UNIVERSITÀ DEGLI STUDI DI PADOVA

UNIVERSITA' DEGLI STUDI DI PADOVA

Dipartimento di Ingegneria Industriale DII

Corso di Laurea Magistrale in Ingegneria dei Materiali

Sodium hydroxide chemical etching of silicon surfaces from end-of-life solar panels

ABSTRACT - The aim of this work is to determine the best combination of parameters for the recycling of silicon from end-of-life solar cells. A chemical etching in hot sodium hydroxide solutions is the proposed treatment for the removal of the back-surface field and the emitter.

The etching kinetic has been studied on the back side of the cell. The best combination of time, temperature and solution concentration for the process is proposed. Then, the time when the emitter is removed has been studied too.

Relatore:

Prof.ssa Calliari Irene

Prof. Kaptay George

Candidato:

Civiero Riccardo, 1154314

Anno Accademico 2018/2019

To my grandmother

INDEX

1. INTRODUCTION

"Silicon is a business", someone would say. As regards the photovoltaic (PV) industry at least, it really is. That is very easy to be determined considering the global PV capacity, and its fashion over years: from 2 GW to 178 GW installed in ten-years' time from 2004 to 2014, up to 700 GW predicted by the year 2020. Since wafer-Si modules are typically ~270 W each, this means ~2,6 million modules in a few years' time.

Earth receives from the sun $1{,}2 \cdot 10^{17}$ W of solar power, while the worldwide energy consumption is only $1{,}3 \cdot 10^{13}$ W. This means that our planet receives more energy from the sun in an hour than the total energy consumed by humans in an entire year. Furthermore, the increasing of energy consumption, higher costs and the awareness of global warming led to a very high growth rate for the PV industry. However, this outstanding growth rate caused a shortage of solar-grade silicon (SoG-Si), and so the demand for PV panels overcame the production.

Silicon contributes for the final cost and energy requirement more than any other component. So, it is important to reduce the price per watt (that is, the ratio between the price of the panel and the nominal number of watts) or the price per kg by means of refining processes. The aim is to bring the price to a level of 2,50 €/W (3 $/W): this is the critical barrier for transition of solar cells industry from small contractor business into large companies, which will further lead the price to less than 1 €/W (~1 $/W).

Semiconductor-grade silicon (SeG-Si), also known as electronic-grade silicon (EG-Si), is widely used for the production of solar cells, typically coming from wastes of the semiconductor industry. This grade is really expensive, more or less 65 €/kg (75 $/kg), due to the high purity level: the total impurity content is 9N (99,9999999%). However, the silicon needed for photo-voltaic purposes does not need to be this pure. Solar-grade silicon must be 5-6N pure (99,999-99,9999%), that means an impurity level of 1-50 ppm. Reducing the purity requirements for SoG-Si leads to a cost decreasing, since a linear relationship can be found, as it is possible to see from Fig. 1.1.

Hence, decreasing the quality of the initial feedstock for solar cells will lead to lots of saving in terms of costs. Using upgraded metallurgical grade silicon (UMG-Si) will reduce costs to 10 €/kg, while the cheapest SeG-Si, that is the near semiconductor-grade silicon, is at most 30 €/kg. However, since near SeG-Si quality is very good, its utilization is supposed to yield a relative efficiency of 1, a relative feedstock yield of 1 and a relative ingot-growth fraction of 1.

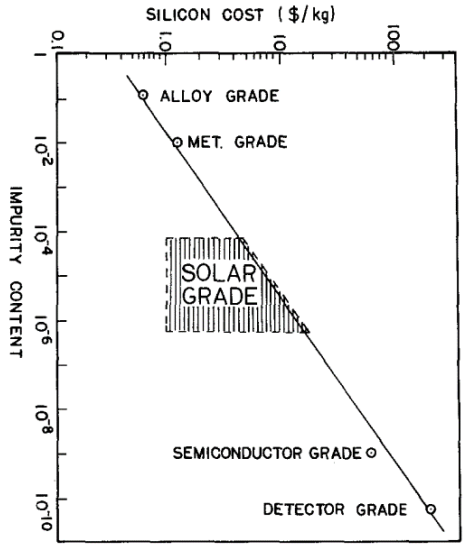

Fig 1.1: *Relation between purity and the cost of silicon (Bathey and Cretella, 1982)*

So, if there are no strong changes of the efficiency, using UMG-Si as feedstock to produce SoG-Si leads to savings for the crystalline Si module of 7% to 11%, while the cost effectiveness is lost if efficiency varies of 1,3-1,7% (del Coso, del Cañizo and Sinke, 2010).

From this it is understandable that the solar cells market needs a feedstock in high quantity and low costs, to satisfy the market needs. This feedstock must also meet the technological requirements, that are good efficiency, 1 Ω·cm resistivity, 6N purity and low boron and phosphorus concentration, since these two elements are detrimental for the semiconductive characteristics of Si if in excess of the required values. Given that in literature there is no complete agreement on those contaminant levels, in this work the ReSiELP project requirements are taken as reference: B below 0,38 ppm_w and P below 0,79 ppm_w. The minority-carrier lifetime must be at least 25 μs.

One way to achieve this kind of product is upgrading metallurgical-grade silicon (MG-Si), which is obtained from the carbothermic reduction of silica. The refining process can be done in different ways, as it will be discussed in the following section. Another way is to take end-of-life PV panels and recycle them to recollect SoG-Si again. However, in the latter case a refining treatment is needed too, since the Si in the cell is doped with B and P to make a p-n junction, which is the basis for the solar panel working.

Recycling is certainly the most attractive way to get new SoG-Si for the solar cells by now, since it responds to the shortage of feedstock. Indeed, even if Si constitutes about the 26% of the earth crust, mostly if form of silica and aluminosilicates, and it is the second most abundant element in weight, after oxygen, to get a Si pure enough for PV applications, very pure raw materials (pure quartz) are needed, and its sources are inexorably lowering.

ReSiELP (**Re**covery of **Si**licon and other materials from **E**nd-of-**L**ife **P**hotovoltaic panels) is a European project that takes care of the recovering and purification of precious raw materials,

such as silicon and silver, but also by-product materials. The aim of this project is to identify an end-of-life environmentally-friendly process with zero or almost-zero waste. Different research and industrial partners are involved, in order to improve the technology from TRL0 to TRL7 by year 2020 and to reach TRL9 within three years from the end of the project.

In this work, a technique to recover silicon to the solar-grade is studied. Since more than half of the total PV panels are **multi-crystalline** wafers, this technology has been studied to reach the required purity on this kind of cells, not only on monocrystalline ones. This process consists on silicon wafers etching in a hot sodium hydroxide solution. The aim is to remove the back-surface field and emitter layers, to get the lightly doped base that can be used to create new wafers. In this way, the recovered material is around 90%, with only 10% of silicon lost.

The kinetic of the etching process has been studied for the back side of the cells, since in this side the thickness that should be removed is higher than the emitter (more than 5 μm versus 1 micron). Different combinations of concentration of the sodium hydroxide in the solution, temperature and time have been tested: the aim is to define the best conditions for the silicon etching. The removal rate is determined from mass and thickness change, while resistivity measurements have been done to have a confirmation of the results.

As for the emitter, the aim is to completely remove it. Since the thickness is very low, the techniques used for the back side are not adequate anymore. So, the samples have been treated with different combinations of time and temperature, keeping constant concentration of the solution, in view of the preliminary results for the back-side etching. The best way to determine when the emitter is successfully removed is to check the type with a p/n tester.

Finally, a combination of concentration of the solution, temperature and time is proposed for a good etching of the silicon. The process consists on etch part of the back-side of the cell, leaving the nitride on the front side to act as a barrier for the silicon, since it is not attacked. When almost all the BSF is etched by the solution, the cell is removed from the NaOH solution and put inside another acid for the anti-reflection silicon nitride coating removal, and then the etching is completed on both sides, to collect the base. In this way, the silicon recovery yield is almost 94%, since part of the silicon is lost in the solution as sodium silicates.

2. LITERATURE REVIEW

Silicon is the second most abundant element in the Earth's crust making up the 25,7% of its mass. Silicon density at room temperature is 2,329 g/cm^3 and the melting point is 1410°C. It possesses an energy gap of 1,12 eV at room temperature and 4 electrons in the outer shell.

Silicon has high affinity with various elements: with oxygen it forms stable oxides as silica SiO_2; with carbon Si-C bonds are very stable, thus forming SiC; also, hydrides as silane SiH_4 can be formed; it also displays high affinity with chlorine Cl_2, forming compounds as trichlorosilane or tetrachlorosilane.

The silicon used in the industries is divided into three purity levels: metallurgical-grade silicon (MG-Si), 98-99% pure, is used as alloying agent or as the starting point to produce higher purity silicon; electronic-grade silicon (EG-Si), 9-11N pure, is used in the electronic industry, for example for the production of transistors; solar-grade silicon (SoG-Si), 6N pure, is used in photovoltaic panels. Due to difficulties in the process, the price of silicon increases as purity increases.

The purest types of silicon can be found in the market with amorphous or crystalline microstructures. The second one is dominant, due to the easier process, and multi-crystalline silicon accounts for the 55% of the total silicon in the market.

2.0.1 Contaminants

The reason for these purity levels is that certain elements different than Si can be incorporated in the lattice. The most important ones are the elements from group III and V of the periodic table. The first ones, like B, originate bonds with one missing electron, thus giving acceptors level in the band gap; vice versa, the second ones bind with other Si atoms with four of their five d-electrons, and so they originate donor levels. As the concentration of these doping elements increases, the resistivity of silicon decreases.

Also transition metals impurities have a relevant effect on silicon, since they affect the minority carriers' diffusion length and lifetime. The minority carrier lifetime τ_0 follows the equation $\tau_0=(\sigma\nu N)^{-1}$, where N is the impurity concentration (atoms/cm^3), σ (cm^2) is the impurity atoms effective cross-section for capturing the minority carrier, and ν the thermal velocity, that

is the average velocity of the electrons. So, the highest is σ, the lowest is τ_0, and, if an impurity is a "lifetime killer" (as Fe and Ti), a minor concentration can be very effective. Fortunately, the impurities in silicon wafers are found in form of precipitates or inclusion, so the recombination activity per metal atom is reduced. High purity Si crystals, with impurity content lower than 10 ppb_w, have a minority carrier lifetime of 10 000 μs, while it is in the range of 50÷300 μs for B or P doped wafers. To increase this lifetime a good technique is to cool the melt down in a way that leads to the formation of precipitates: this practice is the so called "defect distribution engineering".

The most common contamination sources are the raw material and the crucible. The most common raw material for silicon is quartz, which can contain B, P, Ca, Al and Fe as contaminants, so high-grade quartz is needed to get pure results. Most of the crucibles are made by high-purity fused silica or graphite, but the contamination comes from the silicon nitride lining. The proofs of that are that the concentration and the chemical states of the inclusion are similar in the edges of the ingot and in the lining, and that Si_3N_4 particles can be found in the upper part of the solidified ingot due to supersaturation. So, it is necessary to reduce the impurity content in α- Si_3N_4.

To get solar-grade silicon, with the target resistivity, contaminants should be lower than one ppm_w, but this level is hard to get. Anyhow, the required resistivity can be obtained also with higher amount of contaminants, if they compensate each other. In fact, the SEMI PV group in 2011 published the SEMI-PV 17-0611 standard, in which three categories of silicon are listed: "undoped", with less than 0,1 ppm_a of contaminants, the "compensated", with low quantity of doping elements ([B]<0,5 ppm_w and [P]<1,5 ppm_w), and the "heavily compensated", with boron and phosphorus lower than 4 ppm_w.

2.0.1.1 Analytical techniques

The best chemical technique to determine the concentration in the ppb-ppm range is the inductively coupled plasma (ICP). This is a very fast and accurate (the error is 1-2%) way to determine the concentration of trace elements. Since the sample must be liquid, a digestion process is needed as the sample preparation, but in the latest laser-ablation ICPs also solid samples can be measured. The main drawbacks are that the equipment is really expensive and that a calibration with standards is needed each time.

Another physical way to determine the purity of the silicon wafers is the 4-point-probe sheet resistivity measurements. In fact, the resistivity of a semiconductor is controlled by the concentration of the doping elements, as it is confirmed in Fig. 2.1 by Irvin graphs (Irvin, 1962) and by the corrections by Thurber (Thurber, Mattis, Liu, & Filliben, 1980).

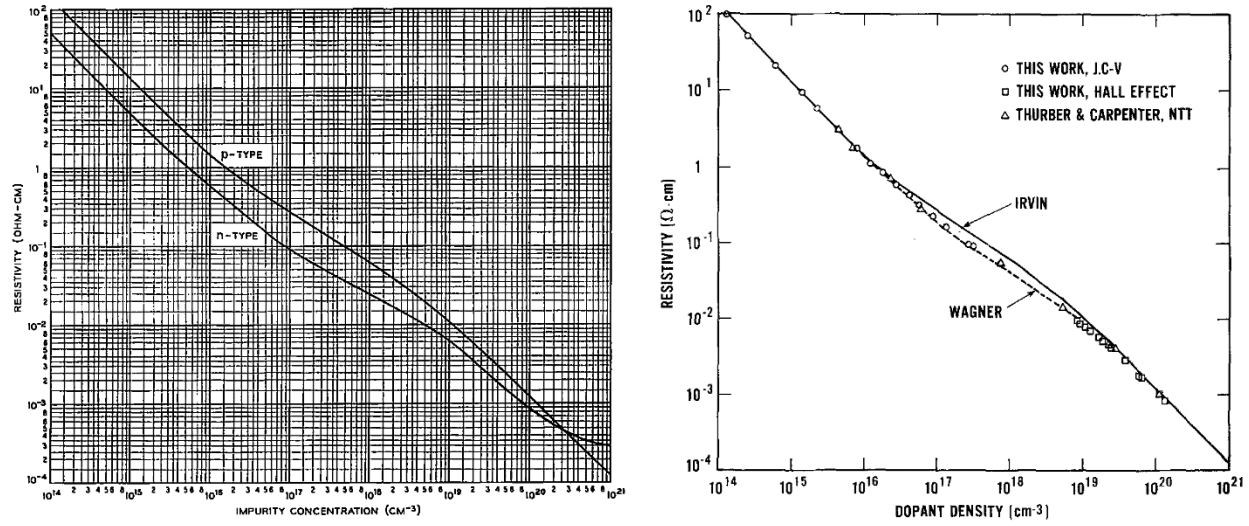

Fig. 2.1 *(*left*) resistivity of silicon at 300 K as a function of acceptor or donor concentration (Irvin, 1962); (*right*) resistivity of silicon at 300 K as a function of acceptor concentration (Thurber, Mattis, Liu, & Filliben, 1980)*

This method consists on placing four probes on a flat surface of the material, to let a current flow through the two outer electrodes and measure the potential difference between the two inner ones. In the simplest configuration the probes are aligned, but other configurations are also possible, as displayed in Fig. 2.2. One of the most important assumptions for the validity of this measurement is that the minority-carriers introduced by the electrodes should easily recombine near the contact area, and this is possible with a high-recombination surface, for example if it is mechanically lapped.

The resistivity can be derived for a semi-infinite material by measuring of the voltage V and by the current applied i by the equation:

$$\varrho = \frac{V}{i} 2\pi s \tag{2.1}$$

where s is the spacing between the probes, considered as constant. If the configuration is not the same as above, some correction factors must be applied to the measured value. For example, for a thin, homogeneous semiconductor slice at temperature T_0:

$$\varrho = \frac{V}{i} w F_2 F(w/s) F_{sp} F_T \tag{2.2}$$

where F_2 is the correction factor for a finite slice $F_2 = 2ln2\frac{s}{w}$, $F(w/s)$ for a finite thickness, F_{sp} for the probe spacing and F_T for the temperature. For the square arrangement with thin infinite slices with nonconductive faces $\varrho \approx \frac{2\pi w}{ln2}\frac{V}{i}$.

This is a fast method which does not need any difficult sample preparation, and it is accurate for measuring in the range of 0,001÷50 Ω·cm. However, with some attentions, it is possible to measure up to 1000 Ω·cm with an error lower than 5%.

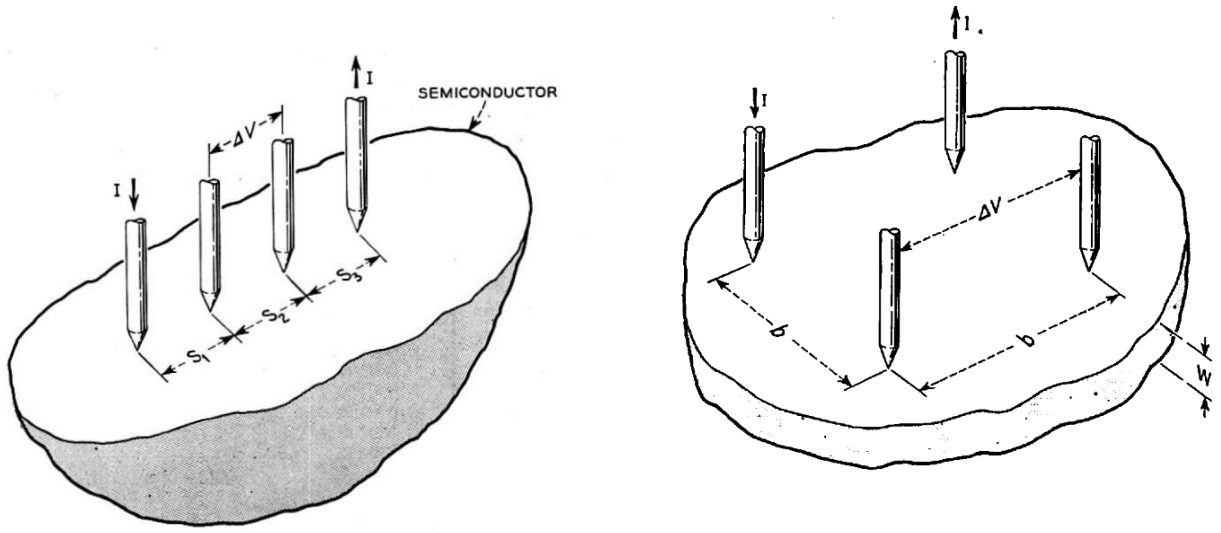

Fig. 2.2 *(*left*) linear and (*right*) square arrangement for the four-point probe (Uhlir, 1955)*

2.1 METALLURGICAL-GRADE SILICON

Silicon, as already said, is a very abundant element in the Earth's crust, but it is present in the oxide or silicate form. In fact, the Gibbs free energy change for the Si oxidation reaction is highly negative, and so SiO_2 is quite stable, it is difficult to find a suitable reductant and not so much elements can be removed from silicon by oxidation. Anyway, it is possible in some ways to reduce silica to get a 98-99% pure product, called metallurgical-grade silicon (MG-Si), for approximately 2,75 €/kg. The impurity content is listed in Tab 2.1: since the too high contamination a further process of purification is needed for the use in photovoltaic applications.

Tab 2.1 Typical analysis of MG-Si (Bathey and Cretella, 1982)

Impurity element	Concentration range (ppm)
Al	1000-4000
B	40-60
P	20-45
Cr	40-220
Fe	1500-6000
Cu	15-40
Mn	10-80
Ni	10-95
Ti	120-275
V	50-275
C	1000-3000
Ca	250-620
Zr	15-25

2.1.1 Carbothermic reaction

Silica can be reduced by carbon at temperatures higher than 1900°C in submerged electric arc furnaces, as in Fig. 2.3. The general form of this reaction is:

$$SiO_2(s) + 2C(s) \rightarrow Si(l) + 2CO(g) \tag{2.3}$$

Actually, the real process is more complex and proceeds through two intermediates, namely SiO and SiC. In fact, the furnace can be divided into two different parts. In the inner zone solid silica is reduced to liquid silicon in a two-steps process at 1900-2100°C through the formation of gaseous SiO:

$$\begin{cases} 2SiO_2(l) + SiC(s) \rightarrow 3SiO(g) + CO(g) \\ SiO(g) + SiC(s) \rightarrow 2Si(l) + CO(g) \end{cases} \tag{2.4}$$

In the outer zone, liquid silicon and SiC for the inner-zone reactions is produced:

$$\begin{cases} SiO(g) + 2C(s) \rightarrow SiC(s) + CO(g) \\ 2SiO(g) \rightarrow Si(l) + SiO_2(g) \end{cases} \tag{2.5}$$

Moreover, side reactions also occur:

$$\begin{cases} Si(l) + \frac{1}{2}O_2(g) \rightarrow SiO(g) \\ SiO(g) + \frac{1}{2}O_2 \rightarrow SiO_2(g) \end{cases} \tag{2.6}$$

producing silica fumes, that are 1 μm fine amorphous silica particles, collected by filters and used as additives in concrete and refractories.

Silica is introduced in the furnace as quartz lumps, while the so-called "reductant mixture" for carbon is made of washed metallurgical-grade coal, lignite, petroleum, coke, charcoal and woodchips. The feedstock must be appropriately pure, in the way that the contamination of

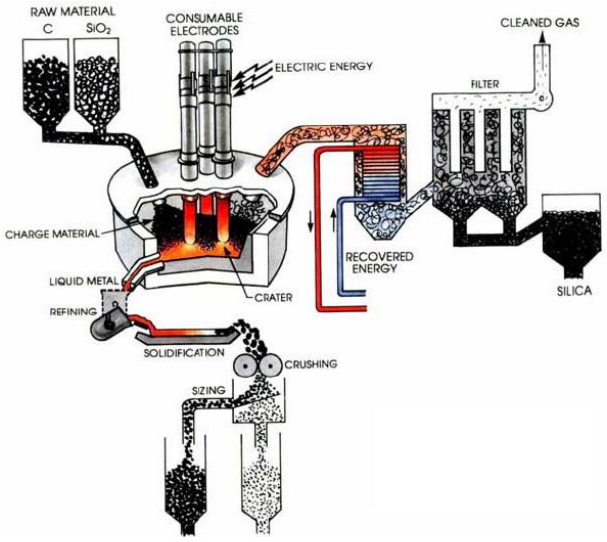

Fig. 2.3 *Schematic representation of a furnace for production of metallurgical grade silicon (Ciftja et al., 2008)*

silicon is minimized. The feedstock is then melted by an arc produced by three submerged carbon electrodes, with a three-phase current applied at a 10-30 MW working electrical load. Finally, liquid silicon is extracted from the bottom, while gaseous CO is oxidized to CO_2 and released into the atmosphere. This is a very energy demanding process (12 kWh/kg of MG-Si produced), with a carbon footprint of 4,3 kg of fossil CO_2/kg of MG-Si produced, and since the temperature are high, it should be as continuous as possible.

2.1.2 Electroreduction

A way to reduce the high energy consumption and carbon emissions of the carbothermic process is the electrodeoxidation of silica in molten salts. In fact, Si(IV) ions can be dissolved into an electrolyte and deposited on a graphite or platinum electrode, following the reaction:

$$SiO_2 + 4e^- \rightarrow Si + 2O^{2-} \tag{2.7}$$

This process is controlled by the ion's diffusion in the electrolyte: SiO_2 is reduced to Si at the cathode, O^{2-} ions migrate to the anode, where they are oxidized to O_2 and/or CO_x. Since silica is an insulant material, it must be coupled with some metals to let the current reach the material, but this usually results in some contamination by intermetallics of the final product. Various salts have been tested: the most promising results have been obtained with $CaCl_2$ at 900°C (Xiao, Jin, Deng, Wang, & Chen, 2010) between -0,65V and -0,95V, and with a LiF-KF electrolyte with 5 mol% K_2SiF_6 at 800°C at moderate current density (~40 mA/cm^2) (Haarberg, Famiyeh, Martinez, & Osen, 2013). All these techniques are characterized by high current efficiencies.

Another chemical way is to reduce SiO_2 porous pellets between two stainless steel plates in molten $CaCl_2$ or $CaCl_2$-NaCl 70:30 mol% mixture. In the final product some $CaCO_3$ can be found, but no $CaSiO_3$, and also some contaminants, like Ni, from the stainless-steel plates, but its brownish colour is due to the nanometric dimension of the particles.

2.1.3 Other routes

There are some other ways to get silicon from silica in a cheaper way, with low carbon emissions and/or leading to purer silicon. One is the aluminothermic reduction of silica:

$$3SiO_2(s) + 4Al(s) \rightarrow Si(l) + 2Al_2O_3(s) \tag{2.8}$$

This way is not so practiced due to the higher cost of Al respect to C, but it is used in some applications, like when the raw material for silicon is phosphorus industry waste (PIW) and/or synthetic slag (SS) (Mukashev et al., 2009). In this process the temperature must be maintained between 1450°C and 1600°C, so that there is low contamination from the crucible refractory material and the silicon floats over the waste. Depending from the ratio between Al and slag different products can be achieved: if the ratio is close to 1, 99,98% pure microcrystalline sili-

con can be obtained with a 80÷90% yield, and the intergranular contaminants can be further removed by acid leaching; if the ratio is more than 1, a Ca-Al-Si alloy is produced, which can be treated with HCl to get monosilane.

Amorphous silicon can also be obtained by rice husks. They are rich in silica, that is captured from the soil by the rice plant, while it does not absorb heavy metals though. These husks are burnt, and the ashes are small, but not submicronic, amorphous, so not carcinogenic, silica particles, very rich in silicon with lower boron and phosphorus content than metallurgical grade silicon. This ash is then reduced by Mg at 900°C, and then the silicon product is purified by acid leaching with a HCl and CH_3COOH mixture 80:20 between 50°C and 70°C.

2.2 ELECTRONIC-GRADE SILICON

Metallurgical grade is too contaminated for application in solar cells, and so it must undergo some refining routes. The most common way is to generate gaseous silicon compounds (mostly chlorides and hydrides) that are purified by distillation and then thermally decomposed into purer Si. The result is a 11N pure silicon, called electronic-grade silicon (EG-Si) or polysilicon: in this way the material has appropriate semiconductor qualities for electronic application, but only a small volume of high-value product can be produced.

2.2.1 Siemens process

The most common process to get EG-Si is the Siemens process, developed in the 1950s. Metallurgical grade silicon undergoes hydrochlorination in a fluidised-bed reactor (FBR) to make trichlorosilane $SiHCl_3$ (TCS):

$$Si(s) + 3HCl(g) \rightarrow SiHCl_3(g) + H_2(g) \tag{2.9}$$

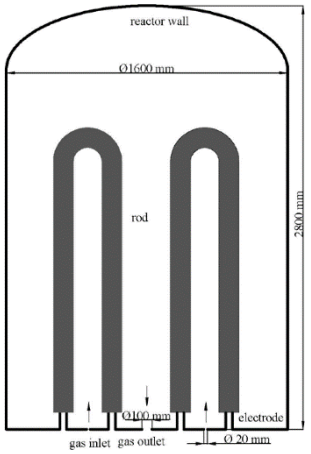

Fig. 2.4 *Frame structure of the traditional polysilicon CVD reactor (Z. Huang, Liu, Yuan, Liu, & Liu, 2013)*

This reaction happens at 350°C without external catalyst, since a good catalyst is Fe, which is naturally found in MG-Si. The trichlorosilane is then purified by the contaminants by fractional distillation in two steps to remove the heavier and the lighter substances. After that, the deposition is done in bell-jar reactors: the reactive gas, that is a mixture of trichlorosilane and hydrogen, undergoes some CVD reactions on some reverse U-shaped high-resistivity silicon rods, which are electrically heated to 1000-1100°C. An example of these reactors can be seen in Fig. 2.4.

This process takes 24-36 hours to be completed, and at the end the silicon has very high purity and fine grains. The by-product is a mixture of produced and reactant gases, that are separated and fed back in the furnace or converted in trichlorosilane again.

The energy requirement for this process is very high, ~200 kWh/kg of silicon produced, but it is calculated that almost 90% of this energy is lost. Moreover, there can be contamination from the graphite contacts on the silicon rods, the process is discontinuous (batch process) and the chlorosilanes are toxic and corrosive. So, the result is a high-cost and low-productivity process, and so some improvements are needed. For example, Huang *et al.* (2013), studied a reactor with a bucket inside to help the control of the outside flow, or another solution can be using multiple bell jar reactors in series, so that the exhaust chlorosilane from a reactor can be deposited in the next one.

2.2.2 Union Carbide process

This process uses silane for the decomposition process: this reaction happens at 800°C, leading to energy savings respect to the Siemens process. However, the whole process is not more economic than the previous one, since the silane is produced via disproportionation of trichlorosilane and dichlorosilane in fixed-bed columns with quaternary ammonium ion exchange. These reactions yield to a 0,2% total silane yield, so the reaction products must be recycled or reintroduced in the reactor. Although, the final silane is very pure.

After distillation, silane is then pyrolyzed onto seed rods on bell-jar reactors:

$$SiH_4(s) \rightarrow 2H_2(g) + Si \tag{2.10}$$

This decomposition can happen in two ways: the heterogeneous decomposition happens on the silicon substrate, and this is the dominant and desirable reaction; the homogeneous decomposition happens away from the structure, leading to big particles that deposit on the substrate or form dust. The by-product is hydrogen, that can be fed again at the beginning of the process, so the only feedstock needed is the MG-Si. No corrosive compounds are formed, and the total conversion efficiency is higher than the Siemens process, but it involves more steps.

2.2.3 Ethyl Corporation process

This process is innovative for two reasons:

I. The silicon feedstock is not metallurgical-grade silicon, but silicon tetrafluoride SiF_4, which is a waste by-product of the fertilisers industry, so it is a low-cost feedstock. The STF is then hydrogenate to monosilane by metal hydrides:

$$\begin{cases} 2H_2 + M + Al \rightarrow AlMH_4 \\ SiF_4 + AlMH_4 \rightarrow SiH_4 + AlMF_4 \end{cases} (M\ being\ Na\ or\ Li) \tag{2.11}$$

$AlMF_4$ can be sold to the aluminium industry.

II. The silane is decomposed in silicon seeds spheres that are moving in a fluidized bed thanks to a gas stream of silane and hydrogen, as it is possible to see from Fig. 2.5. In this way the surface area for the deposition is higher, and when the particles are big enough they fall down in the reactor and they can be collected.

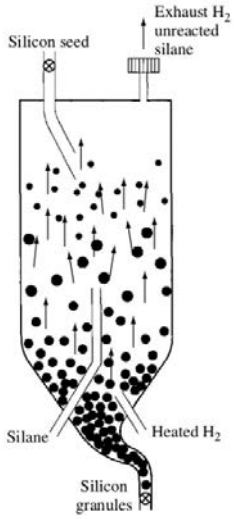

Fig. 2.5 *A schematic representation of a fluidised bed reactor for polysilicon production (Ceccaroli & Lohne, 2003)*

In this way the temperature needed is lower, there is no need to cool the walls and the process is continuous, but there can be some deposition on the walls and contamination of the particles.

2.3 SOLAR-GRADE SILICON

To use silicon in solar panels, with a reasonable efficiency (17-18%), the following limits must be respected:

- 6N purity (99,9999% pure);
- Boron concentration [B]<0,38 ppm_w and phosphorus concentration [P]<0,79 ppm_w;
- Resistivity ϱ=0,1÷2 Ω·cm.

The purity must be this high since transition metal elements, as interstitial or substitutional atoms or as precipitates, introduce deep levels in the middle of the band gap, and this lowers the cell efficiency. Different transition metal atoms have different effect on this purpose, so the concentration allowed changes between different elements. On the other hand, boron and phosphorus are doping elements for silicon, so they have a strong effect on the resistivity of the material, if their concentration is not controlled.

In the beginning, EG-Si waste, as the top and bottom parts of the ingots, was used as silicon feedstock for the PV industry. However, due to the big and constant growth of the PV market, new sources are necessary, like purified MG-Si.

2.3.0.1 SoG-SiO_2 as feedstock for SoG-Si

In section 2.1.2 a method to get silicon by reducing silica with electroreduction is displayed. If the starting silica is pure enough, also the product will be adequately pure for application in solar panels. Solar-grade silica is easy to obtain by leaching treatments. Various molten salts have been found to be good for this purpose, like LiCl-LiO_2 (Lee, Hur, & Seo, 2008) or $CaCl_2$ (Yasuda, Nohira, Hagiwara, & Ogata, 2007).

Another way to get solar-grade silicon from solar-grade silica is with a combustion of an exothermic mixture of silica and magnesium in inert atmosphere, followed by a hydrometallurgical treatment (Won, Nersisyan, & Won, 2011). The hydrometallurgical treatment consists of three steps:

1. Diluted sulphuric acid (H_2SO_4/H_2O 1:4);
2. Leaching in HCl + HNO_3 + C_2H_5OH at 40-50°C with the adding of a mixture of HF + H_2O + C_2H_5OH;
3. Leaching in HF + H_2O + C_2H_5OH at 40-50°C with the adding of a mixture of HNO_3 + H_2O + C_2H_5OH.

The combustion products are mainly Si, MgO and Mg_2Si: the Mg-rich substances are eliminated with the first step of the hydrometallurgical treatment, which is useful to remove also the transition metal impurities. On the other hand, boron, phosphorus and oxygen cannot be removed by step 1, so the other two are needed. Since the combustion product consists on microporous particles, the hydrometallurgical treatment is useful to remove not only the surface impurities, but also the intergranular ones.

2.3.0.2 Other routes

Pure silicon can be obtained by optical fibres waste, since they are made by ultra-high pure silica glass. In this case silica is reduced with a thermal plasma treatment, where the hydrogen glass is useful for the reduction and also for the removal of the contaminants (Ciftja, Engh, & Tangstad, 2008).

Another way to produce high-purity silicon with low energy consumption and CO_x emission is a silicon nitride dissociation in a solar furnace, where the solar rays are concentrated by mirrors in one spot to reach high temperatures. This process leads to MG-Si refining to SoG-Si via two steps:

1. Nitride production:

$$3SiO_2 + 6C + 2N_2 \rightarrow Si_3N_4 + 6CO \quad (2.12)$$

This reaction happens at temperatures lower than 1500°C and it lasts 4 hours, since the kinetic is slow. For this reason, it can be done night time with the stored solar energy.

2. Nitride dissociation:

$$Si_3N_4 \rightarrow 3Si + 2N_2 \quad (2.13)$$

This reaction happens at 1600÷1800°C (lower than the carbothermic reaction), and so during the day. The recombination is thermodynamically unfavoured and a purification step with hydrogen, oxygen or nitrogen is needed to remove the contaminants.

2.4 TRANSITION METAL ELEMENTS

As it is already stated in section 2.0.1, transition metal elements reduce significantly the solar cell efficiency. So, there are specific thresholds for each impurity atom, since their effect is different. However, the tolerable content for each impurity depends on the growth technique and process. So, several ppb_w of contaminants are accepted in solar-grade silicon.

2.4.1 Solidification

The problem/bright side of the solidification is that form a homogeneous melt is not possible to get a homogeneous solid. At a certain temperature T_0 the melt of concentration X_0 start solidifying; at $T_1<T_0$ the solid has concentration X_S and the melt X_L, as it is possible to observe in Fig. 2.6(left): it is possible to define the distribution coefficient as $k_0 \equiv X_S/X_L$.

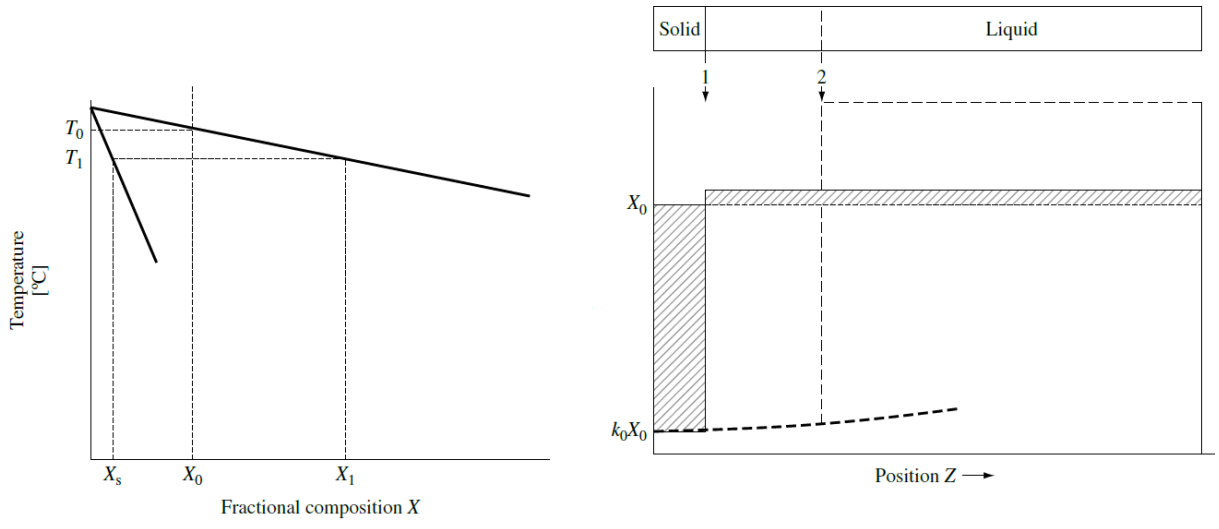

Fig. 2.6 *(*left*) left side of a phase diagram with $k_0<1$ and (*right*) composition development in solid and liquid along a rod solidified from the left end under "normal freezing" (Ceccaroli & Lohne, 2003)*

Let's suppose that at temperature T_0 a fraction of the melt has solidified, as in Fig. 2.6(right). At this temperature the liquid has concentration of component B $X_L = X_0$, so the solid has concentration $X_S = k_0 X_L = k_0 X_0$. However, the solid gets richer in the component A than X_0, so the concentration of B in the melt increases. Furthermore, at the solid-liquid interface the local equilibrium forces the concentrations to follow the rule $X_S = k_0 X_L$, so as the concentration in the liquid increases, also the concentration in the solid does. So, the effect is that, as the solidification proceeds, the concentration of component B increases in both liquid and solid phase. However, if the impurities have a low k_0 (for iron is $8 \cdot 10^{-6}$), almost one atom on 100000 enters in the solid, so the purification effect is high.

If the mixing effect is considered too, then the effective distribution coefficient is $k_{eff} = X_{S,interface}/X_{L,bulk}$: when the mixing is good, $k_0 = k_{eff}$. For the rotational pulling of a rod from the melt the effective distribution coefficient is $k_{eff} = k_0/[k_0 + (1 - k_0)]\exp(-\Delta)$, where $\Delta = v\delta/D_1$, $\delta = 1{,}6 {D_1}^{1/3} \nu^{1/6} \omega^{-1/2}$, D_1 is the diffusion coefficient of the solute, v the pull-out velocity, ν the viscosity and ω the rotational velocity).

Transition metal elements have distribution coefficients in the range between $10^{-6} \div 10^{-4}$. This means these impurities tend to remain in the liquid phase, and so an easy purification process which does not involve any chemical reaction can be done. The main drawbacks of this technique are that, since the last solidified layer, full of impurities, must be cut, some silicon gets lost, and dopant impurities, as boron, phosphorus and aluminium, cannot be removed, due to their high coefficient (in order: 0,8, 0,35 and $2 \cdot 10^{-3}$).

2.4.1.1 Single-crystalline silicon

To produce single-crystalline silicon the most famous way is the Czochralski method (Fig. 2.7 (*left*)). A spinning rod, with a silicon seed attached to it, gets in contact with the molten silicon and it is slowly pulled out. In this way it is possible to control the rod diameter and to prevent spurious nucleation. Rods are generally 2 m long and their diameter is around 30 cm. It is a high energy-consuming process, since the silicon must be maintained in the molten state for a long period.

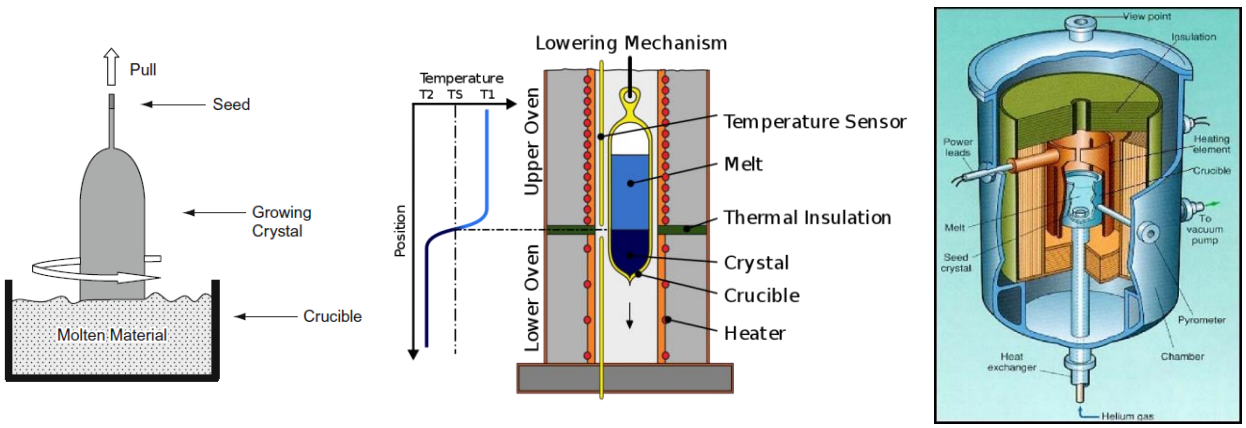

Fig. 2.7 *Schematic representation of: (left) Czochralski method (Ferrazza, 2012); (centre) Bridgman method (https://commons.wikimedia.org); (right) HEM furnace (Ciftja et al., 2008)*

Another method to produce single-crystalline silicon is the Bridgman method (Fig. 2.7 (*centre*)). In a vertical tubular electric furnace the molten silicon is slowly lowered from a region where it is keeped at a temperature above the melting point to a cooling bath of oil. If the speed is low enough, a single-crystalline ingot is obtained.

2.4.1.2 Multi-crystalline silicon

An easier and faster way to produce silicon ingots is the ingot casting. The melt is poured into a crucible and temperature is lowered on the bottom, so solidification starts from there and the front moves upwards. The mostly used equipment for this purpose is the HEM (heat-exchange method) furnace (Fig. 2.7(*right*)): this furnace allows good vacuum and the best directional solidification. In this way multi-crystalline ingots are produced, so the cells have lower efficiency respect to the single-crystalline ones.

2.4.1.3 Zone refining

Zone refining takes advantage of the idea of solidification refining and uses it to purify already solidified ingots. One end of the ingot is slowly heated up to the solid-liquid region, so that the impurities diffuse into the liquid; then this molten part is moved to the other end, so that the liquid phase captures the impurity all along the ingot length. In this way the solute is redistributed, and finally the impurity-rich liquid phase is removed by the "cake", the solid-liquid mixture. The heating velocity is the most important parameter to be controlled, in connection to the diffusion and coalescence of impurities.

2.4.2 Solvent refining

Solvent refining consists on alloying silicon with another metallic element, immiscible with silicon in the liquid phase, up to the hypereutectic concentration. In this way the primary silicon precipitation happens below the melting temperature of pure silicon, and this decreases the distribution coefficient of all the impurities, including boron and phosphorus, as it is displayed in Fig. 2.8. Indeed the solute becomes instable as temperature decreases, and, since the dissolution is endothermic, the activity increases as temperature decreases.The heavy metal impurities are reject from the silicon into the melt, that is a metal-silicon mixture.

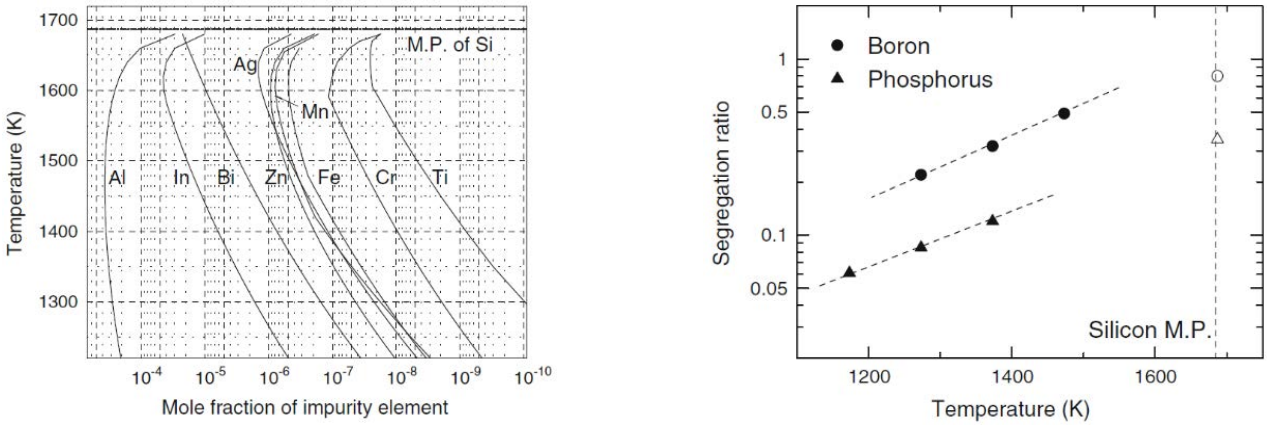

Fig. 2.8 *(left) Solid solubilities of impurity elements in silicon; (right) Temperature dependence of segregation ratios of boron and phosphorus between solid silicon and Si-Al solvent (Yoshikawa & Morita, 2012)*

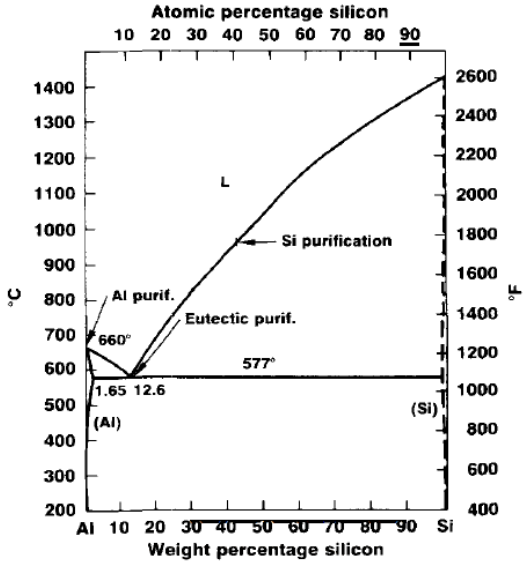

Fig. 2.9 *Aluminium-silicon system binary phase diagram (Dawless, Troup, Meier, & Rohatgi, 1988)*

2.4.2.1 Aluminium

Aluminium is the mostly used metal for solvent refining, because it is cheap and, as it is possible to observe in the phase diagram in Fig. 2.9, no intermetallics between Si and Al exist. So, if more of the 12,6 wt.% of silicon is added, pure silicon crystals precipitate as needle-like crystals, rejecting the impurities into the eutectic melt.

To get the pure silicon, it must be separated from the eutectic phase. The main drawback of using aluminium as the solvent is that the acid leaching is difficult due to the presence of aluminium oxides and hydrides. So other strategies had been developed: if some calcium is added, $CaSi_2$ is formed and it incorporates the silicide particles, being easily leached after all or either way the primary silicon can be separated from the liquid phase by an electromagnetic field in an induction furnace or by supergravity.

Even if the distribution coefficient for boron and phosphorus is reduced, the solvent refining is not enough to reach B and P levels for solar-grade silicon. For this purpose, adding some titanium helps the boron removal, since stable TiB_2 precipitates, and adding calcium reduces the phosphorus concentration in the final pure silicon.

2.4.2.2 Copper

Copper, even if more expensive than aluminium, is frequently used in solvent refining due to the low ionic radius and its faster diffusion in the silicon lattice. In fact, since copper silicides formation is unlikely in the silicon lattice, due to the high volume difference, copper moves in the silcon dendrites up to the liquid phase, full of impurities, until Cu_3Si is formed there. Then the pure silicon dendrites are separated by the copper silicide phase by crushing in micrometric particles.

If some calcium is added in the Si-Cu 50:50 solution, $CaCu_2Si_2$ is formed. This component has great affinity with phosphorus, which is thus trapped, and it can be easily eliminated via acid leaching. If 5% of Ca is added, the phosphorus removal efficiency reaches 82%.

2.4.2.3 Iron

Iron can be a very cheap alternative to aluminum and copper, due to the fast diffusion and the reactivity with boron and phosphorus, and the by-product can be sold to the steelmaking industry as ferrosilicon. The main problem is that the microstructure is composed by silicon and α-$FeSi_2$, and the interface between them is full of impurities. However, quenching above the eutectic temperature and then a slow cooling leads to a 98,9% separation efficiency.

2.4.3 Acid leaching

During solidification, impurities segregate as intermetallics, silicides, silicates, alloys and complex compunds at the grain boundaries, which for this reason become more brittle. A way to remove these impurities is to crush the silicon and treat the particles with acids. In fact, the cracks propagate in the grain boundaries, due to their brittleness, and so the impurities are exposed on the particles surface. Acids dissolve them, but not the metallic silicon, which is more resistant. Thus, the solidified silicon must be crushed into 50÷70 μm particles, so that the impurities at the grain boundaries, but also the ones inside the grains, are exposed. In this way, a 99,9÷99,99% pure silicon can be obtained with an easy and cheap process. However, this is not enough to reach solar-grade purity, so a directional solidification is needed.

The most important parameters to be controlled are the temperature, the time and the type of acid and its concentration. The best acid mixture is aqua regia: in fact, hydrofluoric acid is a must-have in the leaching mixture, because, differently from hydrochloric and nitric acid, dissolves the silica layer which forms on the particles surface. The ultrasonic stirring also improves the purification efficiency, since the cavitation bubbles, exploding when in contact with the particles surface, form cavities which help to remove the impurities also from inside the silicon particles.

However, this treatment is ineffective for the removal of interstitial and substitutional elements, like boron and phosphorus. To remove them, some strategies can be implemented to the leaching treatment. If calcium is added, it dissolves phosphorus in the calcium silicide or forms Ca_3P_4, both leachable; barium has the same effect on boron. For the boron removal, a complexing agent can be added so the acid mixture: boron in silicon can react with hydrofluoric and nitric acid to form boric acid H_3BO_3 or fluoroboric acid HBF_4 and then, since it has an empty orbital, it can form a complex borrowing an electron pair by some complexing agent. The best complexing agent is glycerine, that leads to a 91,5% removal efficiency for boron (Sun et al., 2013).

2.5 BORON AND PHOSPHORUS

Boron and phosphorus are problematic elements, because they cannot be effectively removed with the techniques just described. Their distribution coefficient is too high (k_B=0,8 and k_p= 0,35) to be removed by directional solidification, and solvent refining does not improve it so much. Furthermore, since they are substitutional elements for silicon, they are not removed by

acid leaching. Therefore, other techniques must be applied to reach the required levels of these elements for solar grade silicon (B=0,38 ppm_w and P=0,79 ppm_w).

2.5.1 Vaporization

Impurity elements, including boron and phosphorus, can be eliminated from molten silicon via gas phase. This refining treatment can be done under vacuum, effective condition for P removal, or with reaction with oxidizing gases, as H_2, O_2 or Cl_2, which form volatile compound with the impurities. The ideal temperature range for an effective B and P removal is between 1500°C and 1700°C.

2.5.1.1 Vacuum refining

Vacuum refining is based on the difference of partial pressure between the components of a solution: the higher is the partial pressure of the solute, compared to the solvent, the easier is its removal. Since the partial pressures for phosphorus is p_P^0=2,627·10^8 Pa and for silicon p_{Si}^0=0,191 Pa at 1500°C, and p_P^0=3,177·10^8 Pa and p_{Si}^0=0,789 Pa at 1600°C (Safarian & Tangstad, 2012), vacuum refining can be a useful way to remove phosphorus from the silicon melt. It is done at temperatures between 1500°C and 1700°C at pressures around 0,5 ± 0,2 Pa.

Considering it as a non-equilibrium process and a Raoultian behaviour for silicon and Henrian behaviour for phosphorus, the evaporation coefficient can be defined as:

$$\alpha_P \equiv \frac{\gamma_P^0 p_P^0}{p_{Si}^0}\left(\frac{M_{Si}}{M_P}\right) \tag{2.14}$$

where M_i is the atomic weight and γ_P^0 phosphorus activity coefficient at the standard state. If this coefficient is higher than 1, the removal is possible. This is the case for phosphorus, as displayed in Fig. 2.10.

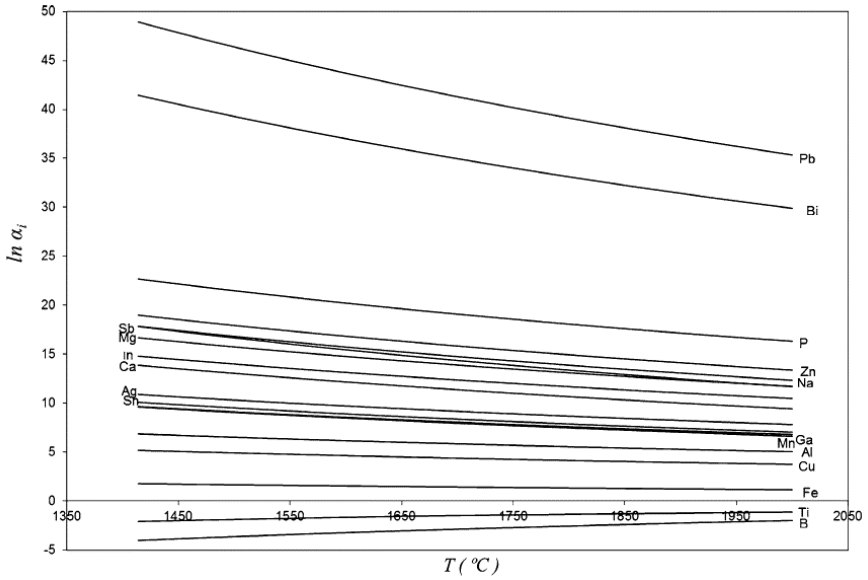

Fig. 2.10 *The relationship between the volatility coefficient a_i and temperature for the dissolved elements in molten silicon (Safarian & Tangstad, 2012)*

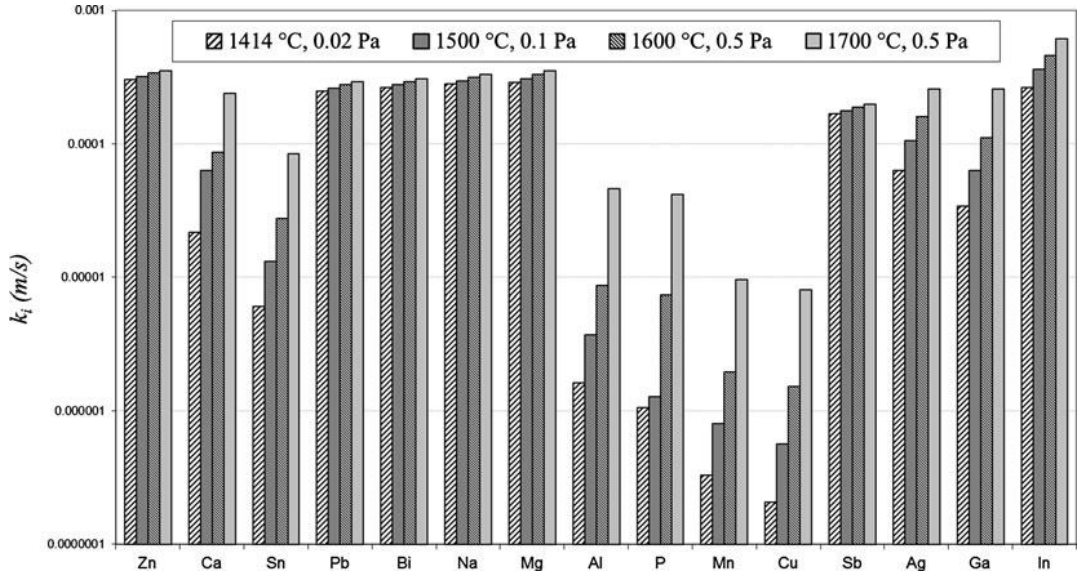

Fig. 2.11 *Total mass transfer coefficients for the dissolved volatile elements in silicon under typical process conditions (Safarian & Tangstad, 2012)*

Phosphorus removal is controlled by the chemical reactions and the mass tranfer in the gas phase. In fact, the flux of phosphorus from the liquid to the gas phase is divided into three parts: the transport through the melt boundary layer, the chemical evaporation and the mass transfer in the gas phase. Each one of these steps is governed by a mass transfer coefficient, respectively:

$$k_{m,P} \equiv \left(\frac{8D_{m,P}v_m}{\pi r_m}\right)^{1/2} \qquad k_{c,P} \equiv \frac{\eta M_{Si}\lambda_P}{\varrho_{Si}\sqrt{2\pi M_P RT}} \qquad k_{g,P} \equiv \frac{v_g \gamma_P^0 p_P^0 M_{Si}}{RT\varrho_{Si}} \tag{2.15}$$

The values of this coefficients between the silicon melting point, 1414°C, and 1700°C, are in the range of $k_{m,P}$=0,0003÷0,0004, $k_{c,P}$=0,000001÷0,0001 and $k_{g,P}$=0,000001÷0,0002. Since the flux of phosphorus is defined as

$$\dot{n}_P \equiv k_P C_P \qquad \text{with} \qquad k_P \equiv \left(\frac{1}{k_{m,P}} + \frac{1}{k_{c,P}} + \frac{1}{k_{g,P}}\right)^{-1} \tag{2.16}$$

the rate determining steps are the ones with lower mass transfer coefficient, ergo, the chemical reactions and the mass transfer in the gas phase. Therefore, from the value of k_P, reported in Fig. 2.11, it is possible to define the P removal flux.

From the figure it is possible to see that the mass coefficient, and so the phosphorus flux, changes with the temperature. In fact, for a pressure of 0,5 Pa, it is possible to calculate the mass trasfer coefficient in function of temperature as:

$$k_P = -\frac{25633}{T} + 1{,}4645 \tag{2.17}$$

According to the kinetic priciple, the general equation for the concentration of phosphorus during the treatment is

$$ln\left(\frac{C_i}{C}\right) = k_P \frac{A}{V} t \tag{2.18}$$

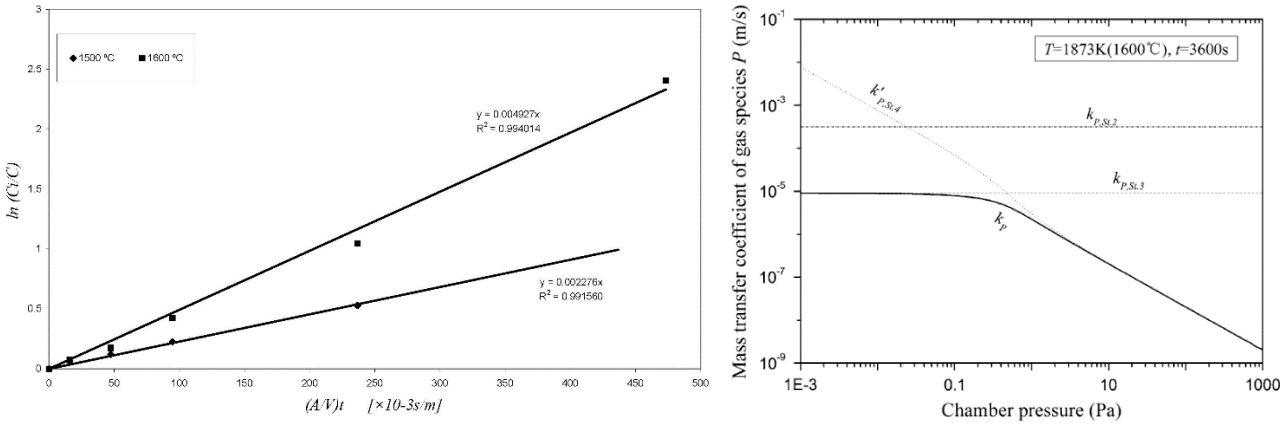

Fig. 2.12 *(left) Relationship between* $ln\left(\frac{C_i}{C}\right)$ *and* $\frac{A}{V}t$ *for phosphorus removal at different temperatures (Safarian & Tangstad, 2012); (right) Plot of mass transfer coefficients as a function of chamber pressure for gas species P (Zheng, Engh, Tangstad, & Luo, 2011)*

which, in the $ln\left(\frac{C_i}{C}\right)$ versus $\frac{A}{V}t$ plot in Fig. 2.12 (left), gives a linear relation, meaning that the process follows a first order kinetics. So it is possible to calculate the concentration of phosphorus at time t as:

$$C = C_i \exp\left(-4{,}325 \exp\left(-\frac{25633}{T}\right) \cdot \frac{A}{V}t\right) \tag{2.19}$$

Also the chamber pressure influences the impurity flux: as the pressure decreases, the mass transfer coefficient increases. However, if pressure becomes lower than 0,471 Pa, the free evaporation of phosphorus becomes the rate determining step, and so k_P becomes constant with pressure, as it is shown in Fig. 2.12 (right).

When the concentration is higher than 50 ppm_w, phosphorus is mainy removed as diatomic specie P_2, while at lower concentrations as monoatomic P, since the partial pressure is higher.

2.5.1.2 Reactive gas blowing

To remove impurities it is possible to make them react with certain gases purged on the surface or through the melt, in order to form volatile compunds that can evaporate from the molten silicon. This method is useful for the removal of boron. These reactive gases are also mixed with some inert gas, mainly argon, that improves the stirring of the melt and so enhances the reaction of impurities elements with the gases. The most used reactive gases are hydrogen H_2, oxygen O_2, water vapour and mixture of them.

When Ar-H_2 mixture is blowed into the melt, hydrogen dissolves into the melt as [H], and reacts with dissolved boron to generate BH or BH_2. When Ar-O_2 mixture is introduced, the silicon oxidation is thermodynamically favoured over the boron oxidation. Therefore the melt is refined by the reactions between silica and dissolved boron, mainly with production of BO and B_2O_2.

When a mixture of Ar-H_2O-H_2 is introduced, boron is removed through the generation of BHO. The longer is the treatment time, the larger is boron removal, with an exponential decreasing, as it is possible to see from Fig. 2.13: this suggests a first order kinetics

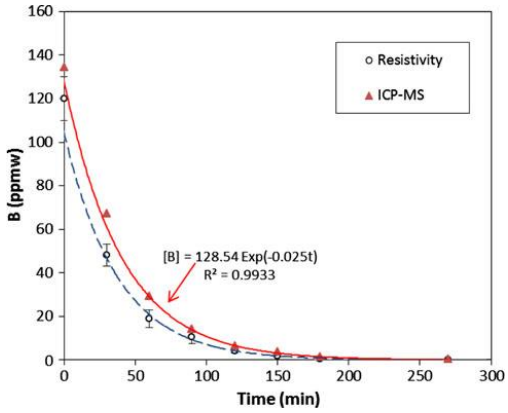

Fig. 2.13 *Comparison of the B contents determined by resistivity meter and ICP-MS (Tang et al., 2012)*

$$\ln\left(\frac{B}{B_0}\right) = -k\sqrt{p_{H_2O}}\frac{A}{V}t \tag{2.20}$$

From the experiments (Tang, Andersson, Nordstrand, & Tangstad, 2012), it is possible to observe that reduction rate is faster at lower temperatures. This suggests that the kinetics is controlled by the heterogeneous chemical reactions occurring at the surface of molten silicon.

A mixture of Ar-H_2O-O_2 can be used to for the refining of molten silicon. In this case, the reactions that occurr have the form:

$$\frac{4x}{2y-z}[B] + \frac{2z}{2y-z}H_2O(g) + O_2 \rightarrow \frac{4}{2y-z}B_xH_zO_y(g) \tag{2.21}$$

At the silicon melting point the most easily formed compound is $B_3H_3O_3$, while at temperatures higher than 1700°C is BHO. However, the partial pressure of hydrides, except BHO, decreases with temperature, so it is recommend to do the refinement at temperatures slightly higher than the silicon melting point. In this region, the most volatile compound, that is the one with higher partial pressure, is $B_3H_3O_6$. However, the partial pressures are $10^5 \div 10^{10}$ times higher than without water wapour.

With this technique it is possible to reduce the boron content to acceptable levels, but further refining techniques are needed to remove the metallic impurities. So, it must be coupled for example with directional solidification.

2.5.1.3 Plasma refining

In an induction furnace, such as the one in Fig. 2.14, a plasma of argon and oxidizing gas flows on the surface of silicon and helps eliminating impurities, both metallic and dopant. Boron can effectively removed so solar-grade concentration in a few minutes, thanks to the formation of oxides and hydrides. Phosphorus should be removed too as P_2, but this does not happen in practice; however, the silicon is not n-type, even if the P concentration is high, meaning that phosphates have been formed, which neutralise P.

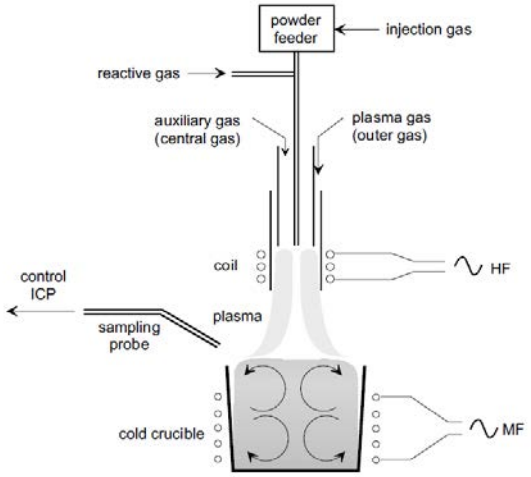

Fig. 2.14 *Schematic diagram of the induction furnace with plasma torch (Alemany, Trassy, Pateyron, Li, & Delannoy, 2002)*

At room temperature the Si is not conductive, so it is heated up by the argon plasma. When it starts melting, the induction heating system takes part in melting the remaining part, so the plasma power can be reduced, since it is less effective, and the oxidizing gas can be introduced. The gas used are a mixture of H_2 and O_2 or water vapour. Hydrogen is useful for the removal of metallic impurities, to eliminate the residual oxygen on the silicon lattice and passivate the defects. On the other way, if too much oxygen is introduced, a white layer of silica forms on the top of the melt, drastically decreasing the volatilization rate.

The main drawbacks of this method are that it is not cost-effective, due to the high cost of the high-vacuum systems to generate plasma, and that the elimination of impurities happens only in the surface. For this reason, a good mixing is necessary for a good refining, guaranteed by the induction furnace.

2.5.1.4 Electron beam refining

This refining technique uses a beam of accelerated electrons to remove the impurities. In the silicon lattice, these electrons interact with impurity atoms and convert their kinetic energy into energy for the evaporation of the impurities with higher vapour pressure than silicon. Therefore, the removal of phosphorus is successful with this method up to more than 90%, but it is ineffective for boron removal.

2.5.2 Slag refining

This refining method uses the liquid-liquid extraction to remove impurities. From the Ellingham diagram, reported in Fig. 2.15, it is possible to observe that the oxidation of most of the metallic impurities in silicon happens spontaneously respect to the silicon itself; however, boron and phosphorus, being more noble than silicon, cannot be oxidised spontaneously. Nevertheless, it is possible to remove boron and phosphorus incorporating them in slags.

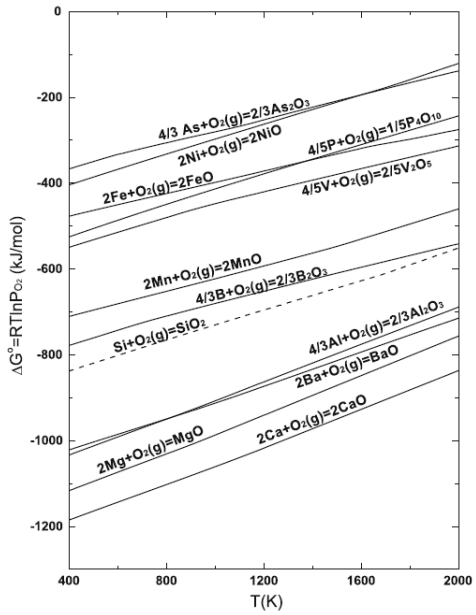

Fig. 2.15 *Ellingham diagram for oxides (Johnston, Khajavi, Li, Sokhanvaran, & Barati, 2012)*

The slag former compounds are generally added in quantitites of 1÷5% of the mass of silicon, they should not contaminate silicon, and they should have different density from silicon. In this way the slag can float or sink, or it can adhere to the mould walls, and in this way it can be easily removed.

Boron can be removed by oxidation and adsorption as borate, as follows:

$$[B] + \frac{3}{4}O_2 = \frac{1}{2}B_2O_3 \qquad \frac{1}{2}B_2O_3 + \frac{3}{2}O^{2-} = BO_3^{3-} \tag{2.22}$$

The O_2 atoms are given by the silica ($SiO_2 = Si + O_2$), while the O^{2-} ions are given by the calcium oxyde ($CaO = Ca^{2+} + O^{2-}$). The slag boron capacity, $\mathcal{L}_B = (B)/[B]$, that is how much boron can be trapped in the slag, can be defined as:

$$\mathcal{L}_B = k_1 \frac{\gamma_B a_{O^{2-}}^{3/2}}{\gamma_{BO_3^{3-}}} p_{O_2}^{3/4} \tag{2.23}$$

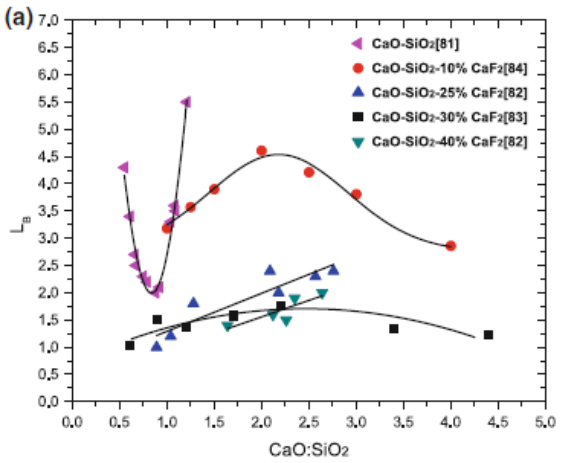

Fig. 2.16 *Boron distribution versus a function of slag composition expressed in CaO-SiO2 binary and CaO-SiO2-CaF2 ternary system (Johnston et al., 2012)*

The two requirements, $a_{O^{2-}}$ and p_{O_2}, are in conflict: increasing the CaO/SiO_2 increases the slag basicity, but at the same time decreases the oxygen partial pressure, given by the silica. So a maximum of the value of the boron capacity can be obtained when $CaO/SiO_2=2$ (Fig. 2.16).

The rate determining step for the boron removal kinetics is the mass transfer, since the temperatures are very high and so the chemical reactions are fast. The relation between the mass transfer coefficient and the refining time is given by:

$$\frac{M_{Si}}{\varrho_{Si} A_S \left(1 + \frac{M_{Si}}{L_B M_{slag}}\right)} ln \frac{[B] - [B]_e}{[B]_{in} - [B]_e} = -k_t t \tag{2.24}$$

By the experimental data it is possible to define that the reaction follows a first order kinetics and that the mass trasnfer coefficient has values between 1,7÷4,3 μm/s (Krystad, Tang, & Tranell, 2012).

The dephosphorization by slag refining happens mostly with the formation of phosphides.

$$\frac{1}{2} P_2 + \frac{3}{2} O^{2-} = P^{3-} + \frac{3}{4} O_2 \tag{2.25}$$

Phosphorus dissolves as Ca_3P_2 and the phosphorus capacity follows the same trends of the boron capacity for $CaO\text{-}SiO_2$ slags, but if other components are added to the slag, such as aluminum oxide, it can follow a linear trend. Phosphorus gas can be removed from the slag, as P_2, P_4, or, if H_2 gas is added, as PH_3.

The best slags for boron and phosphorus refining are ternary or quaternary systems which include MgO or Al_2O_3: magnesium oxide gives the highest mass transfer coefficients for boron removal, while aluminium oxide largely improves the phosphorus removal. The maximum boron and phosphorus capacity reported in literature amount to 5,5 and 9 respectively. The removal efficiency clearly increases with the silicon-to-slag mass ratio, but if too much slag is added, this refining technique is not cost-effective anymore. In fact this method is very easy to be controlled, but the main difficulty is to get very clean slag formers.

2.5.3 Electrorefining

Another way to remove impurities is the electrodeposition of silicon in molten salts: at temperatures between 700°C and 1100°C silicon has good electric properties. The impurities which have

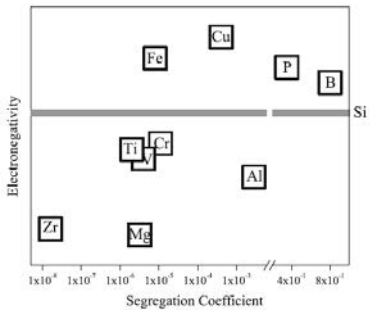

Fig. 2.17 *Comparison of segregation coefficient and electronegativity of impurities in MG-Si (Johnston et al., 2012)*

positive electronegative respect to silicon do not dissolve from the anode, while the others do not deposit to the cathode, and so they remain in the electrolyte: as it is possible to observe from Fig. 2.17, boron and phosphorus remain in the anode, and so the purification can be good.

Generally the electrolyte is made by cryolite (Na_3AlF_6) and silica or molten fluorides and K_2SiF_6: since Si(IV) ions are solvated as Si_{4+x}^{x-}, and this is in equilibrium with gaseous silicon fluoride ($Si_{4+x}^{x-} = SiF_4 + xF^-$), Si_{4+x}^{x-} is more stable in the basic molten baths, and the better one is NaF-KF 40:60 mol. The anode is generally a M-Si alloy, where M is mostly Cu or Fe: this avoids the passivation of the anode, as it happens for MG-Si. The Cu-Si can be in liquid form, but also in solid state, as, if the alloy is solidified from the melt, the microstructure is composed by primary silicon crystals in a Cu_3Si matrix: this allows the treatment to be done at lower temperatures.

At the tungsten cathode a 4-5N silicon deposits in powdery or nano-fibrous form, depending on the K_2SiF_6 concentration in the electrolyte, and it is generally brittle. The boron and phosphorus removal is around 90%. The main difficulty of this process is to find clean electrolytes.

A variant of this process is the three-layer electrorefining: the anode is the molten M-Si alloy, which deposits on the bottom of the cell, the molten fluorides electrolyte stays in the middle, while the pure silicon cathode floats on the top of the cell. Due to the fact that the silicon must be liquid, temperatures higher than the silicon melting point are needed. The main drawback is that boron is not effectively removed, due to the similar thermodynamic properties to silicon. To solve this problem the electrorefining can be coupled to the electrocatalyzed reaction of B with metals, like Fe and Ti: in this way heavy metal compunds precipitate at the anode-electrolyte interface.

2.6 PROCESSES TO SOLAR-GRADE SILICON

The Crystal System Inc. developed a single step process in a modified HEM furnace, combining the gas blowing, the vacuum refining, the slagging refining and the directional solidifiction. Also the using of scavengers, like tungsten, helps the refining, forming complexes with impurities. A " cold finger" made by a tungsten rod with a molybdenum wire inside flowing cold argon gas, is used to capture evaporating silicon, very rich in phosphorus. This route is very effective in removing phosphorus, while it is not so effective for boron (Crystal Systems Inc., 2008; Schmid & Joyce, 2009).

ProPower developed the so-called "Chemical Phisics" method: the metallurgical-grade silicon is melted in vacuum and refined by oxygen gas blowing, then a magnetic field and vacuum are applied to separate the impurities and then the melt is directionally solidified. The product reaches a 5N purity, with a resistivity of 0,5÷3 Ω·cm, while de cells produced with this material show a 15% efficiency, though with a 10÷15% of light-induced degradation (Liang et al., 2010).

Silicor Materials developed a method which allows to produce cells with an efficiency higher than 16,5% with only a 2% light-induced degradation. This process starts from dissolving impuri-

ties into aluminium. The aim of the company is not to get 6N silicon, but compensated silicon useful for p-type solar cells production, so the relative mix of B and P is monitored. After the precipitation of silicon crystal from the melt, an acid cleaning step is done and after the crystals are melted again and directionally solidified (Silicor Materials, 2012).

The NEDO process, by the Kawasaki Steel Corporation, consists on three different stages: the phosphorus is removed to levels lower than 0,1 ppm_w in an electron beam furnace, where also the metallic elements are removed to levels lower than 10 ppm_w in the purified part by directional solidification; the boron is reduced to levels lower than 0,1 ppm_w with plasma melting in oxidizing atmosphere; then a final directional solidification follows. This method leads to the production of a material with a final resistivity of 1 Ω·cm, that generates a cell with 14% efficiency (Yuge et al., 2001).

The Elkem Solar developed a process which purifies metallurgical-grade silicon by a slag treatment, a leaching and a directional solidification, follwed by a post-purification step to prepare the material for the wafer production. In the last years they also developed a simplification process which improves the acid leaching step in order to avoid the directional solidification and the post-treatment. The Elkem process produces silicon with a 70% less energy and four times lower greenhouse gas emissions than the Siemens process (Glöckner & de Wild-Scholten, 2012; Søiland et al., 2014).

2.7 PHOTOVOLTAIC CELLS

The dominant structure of the cells that can be found in the PV panels is the co-fired screen printed Aluminium Back Surface Field cell, which is schematically represented in Fig. 2.18. The usual dimensions are 156x156x0,18 mm^3. This low thickness if effective for the reduced amount of material needed

The main part od the cell is a B-doped p-type silicon wafer, with a concentration of boron (acceptor) of 10^{16} atoms/cm^3, with a bulk resistivity of almost 1 Ω·cm. The main function of this

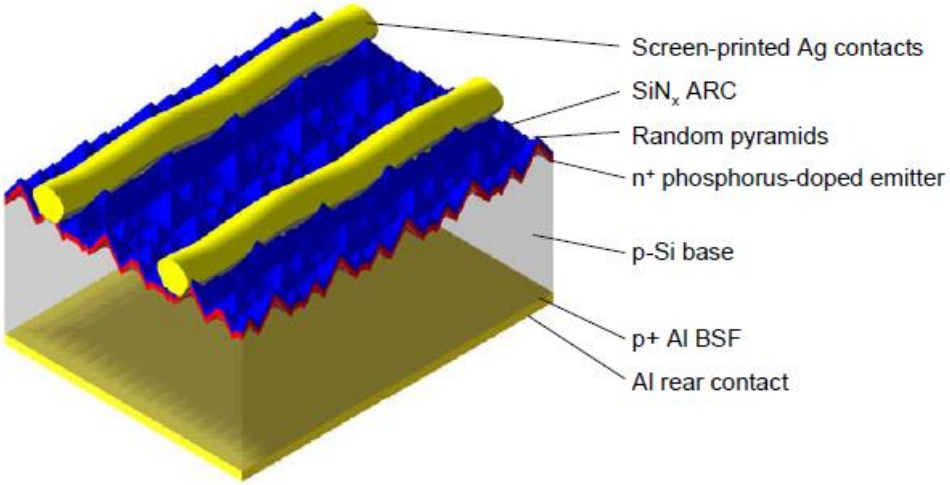

Fig. 2.18 *Structure of Al-BSF solar cell (Glunz, Preu, & Biro, 2012)*

substrate it to absorb the photons and enable the transport of majority (holes) and minority (electrons) carriers.

On the top of this substrate there is a P-doped n-type layer. The phosphorus concentration in this layer changes between 10^{20} atoms/cm^3 near to the outer surface to 10^{16} atoms/cm^3 in the inner part. This doped layer extends for almost 1 μm inside the substrate, and its main function is to generate a several hundreds of nanometers p-n junction, which allows the carriers movement through the cell. The top side is texturized, namely a pyramidal structure is generated, to improve the capturing of photons. The top surface is then covered with a 75 nm thick silicon nitride antireflection layer.

In the top layer a H-like grid of silver paste is applied to create the metallic contact and so to collect the current. Generally, three busbars are formed, and they are linked by a great number of contact fingers. A silver paste is applied on them, and, below it, silver crystallites penetrate the silicon via the (111) planes. The rear side is fully metallized for efficient carrier transport: 5% of the surface is covered by the silver contact pads, soldered to silicon; the remaining surface is covered with an aluminium paste, while the Si region below is doped with Al to $3 \div 4 \cdot 10^{18}$ atoms/cm^3 for almost 5 μm.

2.7.0.1 P-doped layer

The top layer of the cell is heavily n-type, and it is doped by the diffusion of phosphorus atoms: P atoms are donor impurities for silicon, namely they introduce free electrons in the silicon lattice.

The main aim of this layer is to create a p-n (or better, p-n$^+$) junction. When a p-type and an n-type material are juxtaposed, some electrons from the n-layer migrate in the p-layer, where there is a lack of electrons, recombining with the holes: in this way, near the boundary between the n-side and the p-side a depletion region is formed, where there are no free electrons or holes. Due to the migration of electrons, the n-side boundary becomes positively charged, since it lost electrons, while the p-side boundary becomes negatively charged, since it lost holes that recombined with the electrons. In this way an electric field generates in the depletion region. When solar rays hit the cell, the energy they bring is enough to generate in the depletion region

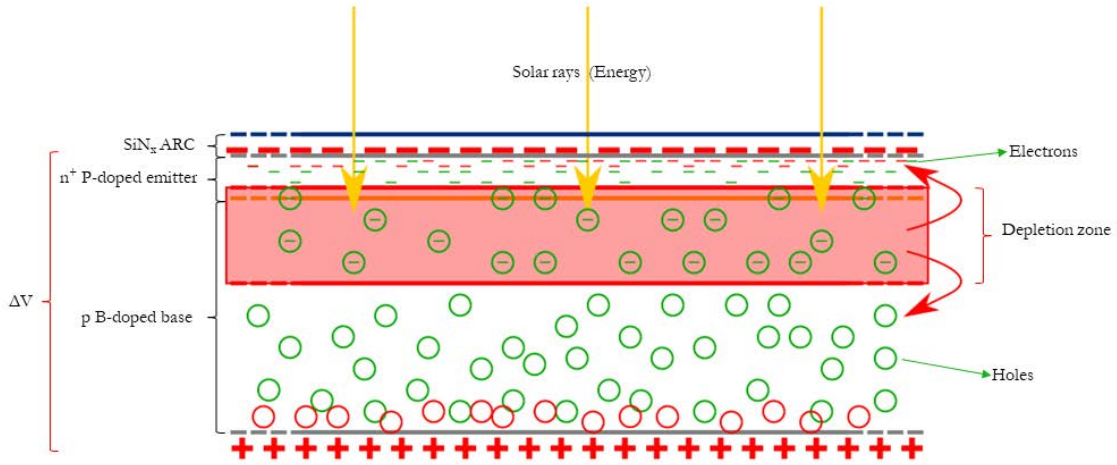

Fig. 2.19 *Schematic view of the structure and operating principle of a p-n$^+$ junction in a solar cell*

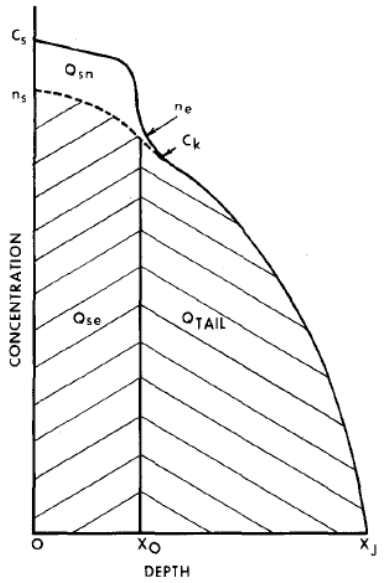

Fig. 2.20 *(left) A typical high concentration phosphorus diffusion profile in silicon (Fair, 1978)*

an electron-hole pair. These particles are driven out of the depletion region by the electric field. Thus, the concentration of electrons in the n-side and holes in the p-side increases enough to generate a potential difference between the two sides of the cell.

The diffusion profile of phosphorus in the emitter follows a typical trend, and two different regions can be defined: an highly-doped surface Q_{se}, a tail region Q_{TAIL} and the inactive doping Q_{sn}. The total phosphorus concentration can be calculated as $Q_T = Q_{se} + Q_{sn} + Q_{TAIL}$. The concentration profile for the total phopshorous concentration is:

$$Q_T = n_s^{3/2}\sqrt{\frac{t}{n_i}}\left\{(1+2{,}04\cdot 10^{-41}n_s^2)\sqrt{\frac{D_i^{=}n_s h}{n_i}}+\frac{1}{2}\sqrt{D_i^{-}\left[1+\exp\left(\frac{0{,}3eV}{KT}\right)\right]}\right\} \qquad (2.26)$$

while the active phosphorus profile can be calculated as:

$$Q_{el} = n_s^{3/2}\sqrt{\frac{t}{n_i}}\left\{\sqrt{\frac{D_i^{=}n_s h}{n_i}}+\frac{1}{2}\sqrt{D_i^{-}\left[1+\exp\left(\frac{0{,}3eV}{KT}\right)\right]}\right\} \qquad (2.27)$$

where D_i^{-} and $D_i^{=}$ are the diffusion coefficients for the vacancies in V^- and $V^=$ state, n_s the electrons concentration at the silicon surface and h=2 is the electric field enhancement factor. Q_{el} influences the sheet resistance and the emitter saturation current density, which should be lowered.

2.7.0.2 Surface passivation and Back-Surface Field

At the cell surfaces the continuity of the silicon lattice is broken. Thus, surface states generate in the band gap close to the surface, acting as traps and recombination sites for electrons and holes. In this way a difference between the excess of carriers, Δn if electrons are considered, generates between the surface and the bulk on the doped layer. A difference of concentration of

carriers originates a diffusion current, that leads to the definition of a new quantity, called "surface recombination velocity", S_R:

$$-\left[D_P \frac{\partial \Delta n}{\partial x}\right]_{surf} = -S_R \cdot \Delta n \tag{2.28}$$

A decreasing of the surface recombination velocity leads to the increment of the short-circuit current density J_{sc} and the open-circuit potential V_{oc}, and so the cell efficiency. To annihilate these surface states different ways are possible. One is to grow or deposit a passivating layer, such as SiO_2, Al_2O_3 or hydrated-SiN_x: the latter is effectively used for the front side of the cell, as well as for the anti-reflection properties.

Another way is to generate a low-high junction at the surface: this is also called "Back-Surface Field", and it is effectively used for the back contact of the cell. In fact, the electrons in the p-type base should be collected at the emitter, not recombined at the back surface. So, a thin layer at the back side is heavily doped with aluminium or boron, so a p^+-p junction is formed. This junction generates an electric field:

$$V_{b2} = \frac{KT}{q} ln\left(\frac{N_{A^+}}{N_A}\right) \tag{2.29}$$

which has the same direction of the field induced by the depletion region. In this way electrons are repulsed away from the back surface, and they do not recombine at the surface. The lowest values of the surface recombination velocity in crystalline silicon reported are 1-10 cm/s, while for most solar cells is around 100-1000 cm/s.

Most of the solar cells have an aluminium Back-Surface Field, since the production technique is well known and easy to manage. However, Al-BSF suffers of corrosion problems and the maximum doping concentration is around $3 \cdot 10^{18}$ atoms/cm^3. Boron BSF are also possible, and, even if the temperatures and the times for the treatment are higher, the dopant concentration is larger thanks to the greater solubility of boron in silicon.

2.7.1 Efficiency

From the first cell, invented in 1941, with an efficiency of 1%, the main aim of the photovoltaic research has been the improving of this value. In the beginning the first cells were made of n-type silicon, and an almost 15% efficiency was achieved in cells for the satellites. However, the

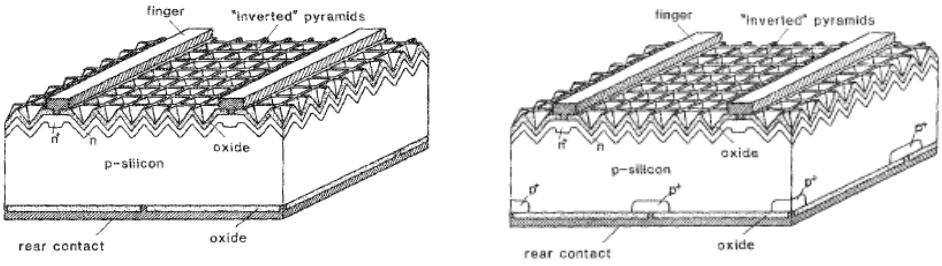

Fig. 2.21 *Schematic view of a (left) PERC (Wang, Zhao, & Green, 1990) and (right) PERL solar cell (Blakers, Wang, Milne, Zhao, & Green, 1989)*

space radiation hardness was too detrimental for the n-type cells, so p-type panels started their expansion, that brought them to be now the most largely diffuse type of solar cells. The same efficiency achieved for the n-type panels was reached by the p-type ones in the '80s. Nowadays, solar cells reached efficiencies of 23% and 25% for respectively PERC (Passivated Emitter and Rear Cell) and PERL (Passivated Emitter, Rear Locally diffused) monocrystalline p-type cells (Fig. 2.21). Industrial cells have an efficiency of 12÷18%.

Not all the solar radiation can be converted into electric energy. The main cause of the reduction of the efficiency is the Auger recombination: the photons with lower energy than 1,1 eV (Si band gap) cannot excite electrons in the cell, and for the others, the energy portion higher than this level is wasted, so approximately % of the sun spectrum is not used, Then there are other causes of efficiency losses, like radial recombination, optical losses, reflection of the incoming rays, electrical resistance losses, contamination, surface effects and material defects. This leads to a maximum theorical efficiency of 29%, while the practical maximum efficiency is around 26%. To calculate the efficiency the equation to be used is:

$$\eta = \frac{P_{max}}{P_{in}} = \frac{J_{sc} \cdot V_{oc} \cdot FF}{1000 \cdot C_r} \tag{2.30}$$

where FF is the fill factor, C_r is the relevant area of a reference cell (=0,015849 m^2), P_{max} is the maximum output power of the solar cell and P_{in} the incident optical power defined by the relevant area of the reference cell.

2.7.2 Production process

2.7.2.1 Wafers

Solidified single- and multi-crystalline ingots are shaped into a pseudo-square shape to increase the power density (in this way the planar surface of the panel is almost completely covered by the cells). Then the ingots are cut into wafers by some thin (160 μm of diameter) wires, arranged to form a web, as in Fig. 2.22. An abrasive slurry, made of fine-grained SiC particles, helps the cutting. To make the process easier the ingots are glued to a glass support and after the cutting they detach. The process parameters must be controlled in order to get homogeneous thickness. The main problem is that the wires have almost the same thickness as the wafers, so almost 50%

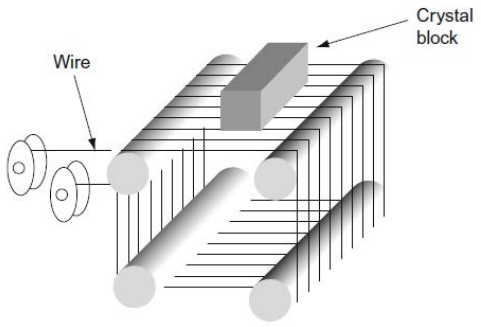

Fig. 2.22 *Principle of wire sawing (Ferrazza, 2012)*

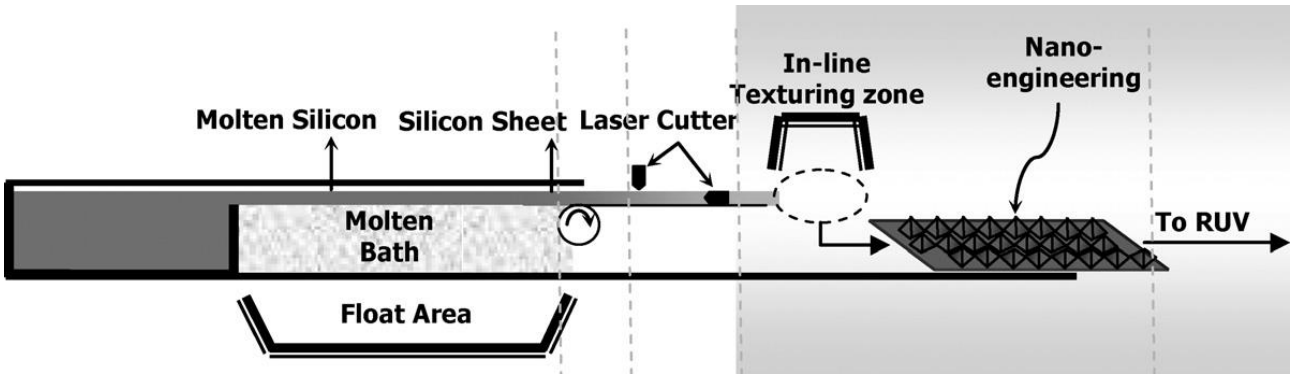

Fig. 2.23 *Float process for producing silicon wafers (Ranjan, Balaji, Panella, & Ydstie, 2011)*

of the silicon is lost and needs to be recycled. Also, if the wafer thickness is lowered, more wafers per ingot can be made, and so the productivity increases.

To solve the problem of the silicon losses, some continuous techniques have been improved. In the string ribbon process some high-temperature resistant wires are pulled through the silicon melt and the ribbons are then cut into strips; in the ribbon growth on substrate some silicon powder, subsequently melted, or already molten silicon are spread on a substrate. These techniques unfortunately lead to low-efficiency cells. An interesting technique is a modification of the Pilkington process, displayed in Fig. 2.23. Molten silicon is spread on the top of a more dense and immiscible liquid, and a single-crystalline silicon sheet of the desired thickness solidifies on the top of it.

2.7.2.2 Non-wafers

The most interesting non-wafer manufacturing of silicon for solar cells is the epitaxial growth on low-cost MG-Si substrates of very thin film of pure silicon. This technique has been developed to generate high efficiency cells, since the AM1.5 radiation is absorbed in a 30 μm layer. The epitaxial layer is generally generated by the reduction of dichlorosilane or trichlosilane at 1100°C, but it can be originated by a liquid Cu-Al-Si alloy: in the latter case, aluminium is helpful to get rid of the native SiO_2 layer, and with copper also of the impurities.

2.7.2.3 Process

The wafers are first inspected to check the presence of microcracks, the resistivity and the minority carrier lifetime.

The chemical texturization process is different for the case of single- and multi-crystalline wafers. For the monocrystalline a basic solution of potassium or sodium hydroxide is used, and the etching is done at 70-80°C for 20-30 minutes; for the multi-crystalline an acidic mixture of hydrofluoric and nitric acid is used, and the treatment is done for 1-2 minutes at 10-15°C, for a better control of the reaction, since it is highly exothermic. In the latter case great care must be taken of the evaporation of hazardous gases. The main reaction in the two cases are:

$$2KOH + Si + H_2O \rightarrow K_2SiO_3 + 2H_2 \quad (2.31)$$

$$3Si + 4HNO_3 + 12HF \rightarrow 3SiF_4 + 4NO + 8H_2O \quad (2.32)$$

Then, liquid phosphorus oxychloride $POCl_3$ and oxygen are released in a furnace on the wafers. Here a pre-deposition and the subsequent growth of the phosphorus silicate glass take place thanks to the following reactions:

$$4POCl_2 + 3O_2 \rightarrow 2P_2O_5 + 6Cl_2 \quad (2.33)$$

$$2P_2O_5 + 5Si \rightarrow 5SiO_2 + 4P \quad (2.34)$$

After a few tens of nanometers of phosphorus silicate glass is formed, the phosphorus oxychloride flow is stopped, and the temperature is increased to 820-850°C for one hour, so that the P diffusion into the silicon takes place. After it the phosphorus silicate glass is etched by hydrofluoric acid.

Then the hydrogenated silicon nitride anti-reflection layer is deposited on the top surface by plasma-enhanced chemical vapour deposition: the plasma partially dissociates silane and ammonia so that the deposition of silicon nitride can take place.

After that the silver and aluminium pastes are applied to the front and the rear cells to generate the electric contact. The formulation of the pastes has been improved in the years to enhance printability or to guarantee an appropriate BSF generation. A drying at 200°C is needed to remove the solvents in the pastes.

The final step is the contact firing. The wafers are treated at temperatures higher than 800°C in a furnace. In the silver paste the glass frits melt and etch the dielectric layer below. Then, silver and silicon mix in the liquid phase and generate the contact. In the aluminium paste the aluminium melts at temperatures higher than 660°C and reaches the silicon. Some silicon dissolves in the melt and so a Si-Al alloy is formed. As the temperature is lowered, the aluminium is trapped by the epitaxial regrowth of silicon, generating the back-surface field, and at the eutectic temperature (557°C) the remaining alloy solidifies.

2.7.2.4 Recycling

Recycling is rarely practiced industrially because low LCAs have been made in the recent years. However, it can be advantageous from the environmental point of view, for the preservation of rare metals, the use of less chemicals and the lower CO_2 emissions, but also from the economic point of view: recycling a single wafer can lead to an almost €15 saving, thanks to the recollection of precious materials as solar-grade silicon and silver. Lots of different factor can cause the degradation of the solar panels, such as UV rays, but also the snow, and so the efficiency decreasing. In the next years the number of end-of-life panels will start increasing significantly, so the recycling sector should be improved as well.

There are different ways to recycle solar modules. Before 2005 the main technique was to gently separate the cells from the glass, removing the EVA polymer by burning it in an FBR furnace at 480°C in nitrogen atmosphere. If the reclaimed cells were not broken, they could have been recycled in new panels.

After 2005, since the wafer thickness became too low to handle them in the recycling process without breaking them, a new method has been developed. It is based on reclaiming the cells

from the old modules, treating them with chemicals, and so obtaining new wafers. Firstly, the cells must be freed from the glass, then they are treated with different chemicals to collect the various metals (Ag, but also Cu, Al, Sn and Pb) and to remove the silicon nitride, the emitter and the BSF. Different techniques have been developed: Huang proposed an etching in 11,4% HNO_3 subsequent electrowinning at 0,3 V for 20000 seconds to recover pure silver and at -0,3 V for 24 hours for copper (the recovery rate are 74% and 83% respectively), then the cells are treated in 10% HF solution for 15 minutes at room temperature to remove the ARC and the Al contact, and finally they are treated in 3% NaOH solution at 50°C for 30 minutes to remove emitter and BSF (W.-H. Huang & Tao, 2015); Shin proposed an etching in 60% HNO_3 solution for 5 minutes at room temperature to remove Ag and Cu and in 45% KOH at 80°C for 8 minutes to remove Al, then an etching paste is applied to remove the nitride layer after an annealing treatment at 320-360°C and finally the doped layers are peeled off in a 0,05% KOH solution (Shin, Park, & Park, 2017).

Other recycling options are the component repair and the silicon recycling from the wafer cutting sludge. For the latter, the separation of silicon particles from the SiC abrasive particles is really difficult: it can be done by centrifugation, using toxic liquid and for long times though, or by applying a horizontal electric field.

2.8 ETCHING BY SODIUM HYDROXIDE

The reaction of silicon with sodium hydroxide is well known:

$$Si + 2NaOH + H_2O = Na_2SiO_3 + H_2 \tag{2.35}$$

However, it is difficult to find in the literature a comprehensive study on how sodium hydroxide etches multi-crystalline silicon surfaces. Indeed, it is well known that the etching is selective respect to the silicon planes: there can be difference of two orders of magnitude between the etching rate in the {110} planes and the one in the {111} planes, namely the one with lowest rate. The main reason is due to the energy difference of the surface states for different crystal orientations (Seidel, Csepregi, Hauberger, & Baumgärtel, 1990). The calculated etching rate for {100} planes is 120 μm/h, while for the {111} planes is 3 μm/h.

The etching rate can be determined from the treatment time and the thickness decreasing, which can be obtained by the weight decreasing:

$$\Delta d = \frac{\Delta m}{n \cdot \varrho_{Si} \cdot A} \tag{2.36}$$

where n is 1 if only one side is etched or 2 if both sides are. The main assumption under this equation is that the surface area remains the same after the etching, meaning that the lateral surface is much smaller than the faces. In a study by Akhter *et al.*, for {100} planes, the etching rate has been studied in function of the concentration of the solution (Akhter, Baig, & Mufti, 1989). It was possible to see that for low concentration the etching rate follows a logarithmic

trend, while for higher concentration it increases linearly as the concentration increases. The etching rate in function of temperature and concentration can be calculated for the two regions respectively as follows:

$$R(T) = [(4{,}0 \pm 3{,}8) \cdot 10^{10}] ln\left(\frac{M}{M_0(T)}\right) exp\left(-\frac{E}{KT}\right) \quad (2.37)$$

$$R(T) = [(8 \pm 3) \cdot 10^{8}] exp\left(-\frac{E}{KT}\right) \cdot M + B \quad (2.38)$$

where M is the molarity of the solution.

A study from Huang and Tao focused on the effect of concentration and temperature on the etching rate in crystalline solar cells (W.-H. Huang & Tao, 2015). They found that the solution providing at room temperature the best etching rate is the 3 wt.% NaOH solution: this concentration provides the right amount of both sodium hydroxide and water. To have an etching rate high enough for an industrial treatment, the etching should be done at 50°C with the 3% solution, giving a etch rate of 0,53 μm/min: with these conditions, from the resistivity measurements, it is possible to observe that after 30 minutes both the emitter and the back-surface field were effectively removed.

Another big problem of the sodium hydroxide etching is that it leaves a rough surface, that implies a lower minority carrier lifetime. This is due to the fact that the increasing of the surface area leads to additional dangling bonds, so more recombination centres.

2.8.0.1 Silicon oxide layer

Before the etching of silicon starts, the native silicon oxide layer must be removed. It is possible to observe that the etch rate for the first minutes of etching of silicon in sodium hydroxide is much lower than for the other part of the treatment (W.-H. Huang & Tao, 2015). Huang proposed that the reaction that happens is

$$SiO_2 + 2NaOH = Na_2SiO_3 + H_2O \quad (2.39)$$

This is proved by the fact that if the sodium hydroxide concentration in the solution is lowered, the incubation time before the silicon etching starts is longer, because less NaOH is present and so the silica dissolution is slower.

However, it has been studied that the silica dissolution in sodium hydroxide follows a more complex mechanism. In fact, since silica is a polycondensation polymer of silicic acid $Si(OH)_4$, the etching is more like a depolymerization reaction: the NaOH hydrolyse the Si-O-Si bonds and penetrates porous silica; then low molecular weight silicic acid diffuses out in the liquid phase.

2.8.1 Silicon nitride layer

While silicon oxide can be removed by the sodium hydroxide, this solution is not effective for the removal of the anti-reflection silicon nitride coating. So, other chemicals must be used for its removal, to make the emitter etching possible.

Phosphoric acid treatment is an investigated possibility, but for an effective removal the temperature should be brought at 180°C, making the process difficult. A fast way is to remove it with hydrofluoric acid: 15 minutes in a 10% HF solution are sufficient for an effective removal. The etching of the silicon nitride coating is a layer-by-layer process, where the nitrogen atoms must be protonated to ammonia, the surface Si-NH_2 bonds broken and the Si-N bonds replaced with Si-F bonds.

However, phosphoric and hydrofluoric acids are hazardous chemicals. A more environmentally-friendly process is to use tartaric or citric acid. The etching is a layer-by-layer process too, as in the case of HF. However, the etching rate is very low, 4.38 ± 0.02 nm/h at 80°C for a 20% tartaric acid solution: this means that to remove 75-80 nm of silicon nitride more than 18 hours at high temperatures are needed (Kropp & Lang, 2015).

3. GOALS

As it is possible to understand from the previous pages, sodium hydroxide solutions are frequently used for silicon etching for the purpose of the texturization, but not for the removal of the heavily doped layers in the cells, namely the back-surface field and the emitter. Moreover, some preliminary tests made as part of this research did not fit perfectly with the results from the work by Huang (Huang & Tao, 2015): the lowest concentrations were found to be less effective than the highest

One part of the ReSiELP project is about purifying the recovered silicon from the solar panels. One way to do it is to chemically etch the heavily doped layers, namely the emitter, n^+, and the back-surface field, p^+. Anyhow, in this way also part of the silicon is lost. The aim of the project is to optimize the treatment parameters to effectively remove these layers in multicrystalline cells, since this is the most common type. So, a more detailed research was needed to define the best parameters to get a good purification treatment with a high silicon recovery yield.

The goals of the present study are the following:

1. Make a model on the etching rate of silicon as function of the treatment parameters, namely temperature, solution concentration and time (defined as the etching time, i.e. the treatment time t minus the incubation time τ). This to be done in the back-side of the cell, in order to remove 5÷10 μm, so it is possible to study it by thickness and mass changes. The best combinations of these treatment parameters need to be verified by resistivity measurements, to check if the typical resistivity of the p-type base is reached, namely 0,5÷2 Ω·cm.
2. When the best combinations of parameters are found, they need to be optimized also for the emitter removal. The total process consists on etching the back side of the cell for a certain time, leaving the nitride layer on the front surface, in such a way that it protects the silicon from the etching, then removing the layer after this time and finishing the treatment etching both sides with the sodium hydroxide solution. So, the time at which the emitter layer is completely removed needs to be found.

These two goals are discussed respectively in Chapter 5 and Chapter 6, while the proposed treatment can be found in Chapter 7.

4. MATERIALS, EQUIPMENT & METHODS

4.1 MATERIALS

4.1.1 Silicon

The silicon samples used for the back-side experiments come from the FD_PDV_003 batch of cells. Those cells are CEA waste cells treated in the laboratories of Padova University with a sodium hydroxide and nitric acid treatment to remove Al and Ag. The composition of the cells is displayed in Tab 4.1. The original dimension of the cells is 155 x 155 mm, with a thickness around 180÷200 μm. The front side is covered with an 80 nm Si_3N_4 anti-reflection layer, so the colour is violet-blue, but some lines for the metallization are left uncovered. The silicon back side is grey and shiny. Cells can be either single-crystalline or multi-crystalline: in the latter case the crystal pattern is visible at human eye, and the dimension of the grains can be different between the grains of the same cells.

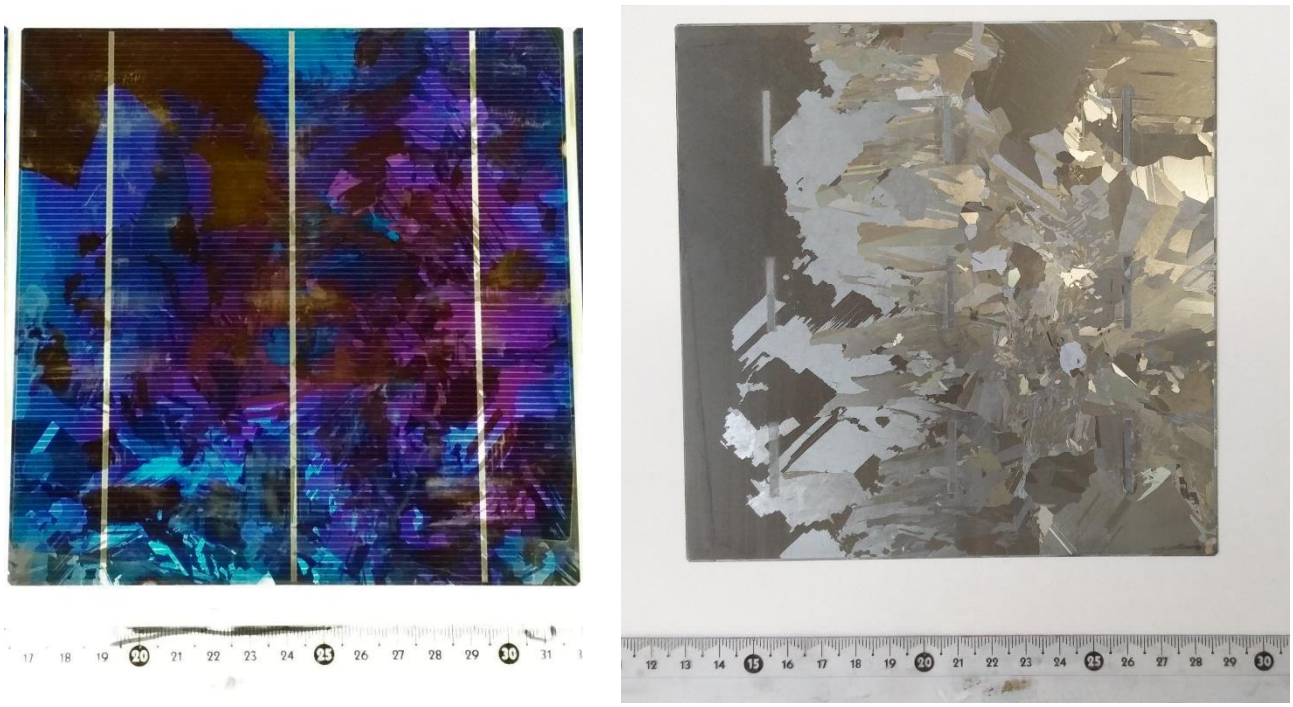

Fig. 4.1 *Front and back side of FD_PDV_003 cells*

The samples have been prepared by breaking the cells with a cutter into pieces with random size: the ones with dimensions around 20 x 20 mm have been collected and used for the experiment.

Fig. 4.2 *All the 252 samples for the back-side etching treatment (a 50 cm long ruler for scale)*

The silicon samples used for the front-side experiments come from CEA waste cells treated with sodium hydroxide and nitric acid.

Tab. 1 Concentration of elements in FDV_PDV_001 cells

Element	Concentration (ppm_w)
C	52
N	22
O	560*
B	0,51
Na	262
Mg	39
Al	216
Si	Matrix
P	1,1
K	0,8
Ca	61
Ti	285
Cr	0,25
Mn	0,32
Fe	1,8
Co	0,03
Ni	<0,05
Cu	79
Zn	2,1
Zr	0,9
Ag	72
Cd	<0,01
In	<0,01
Sn	15
Ba	0,05
Pb	32

4.1.2 Sodium hydroxide

The solutions for the sodium hydroxide treatment of the back side have been prepared with solid sodium hydroxide UN:1823, CAS:1310-73-2, sold by Azúr Chemicals Trading Ltd. It is presented as a white fine powder.

For the treatment of the front side solid sodium hydroxide UN:1823, CAS:1310-73-2 has been used too. It is presented as white chips with different sizes, between 1 and 5 mm.

4.1.3 Acetone

The acetone used through the whole back-side experiment is UN:1090 CAS:67-64-1, produced by MOLAR Chemicals Kft. in March 2018. It is 99,92% pure acetone, with a density of 0,790 g/cm^3. It is transparent. For the front side experiments it has been produced by Prodotti Chimici Riuniti s.r.l.

4.1.4 Polystyrene chips

Some S-shaped polystyrene chips, used for packaging, have been used through the whole experiment to glue the samples to the sample holders. Their weight is approximately 60÷80 mg, and their dimension are approximately 40 mm in length, 20 mm in width and 15 mm in height. The chips that have been used are presented in three different colours: white, green and pink.

4.2 EQUIPMENT

4.2.1 Analytical balance

The balance used to weight the samples before and after the etching treatments is the XS205 DU model by Mettler Toledo©. The calibration had been done by the producers in 2010, and the calibration adjustment has been made on 12th November 2018, before starting the measurements, with 10 g and 200 g reference weights. An electromagnet generates a force that balances the gravity force that acts on the sample. This balance can measure from 20 mg to 220 g, with an accuracy of 0,1 mg.

4.2.2 Micrometer

The electronic micrometer used to measure the thickness of the samples is produced by Horex®. The calibration had been done in 2016 by Bay Zoltán Nonprofit Ltd, Department of material characterization. The micrometer transforms a low distance in a rotation of a screw large enough to be read. This micrometer measures in the range between 0 mm and 25 mm with an accuracy of 0,001 mm.

4.2.3 Surface roughness tester

The portable surface roughness tester SJ-201 by Mitutoyo© has been used to measure the average roughness of the treated samples from the back-side experiment. The calibration had been done by S+V Engineering Kft. in 2014. The detector is a tip that moves along a line in the surface applying a constant force on it, and the instrument detects the height of the tip along this direction. The measurement range of this equipment is 360 μm, from -200 μm to +160 μm, with an accuracy of 0.02 μm.

4.2.4 Four-point sheet resistivity equipment

For the measurements of the p-side treated samples a four-point-probe equipment at Innolabor has been used. This method consists on placing four probes on a flat surface of the material, to let a current flow through the two outer electrodes and measure the potential difference between the two inner ones. A home-made prototype has been used, with a lab-scale power supply unit and high-precision voltammeter and ammeter. The in-line electrodes are applied on the sample with the use of springs, so that a static pressure is applied during measurement. The electrode distance is 1,27 mm. The measurements have been done at 25°C ± 1°C, with an illumination less than 100 lux.

For the n-side treated samples electric measurements the apparatus is a four-point-probe equipment with square-arranged spring-loaded golden tips. The system is also provided with a remote control, a sourcemeter and a switch matrix. For the Hall measurements, a 0,625 T magnet is used.

4.2.5 Profilometer

The profilometer used is the model P-10 by Tencor®. The sample is scanned along one horizontal direction by a tip, which applies a certain force on the sample, and the movement in the vertical direction is measured. The parameters used for the scan are a scan speed of 20 μm/s, a sampling rate of 50 Hz, a vertical range of 131 μm with a resolution of 0,357 Å.

4.2.6 P/N tester

For the measuring of the type of semiconductor the PN-100 pen by Semilab is used. This is a non-contact testing where chopped light excites the sample, generating electron/holes pairs, and a probe measures the difference of the surface potential barrier: the LED display turns red if the sample is p-type, green if n-type. The measurement time is 0,5 seconds, the excitation depth is ~3 μm, and the resistivity range of the measurable samples is between 20 mΩ·cm and 3000 Ω·cm.

4.3 METHOD

4.3.1 Back-side etching

To have results that are representative of the dissolution kinetics of the silicon surface, the etching treatment, and so the dissolution, must be done on just one side. To accomplish this, since silicon nitride is not removed by the sodium hydroxide, and so it acts as a "natural" barrier for the underlying silicon, the etching is done on the back side. However, the sample must be glued on the sample holder: either way, the sample can uplift due to hydrogen bubbles generation because of the NaOH reaction with silicon on the metallization lines on the front side. The sample holder also keeps the sample horizontal, so the originated hydrogen bubbles do not collide with each other on the surface: this would cause the early detachment of some of them.

The etching kinetics is studied in relation of different combination of temperature, time and concentration. Seven different temperatures (30, 40, 50, 60, 70, 80 and 90°C), three different etching times (15, 30 and 60 min) and six different NaOH concentrations (2,5, 5, 10, 15, 20 and 25 wt. %) are tested: for each combination of these parameters, two replicate samples are treated.

The etching kinetic is studied by the thickness variation and the mass lost, while the incubation time of etching due to the oxide layer by the time at which the bubbling starts and at which almost half of the surface is covered by bubbles. At the end, the sheet resistivity measurement is done to state if the silicon reached the levels for solar-grade silicon (0,5÷2 Ω·cm).

4.3.1.1 Procedure 1 (30÷70°C)

Before the experiment all the silicon samples are weighed, and their thickness is measured in three different points on the longest direction in the samples, in a way that they are far from each other.

Six silicon samples are glued with grey side up on six different sample holders. The gluing is achieved by dissolving the PS chips with some acetone and then pushing the silicon on the mixture. The sample holders are made of a steel plate, a steel support and an epoxy disk, glued together by superglue. Then the sample holders are put in the desiccator oven at 90°C for some minutes, to let the acetone evaporate. The free surface is cleaned with acetone with the help of a cotton swab, to remove the excess styrene, and then each sample holder is glued to the bottom of a 100 mL polypropylene beaker with some Blu-Tack®.

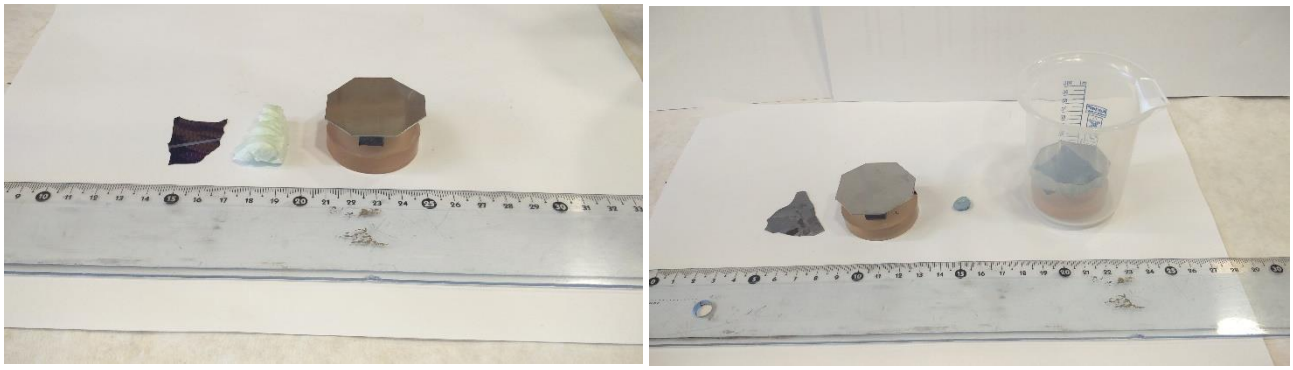

Fig. 4.3 *Sample, PS chip and sample holder for gluing the sample on the holder and sample, sample holder and Blu-Tack® to glue the ensure horizontal position*

Fig. 4.4 *(left) Heating of the different solutions (in this case at 50°C); (right) Etching treatment on the samples (in this case at 40°C for 1 hour)*

A large and short metallic pot is filled with water for its half and put on a heater. Six 100 mL polypropylene beakers filled with 70 mL of the NaOH solutions, plus another beaker filled with distilled water, are put inside the water, close to the edges of the pot, approximately all at the same distance from the center. The beakers are covered with some parafilm to avoid solvent evaporation and consequent massive concentration of the solution. Magnetic stirring is ensured in the pot to homogenize the temperature as much as possible. The temperature is measured with a digital thermometer with 0,1°C sensitivity inside the beaker with distilled water.

When the solution has reached the desired temperature, it is poured inside the beakers which contain the samples. The first bubble time and the time at which approximately half of the Si surface is covered by bubbles are measured by visual examination. When the treatment time is elapsed, the samples are removed from the solution and immediately rinsed in distilled water. Then the samples are carefully removed from the sample holder by dissolving it with acetone and rinsed again with distilled water. Then they are put in the desiccator to dry.

Finally, the dried samples are weighed again, and the thickness is measured in three different points as before. Then, the average roughness and the resistivity of the most interesting samples is measured.

4.3.2 Procedure 2 (80÷90°C)

The silicon samples are measured before the treatment and six of them are glued in six different steel plates. The gluing is achieved by dissolving the PS chips with some acetone and then pushing the silicon on the mixture. Then the plates are put in the desiccator oven at 90°C for some minutes, to let the acetone evaporate. The free surface is cleaned with acetone with the help of a cotton swab, to remove the excess styrene, and then each steel plate is glued to a ceramic disk for desiccators with some Blu-Tack®.

In a steel pot 700 mL of solution is heated to the treatment temperature, with a glass lid which is put on it to avoid solvent evaporation and consequent massive concentration of the solution. The temperature is measured with a digital thermometer, with 0,1°C sensitivity, that is in contact with the solution through a hole in the lid.

When the solution has reached the desired temperature, the disk is immersed inside the pot. The first bubble time and the time at which approximately half of the Si surface is covered by bubbles are measured by visual examination. When the treatment time is elapsed, one pair of samples is removed from the solution and immediately rinsed in distilled water, while the other samples continue their treatment. Then the samples are carefully removed from the sample holder by dissolving it with acetone and rinsed again with distilled water. Then they are put in the desiccator to dry.

Finally, the dried samples are weighed again, and the thickness is measured in three different points as before. Then, the average roughness and the resistivity is measured.

4.3.2 Front-side etching

After the study of the etching kinetics on the back side, it is done also on the front side, under the silicon nitride layer. For a technological reason, the treatment is done at the best concentration found in the back-side experiment, and at high temperature, so that the kinetic is faster and the incubation time is short. Since in this case the phosphorus-doped layer is much thinner than the p^+-doped layer on the back surface, the etching time must be lower.

The etching kinetics is studied in relation of different combination of temperature and time. Three different temperatures (60, 70 and 80°C) and five different etching times (1, 2, 4, 8 and 16 min) are tested: for each combination of these parameters, two replicate samples are treated.

The etching kinetic is studied by the thickness variation. The mass is not of interest, since not all the front surface is treated: it is only measured for the samples whose resistivity is measured. At the end, the sheet resistivity measurement is done to state if the silicon reached the levels for solar-grade silicon (0,5÷2 Ω·cm).

4.3.2.1 Procedure

One piece of masking tape is put on the silicon samples so that half of the surface is covered. Then some temperature-resistant paint is spread on the free surface and it is let drying. The tape is removed and the samples are immersed in a 10% HF solution for 15 minutes, so that the silicon nitride layer is removed from the free surface. The samples are rinsed with distilled water, the paint is removed with some nitro thinner and the samples are rinsed again. Six samples are glued on a steel plate: the gluing is achieved by dissolving the PS chips with some acetone and then

Fig. 4.5 *(from left to right) As-received sample; half of the surface is covered with a high-temperature resistant paint; sample treated in 10% HF solution for 15 minutes; paint removed with nitro thinner; treated sample in sodium hydroxide solution.*

pushing the silicon on the mixture. Then the plates are put in the desiccator oven at 90°C for some minutes, to let the acetone evaporate. The free surface is cleaned with acetone with the help of a cotton swab, to remove the excess styrene.

In a steel pot 500 mL of 20 wt. % solution is heated to the treatment temperature. The temperature is measured with an analogic thermometer with 1°C sensitivity. No lid is placed on the pot since the treatment time is very short, so the solvent evaporation is negligible.

When the solution has reached the desired temperature, the plate is immersed inside the pot. The first bubble time and the time at which approximately half of the Si surface is covered by bubbles are checked if they agree with the previous results by visual examination. When the treatment time is elapsed, one pair of samples is removed from the plate and immediately rinsed in distilled water, while the other samples continue their treatment. Then the glue is carefully removed from the samples by dissolving it with acetone and they are rinsed again with distilled water. Then they are put in the desiccator to dry.

Finally, the profile is measured with the profilometer in three different points straddling the border between the silicon nitride and the treated area. After that, the treatments with the five most promising conditions are re-done on the whole surface of five new pairs of samples. Their initial and final mass is measured and their final sheet resistivity with the four-point probe equipment. Then the samples are sent to CEA for the p/n tester measurements.

5. BACK-SIDE ETCHING

5.1 PRELIMINARY RESULTS

A total number of 252 samples have been treated with different combinations of nine different temperatures (30, 40, 50, 60, 70, 80 and 90°C), six different concentrations of the sodium hydroxide solution (2,5, 5, 10, 15, 20 and 25 wt. %) and three different times (15, 30 and 60 minutes), two replicates for each combination. The dry mass m of the samples has been measured before and after the treatment, and their thickness d in three different points too. Average roughness R_a for the most interesting cases and resistivity ϱ have been measured after the etching treatment. The time when the first bubbles appear τ_{in} and when almost half of the surface of the sample is covered by bubbles $\tau_{50\%}$ has been taken during the experiments.

The samples have been treated with their p-type side upside and the n-type side glued on the sample holder, so that the dissolution on the latter side is inhibited. Hydrogen bubbles were formed during the experiment, according to the reaction:

$$Si + 2NaOH + H_2O = Na_2SiO_3 + H_2 \tag{5.1}$$

Since the solution wets well the Si surface, these bubbles are close to spherical and detach from the surface due to the buoyant force when their size is more or less between 0,5 and 1 mm. For this reason, the sample holder has been kept strictly horizontally, so that the uprising bubbles did not interfere with the detaching of the others.

The results can be seen in Tab. A.1 in appendix A. The area of the sample was needed for the calculation of the resistivity, and it has been obtained knowing the initial mass m in grams, the average initial thickness d in microns and the density of silicon (at room temperature ρ=2,329 g/cm^3), supposing that the etching in the lateral sides of the samples is negligible and that the surface are does not change after the treatment:

$$A = \frac{10^{-6}}{\varrho}\frac{m}{d} \tag{5.2}$$

The relative change in mass and thickness are shown for all the samples in Fig. 5.1. Each dot represents one of the 252 samples treated. The thickness and mass changes are defined as:

$$\Delta m_{\%} = \frac{m_{fin} - m_{in}}{m_{in}} \cdot 100 \qquad \Delta d_{\%} = \frac{d_{fin} - d_{in}}{d_{in}} \cdot 100 \tag{5.3}$$

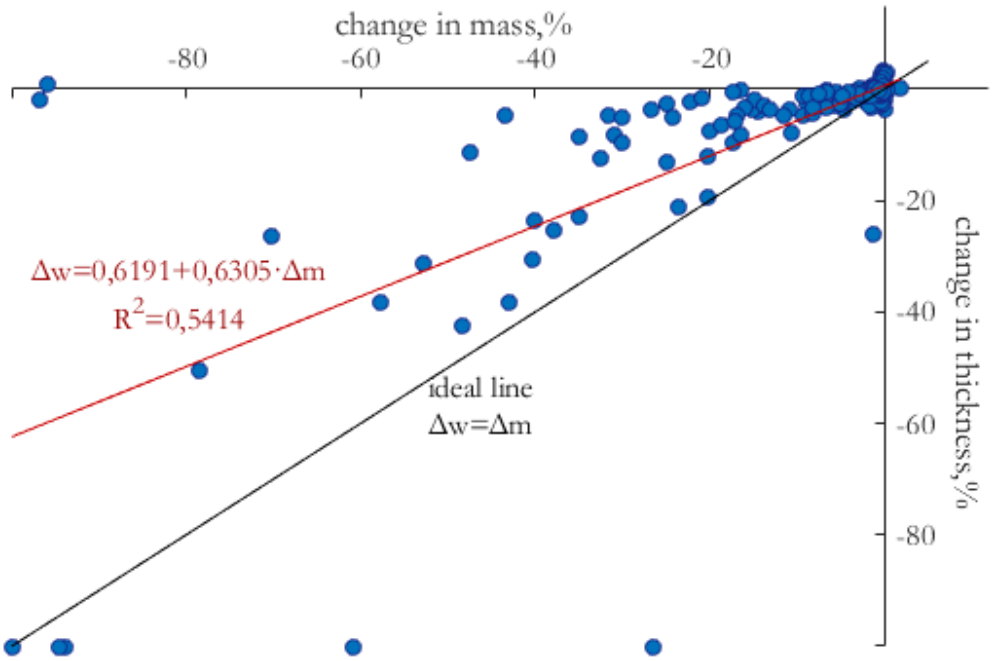

Fig. 5.1 *Relative change of thickness vs relative change of mass of Si for the 252 samples*

It is possible to observe that there is a large scatter of data and no good correlation between changes in measured mass and changes in measured thickness, since the slope is 0,6305 and R^2=0.5414. This can be related to different effects:

- At low temperatures the thickness and mass change are very small. However, the mass measurements are more sensitive to changes respect to the thickness measurements, so this can affect the linearity of the results.
- At low temperatures some positive changes for mass have been calculated. This is probably due to the formation of silicates on the surface of the sample. Sodium silicates are slightly soluble or almost insoluble in cold water (Budavari, S. (ed.). The Merck Index - Encyclopedia of Chemicals, Drugs and Biologicals, 1989., p. 1368), so probably also in the sodium hydroxide solutions at lower temperatures.
- However, also at higher temperatures the linear correlation is not good. The reason should be identified in the fact that sodium hydroxide etching is crystallographic-orientation selective. It is well known that etching in the {100} and {110} planes is 40 times faster than in the {111} planes. From a photoluminescence imaging it is possible to determine the orientation of each crystal in the mc-Si wafers: due to the nature of the solidification process, it is possible to observe that the crystals do not perfectly fit in one of the defined plane orientations, but, even showing different colours, they mostly have an intermediate orientation (Sio, Xiong, Trupke, & Macdonald, 2012). This leads to different etching rates between the different grains: the ones closer to the {111} configuration etch slower, but the difference is not so large. When the thickness is measured, the micrometer tip's diameter is 5 mm, which is larger than the dimension of the smallest grains in the mc-Si. So, the thickness measured is the one of the less-etched grains, while the mass measured is an average through the whole sample.

So, a separate analysis of the thickness and the mass change and a study of only the single-crystalline samples are needed to check if the linear correlation is improved. Fig. 5.2 shows the modification of the linear correlation for only the single-crystalline samples treated. For this case the line fits much better the experimental values (R^2=0.9620), and the slope is closer to 1 than in the previous case. However, the real behaviour is still far from the ideal case.

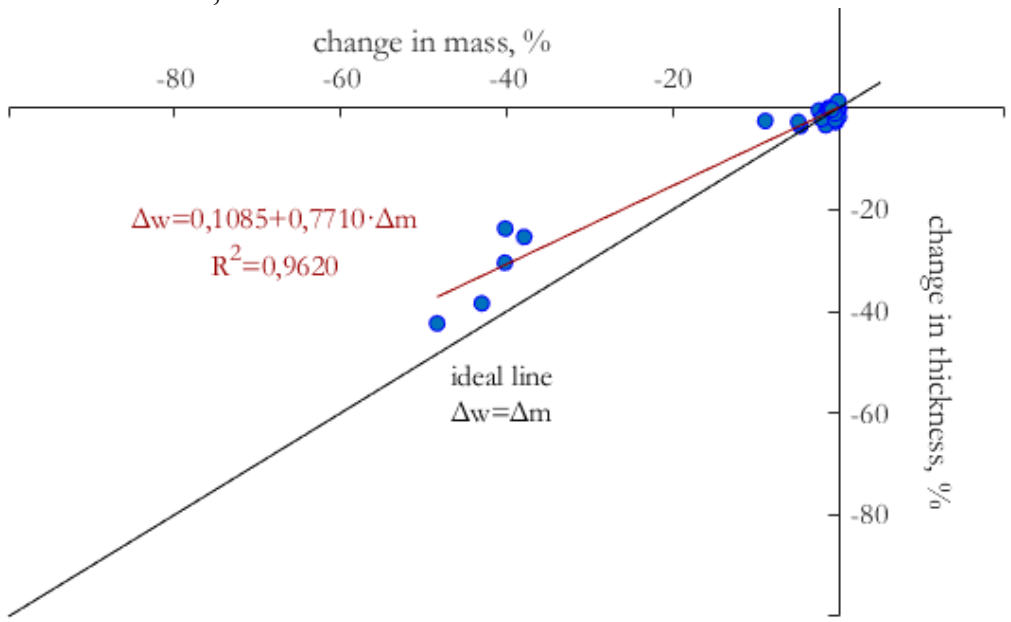

Fig. 5.2 *Relative change of thickness vs relative change of mass of Si for the 34 single-crystalline samples*

The monocrystalline samples show that the main cause of deviation from the linear behaviour when the total number of the samples were considered is the fact that for the multicrystalline samples the etching is selective on the plane orientation. However, the differences from the ideal case should be identified with other causes, such as the different sensitivity of the mass and thickness measurements.

5.1.1 Evaluation of the thickness change

The main aim of the project is to remove the contaminated surface layer of the wafer, rich in aluminium. So, the primary interest is to analyse the thickness change. The results are presented in Tab. 5.1. Here, for each combination of temperature, time and concentration, the thickness change in the two parallel samples is compared: three different signs can be found in the table if the sign change is negative (-) or positive (+) in both samples or if the two parallels have different signs, or one of them appears to be zero with the accuracy of 0,1 μm (?). In each cell the signs are written for the three different times, starting from the shortest one, separated by the oblique stroke.

The optimum cells in Tab. 5.1 are the green ones. These ones have the combination "-/-/-", meaning that the thickness decreased in all the six samples treated with that combination of temperature and concentration. Also the yellow ones are pretty good, although not perfect: the combination "?/-/-" means that in the first 15 minutes the result was undefined, while for the

Tab. 5.1 Evaluation of Δd after the etching treatment

wt. % NaOH °C	2,5	5	10	15	20	25
30	-/?/+	-/?/?	?/ ?/+	-/-/+	-/?/-	-/-/?
40	+/+/+	+/?/?	?/+/-	-/?/-	?/ ?/-	?/ ?/-
50	?/ ?/-	?/-/ ?	?/-/ ?	?/-/-	?/-/-	?/-/-
60	?/-/ ?	?/ ?/-	+/?/?	-/-/-	?/-/-	-/-/-
70	?/ ?/ ?	?/+/-	-/-/?	?/-/-	?/-/-	-/-/-
80	-/-/-	-/-/-	-/-/-	?/-/-	-/-/-	-/-/-
90	+/-/-	?/-/-	-/-/-	-/-/-	-/-/-	-/-/-

longer times a decrement of the thickness can be identified. It is possible to observe that all the best results are placed in the bottom right corner of Tab. 5.1: thus, the best conditions for the treatment are temperatures higher than 50°C and NaOH contents between 15 and 25 wt. %.

5.1.2 Evaluation of the mass change

Since the scattering of the values for thickness is very high, the study should focus on the mass change. Tab. 5.2, such as Tab. 5.1, shows the results for these measurements. Thanks to the special form that the green cells assume, it is possible to prove that the best NaOH concentration for the etching treatment is probably around 20 wt. %. The temperature where the green cells are more is 70°C.

Tab. 5.2 Evaluation of Δm after the etching treatment

wt. % NaOH °C	2,5	5	10	15	20	25
30	?/-/ ?	0/?/?	-/?/?	-/-/?	-/?/-	-/?/-
40	-/?/?	-/+/?	-/?/-	-/?/-	-/-/-	?/-/-
50	?/ ?/-	?/-/-	-/-/-	-/-/-	-/-/-	?/-/-
60	?/ ?/-	-/-/-	-/-/-	-/-/-	-/-/-	-/-/-
70	-/-/-	-/-/-	-/-/-	-/-/-	-/-/-	-/-/-
80	-/?/?	-/-/-	-/-/-	?/-/-	-/-/-	-/-/-
90	+/-/-	?/-/-	-/-/-	-/-/-	-/-/-	-/-/-

5.2 SILICON OXIDE LAYER REMOVAL

The real etching of silicon can be identified by the appearance of bubbles, as shown in Fig. 5.3. Those bubbles are hydrogen bubbles, generated as a product of reaction 5.1. However, these bubbles do not appear as soon as the sample is introduced in the etching solution: an incubation

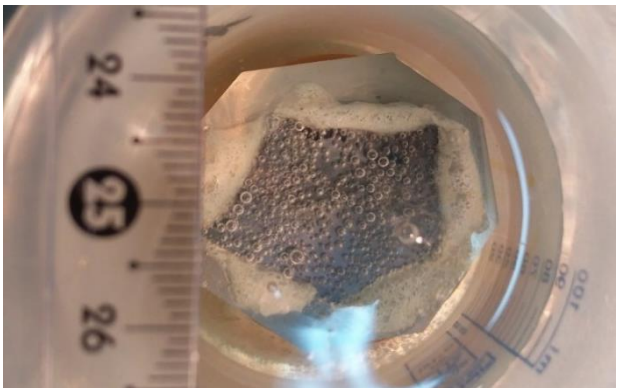

Fig. 5.3 *Example of hydrogen bubbles covering the surface of the silicon sample*

time for the etching process can thus be observed. During this time, the native silicon oxide layer is dissolved by the sodium hydroxide, and when it is completely removed, the silicon removal starts. This process is described by the reaction:

$$SiO_2 + 2NaOH = Na_2SiO_3 + H_2O \tag{5.4}$$

To keep under control this phenomenon, two different times have been measured: the "first bubble time" τ_{in}, namely the time since the starting of the experiment when the first bubbles are visible, and the "50% surface covered time" $\tau_{50\%}$, namely the time since the starting of the experiment when almost half of the surface is covered by bubbles.

From the table A.1 in Appendix A, at pages A-23 and A-24, it is possible to check these measured times. At low temperatures and solution concentrations the treatment time was not long enough to completely dissolve the silica layer in most cases. In few other cases, at higher temperatures but mostly for the low concentration solutions, the bubbling started, but the bubbles never covered half of the surface. However, as temperature increases, it is possible to see that the time decreases, from more than one hour to less than ten seconds.

5.2.1 Modelling

Since the incubation time is independent on the treatment time, except for the fact that in some cases no bubbles are visible during the whole experiment, for each combination of temperature and composition an average τ_{in} and $\tau_{50\%}$ have been calculated. When the incubation time was longer than the treatment time, that value was not considered. Those average incubation times are reported in Tab. 5.3.

It is evident also from this table that as temperature increases, the incubation time decreases. So, it is interesting to check how this parameter changes as function of temperature. In Fig. 5.4 it is possible to observe the trend of the incubation times as function of the temperature. The dots represent the real data, and they appear to follow an exponential trend.

So, the data have been fitted by an exponential model:

$$\tau(T) = a \cdot e^{b \cdot T} \tag{5.5}$$

where the temperature is in °C and the incubation time in seconds. The a and b parameters are listed in Tab. 5.4.

Tab. 5.3 Average incubation time

	30°C		40°C		50°C		60°C
	τ_{in} [s]	$\tau_{50\%}$ [s]	τ_{in} [s]	$\tau_{50\%}$ [s]	τ_{in} [s]	$\tau_{50\%}$ [s]	τ_{in} [s]
2,5 wt.%					1234	1240,667	732,6667
5 wt.%					1707	1428	521,6
10 wt.%	1701	1814	1480	1492	414	488,5	172,5
15 wt.%	743	1249	673,5	754	178,1667	237,8333	77,16667
20 wt.%	950,6667	1040	382,5	454,1667	169	211,8333	57,66667
25 wt.%	584,8	754,6	454,5	606,1667	124,8333	153,5	62,66667

	60°C	70°C		80°C		90°C	
	$\tau_{50\%}$ [s]	τ_{in} [s]	$\tau_{50\%}$ [s]	τ_{in} [s]	$\tau_{50\%}$ [s]	τ_{in} [s]	$\tau_{50\%}$ [s]
2,5 wt.%	1054	377,2	293	87,33333	141,8	45,16667	
5 wt.%	621,75	306,6667	437	62	98,66667	22,83333	75,5
10 wt.%	278,6667	101,8333	202,1667	30,66667	45,16667	18,16667	25
15 wt.%	117,6667	43,66667	67,16667	24,83333	38,5	9,666667	11
20 wt.%	86,33333	39,66667	49,16667	23,33333	34,83333	13,5	14,6666667
25 wt.%	84	31	38,5	14,5	21,5	11	12

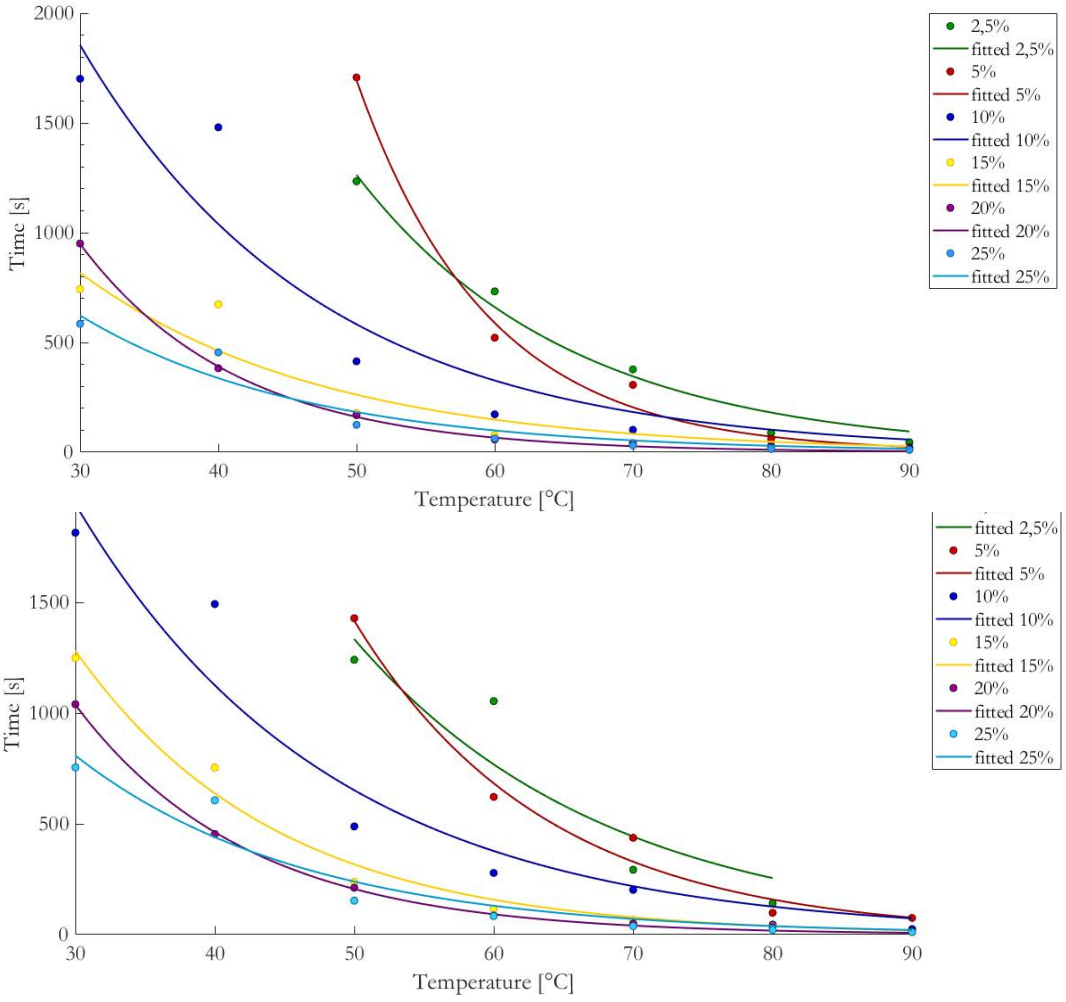

Fig. 5.4 *(above) first bubble time versus temperature plot; (below) 50% surface covered time versus temperature plot*

Tab. 5.4 Model parameters for temperature

		2,5%	5%	10%	15%	20%	25%
τ_{in}	**a**	$3{,}226 \cdot 10^4$	$3{,}353 \cdot 10^5$	$1{,}053 \cdot 10^4$	4492	$1{,}358 \cdot 10^4$	3912
	b	-0,0648	-0,1057	-0,0579	-0,05683	-0,0887	-0,0613
	$\mathbf{R^2}$	0,9815	0,9921	0,9088	0,8940	0,9992	0,9384
$\tau_{50\%}$	**a**	$2{,}1 \cdot 10^4$	$5{,}435 \cdot 10^4$	9999	$1{,}04 \cdot 10^4$	$1{,}17 \cdot 10^4$	5007
	b	-0,0551	-0,07294	-0,0546	-0,0698	-0,0808	-0,0608
	$\mathbf{R^2}$	0,8596	0,9843	0,9381	0,9829	0,9994	0,9274

These parameters "a", as they are, does not seem to follow any particular trend as function of the concentration, but they vary widely, in some cases also orders of magnitude, between each other. However, parameters "b" appear to be almost constant. For this reason, it is possible to correct the model keeping constant b equal to the average of the results in the table. The average value of coefficient b in both cases and updated parameters "a" and R^2 are shown in Tab. 5.5.

Tab. 5.5 Updated model parameters for temperature

		2,5 wt.%	5 wt.%	10 wt.%	15 wt.%	20 wt.%	25 wt.%
τ_{in}	**b**	-0,0725					
	a	$3{,}225 \cdot 10^4$	$3{,}853 \cdot 10^4$	$1{,}331 \cdot 10^4$	5885	6138	4410
	$\mathbf{R^2}$	0,9815	0,9194	0,9030	0,8862	0,9691	0,9370
$\tau_{50\%}$	**b**	-0,0657					
	a	$3{,}702 \cdot 10^4$	$3{,}691 \cdot 10^4$	$1{,}456 \cdot 10^4$	9064	7084	5909
	$\mathbf{R^2}$	0,8405	0,9791	0,9222	0,9815	0,9855	0,9248

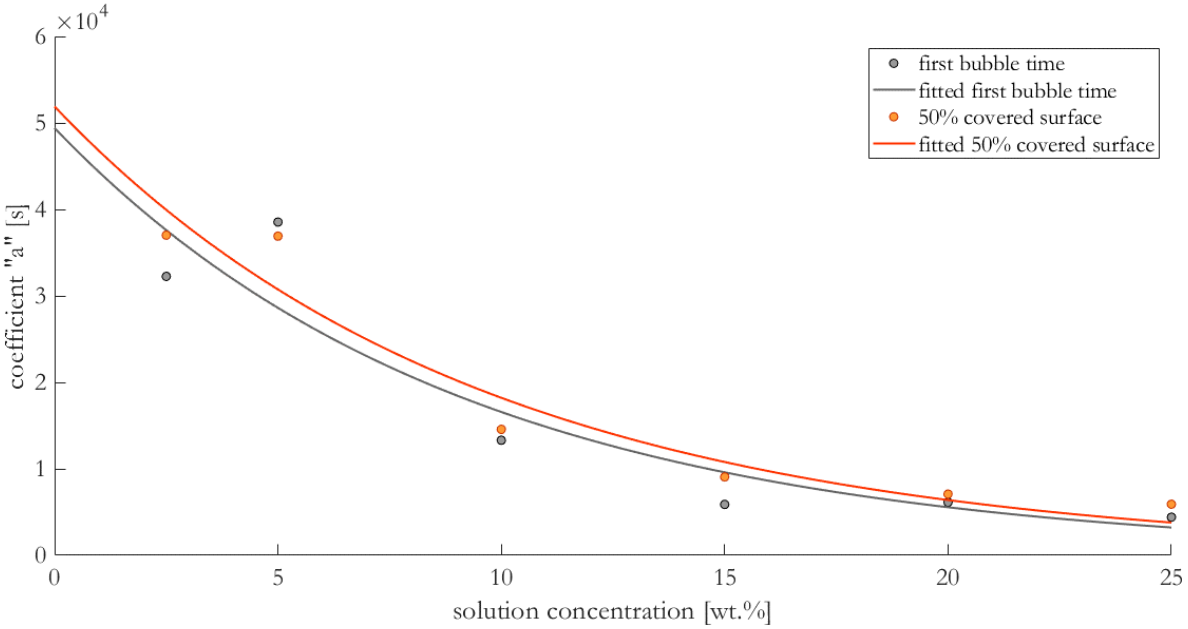

Fig. 5.5 *Coefficient "a" versus concentration for the first bubble time and 50% covered surface models*

As it is possible to see from Fig. 5.5, the coloured marks, that represent the data from the table, appear to follow an exponential trend as function of the concentration of the solution. For this reason, an exponential model can be applied to fit the data. The parameters of the model are listed in Tab. 5.6 with the R^2 value.

$$a(c) = a' \cdot e^{b' \cdot c} \tag{5.6}$$

Tab. 5.6 Model parameters for temperature

	a'	b'	R^2
τ_{in}	$4{,}94 \cdot 10^4$	-0,1092	0,8620
$\tau_{50\%}$	$5{,}189 \cdot 10^4$	-0,1047	0,9369

5.2.2 Discussion

In Fig. 5.4 the dashed lines represent the exponential equation that fits the data. It is possible to see that they fit well the experimental data both visually and from the R^2 values, which are more than 0,9, or close to it, for all the cases. Also, the coefficient a from the first model is pretty well fitted by the second one, even if the R^2 values are a bit lower.

From this model it is possible to state that the incubation time decreases as the temperature decreases, so higher temperatures favour the etching treatment, decreasing the time during that the silicon does not effectively react with the sodium hydroxide. Moreover, as the concentration increases, the pre-exponential factor decreases, thus decreasing all the exponential curve and so the incubation time. This is in accord to the statement by Huang that, as the NaOH concentration increases, more reactant is available for the silicon oxide dissolving, thus speeding up the process (Huang & Tao, 2015).

Thus, the final equation to calculate the incubation time as function of temperature and concentration is:

$$\tau_{in}(T, c) = 4{,}94 \cdot 10^4 \cdot e^{-0{,}1092 \cdot c} \cdot e^{-0{,}0725 \cdot T} \tag{5.7}$$

$$\tau_{50\%}(T, c) = 5{,}189 \cdot 10^4 \cdot e^{-0{,}1047 \cdot c} \cdot e^{-0{,}0657 \cdot T} \tag{5.8}$$

It is possible to observe that the parameters for the two incubation times are quite similar with each other. This mean that the first bubble time and the 50% covered surface time do not differ too much. This is generally true, and the cases when the sample started bubbling but it never reached half of the surface covered are limited. This similarity between the parameters also means that the trend is similar for the two incubation times, and this is proved if the two graphs in Fig. 5.4 are superimposed.

The graphs in Fig. 5.6 show that the models cannot calculate perfectly the incubation times, because the slope is not so close to the ideal line, namely the bisector of the quadrant (calculated τ=measured τ). This is because the incubation times, especially at low temperatures and concen-

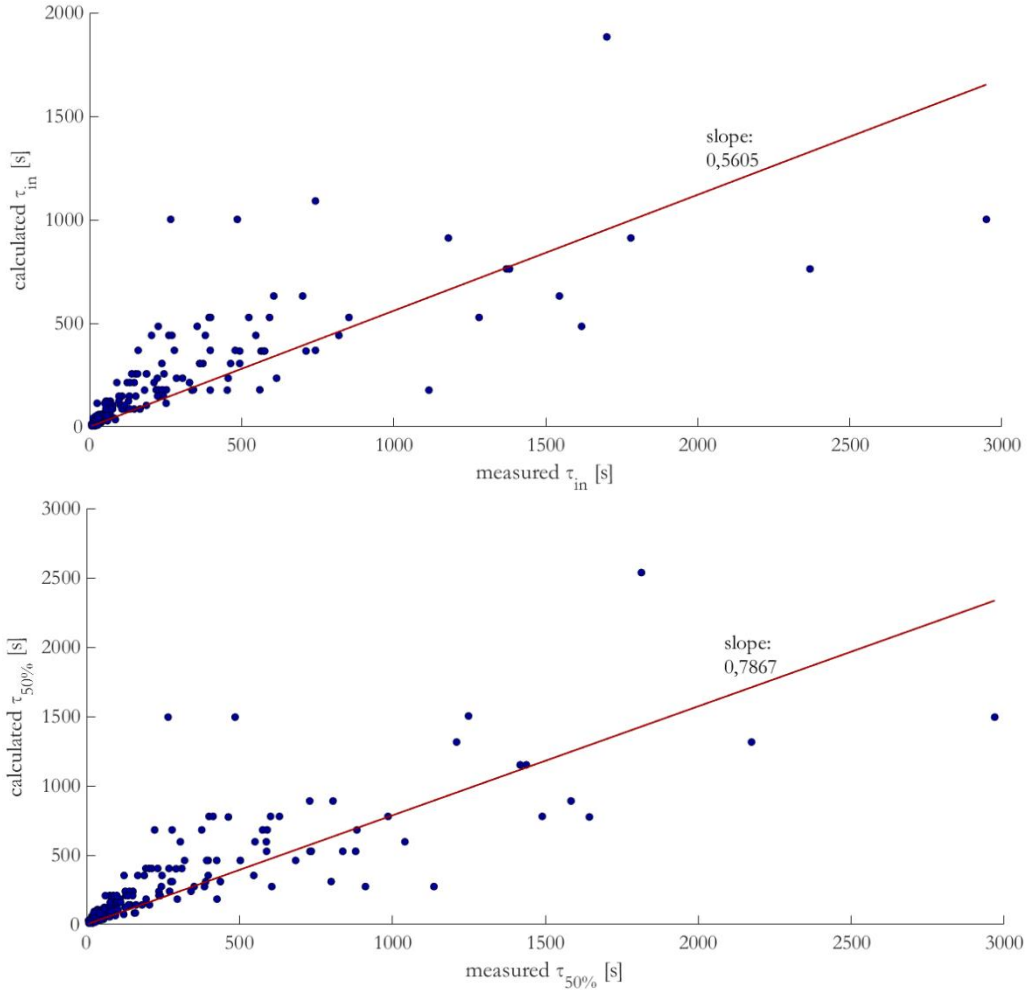

Fig. 5.6 *(above) calculated versus measured initial bubble time; (below) calculated versus measured 50% covered surface time*

trations, differ a lot between each other for the same combination of parameters, and it is confirmed by the large scattering of the data and the low values of R^2 (0,5553 and 0,6037 respectively). However, the model for $\tau_{50\%}$ fits pretty well the experimental data, even if it is not perfect. If the average incubation times are considered, the fitting quality increase considerably and the slopes become respectively 0,7646 and 1,0405.

5.3 SILICON ETCHING

Once the native silicon oxide layer is dissolved in the solution, the etching of the silicon can start. This phenomenon is described by the reaction 5.1, and its beginning can be recognised by the formation of small hydrogen bubbles on the surface of the sample, as it is possible to observe from Fig. 5.3. When a bubble is generated is a fraction of millimetre big, and it increases its size until it reaches almost one millimetre, when it detaches from the surface sample to reach the surface of the solution.

The reaction proceeds until all the sample is dissolved in the solution or until the treatment is stopped. The aim of the study is to etch the silicon to remove a precise layer, corresponding to the back-surface field in this case (or the emitter in the front side). So, the thickness removal rate is studied, in order to identify which are the parameters for an optimal treatment, which combines

short times, low energy requirements and good reproducibility. In fact, the aim is to scale up this technology to industrial levels, and, for this reason, all the samples treated should be etched to the desired level, without unnecessary silicon losses.

To identify the best combinations for the treatment parameters, the thickness reduction rates have been studied for different temperatures as function of the concentration of the solution.

5.3.1 Modelling

During the experiments both initial and final masses and initial and final thicknesses have been calculated. However, it has already been stated that there is no good correlation between these calculated values, and that the mass measurements are better than the thickness measurement because of the higher sensitivity of the equipment and the lower sensitivity to anisotropic etching.

A study of the measured mass variation as function of the treatment time is preferable to the measured thickness variation, but it suffers the problem that it is not directly related to the thickness of the back-surface field. Let's suppose to take two different cells, one 180 μm thick and the other 200 μm thick, and suppose that the back-surface field is in both cases 10 μm thick. If a combination of parameters is found so that a 10 μm thick layer is removed, the BSF is completely removed in both cases, but if the combination is found so that the 5% of the mass of the cell is removed, it is sufficient only for second one.

However, it is possible to combine the mass and thickness measurements to get a precise study on the thickness reduction rate. In fact, from the equation for the density, it is possible to write:

$$d = \frac{10^{-6} m}{A \varrho} \tag{5.9}$$

where d is in μm, m in g, A in mm² and ϱ in g/cm². This equation is similar to equation 5.2. Since it is supposed that the surface area of the sample does not change significantly during the treatment, because the lateral area is much less than it, so the etching on the sides is much lower than on the surface, it is possible to rearrange equation 5.9, using equation 5.2, into:

$$d_{fin}^{avg} = \frac{10^{-6} m_{fin}}{\frac{10^{-6}}{\varrho} \frac{m_{in}}{d_{in}} \varrho} = \frac{m_{fin}}{m_{in}} d_{in}^{avg} \tag{5.10}$$

So, the thickness after the experiment can be calculated just by knowing the initial and final mass and the initial thickness. The latter one does not suffer from the problems of the calculated final thickness, and it is much more reliable.

The treatment time considered is the effective treatment time, calculated by the time of the experiment minus the 50% covered surface time. This value has been chosen between the two incubation times because it is the one that is more indicative of the end of the incubation time, since the oxide layer is removed in most of the surface, and it is better described by the models.

The graphs in the following pages display the removed thickness Δd as function of time for different temperatures and concentrations.

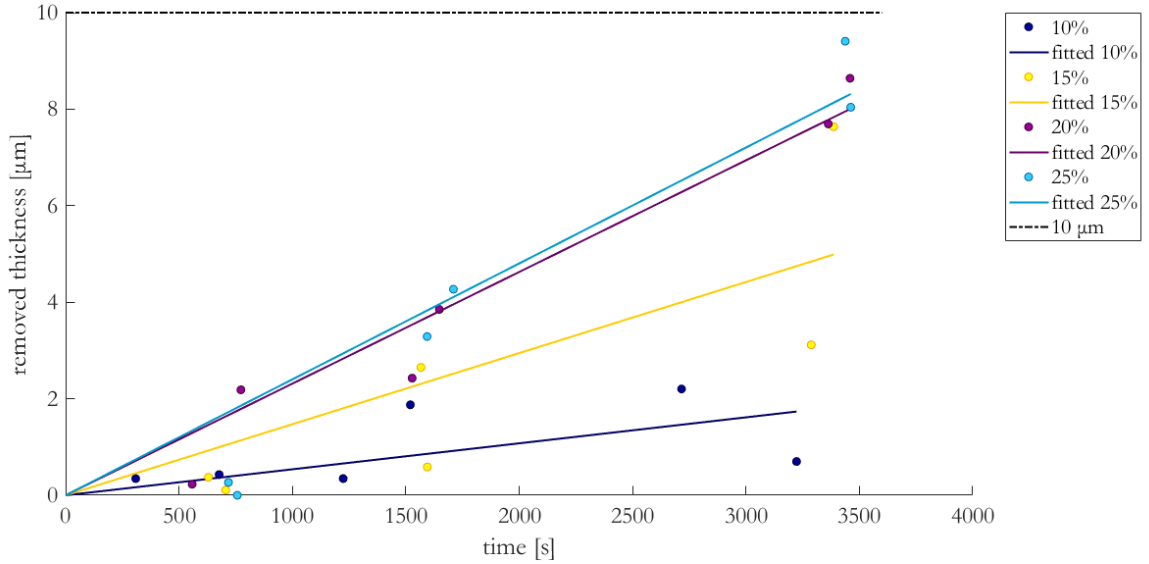

Fig. 5.7 *Removed thickness versus etching time plot for 50°C*

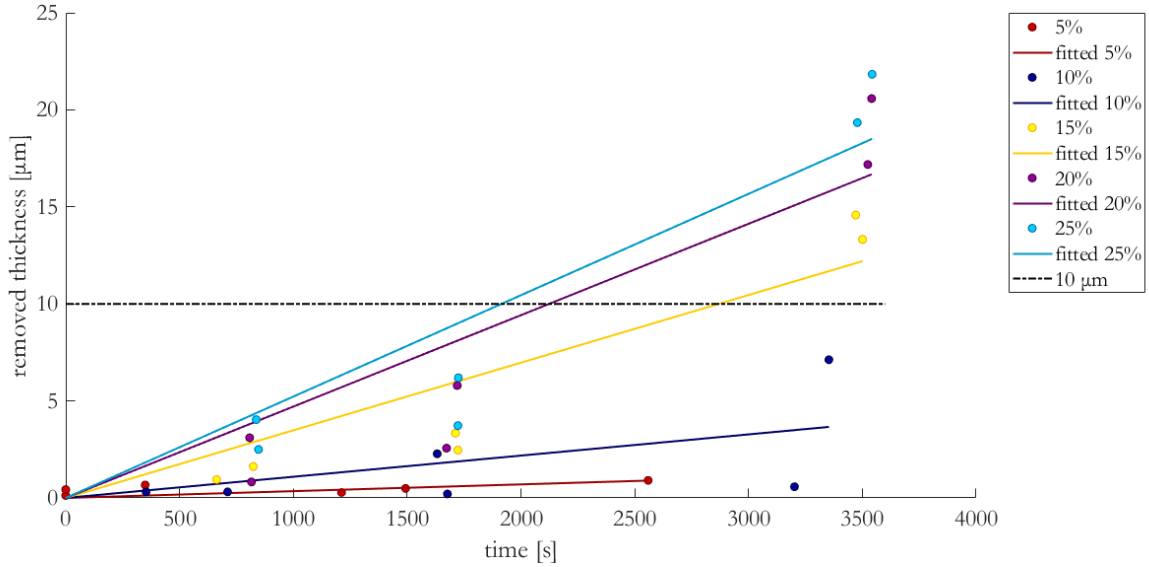

Fig. 5.8 *Removed thickness versus etching time plot for 60°C*

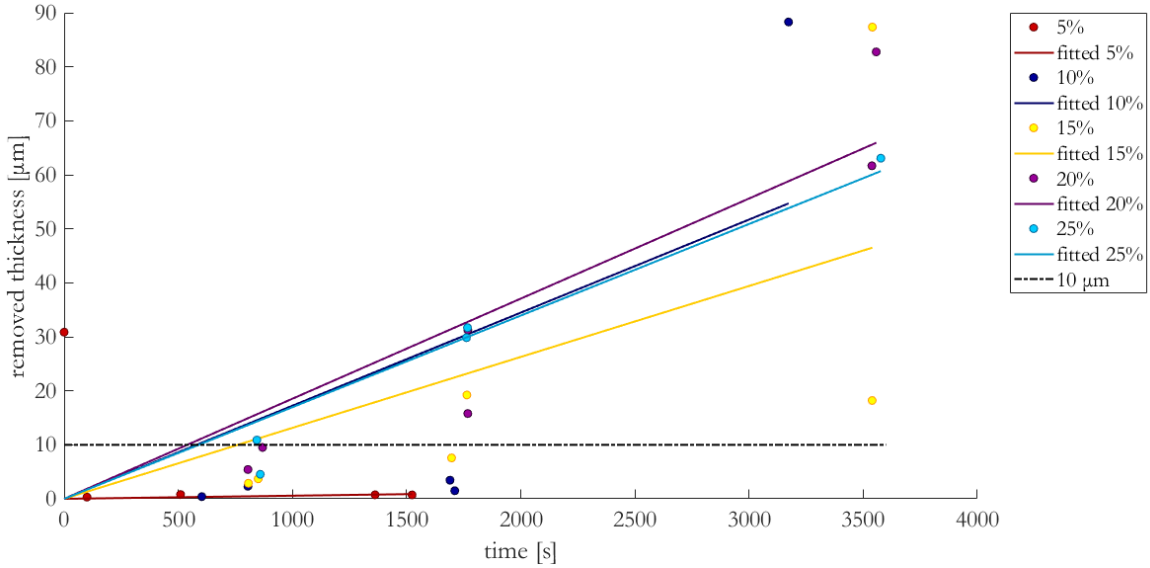

Fig. 5.9 *Removed thickness versus etching time plot for 70°C*

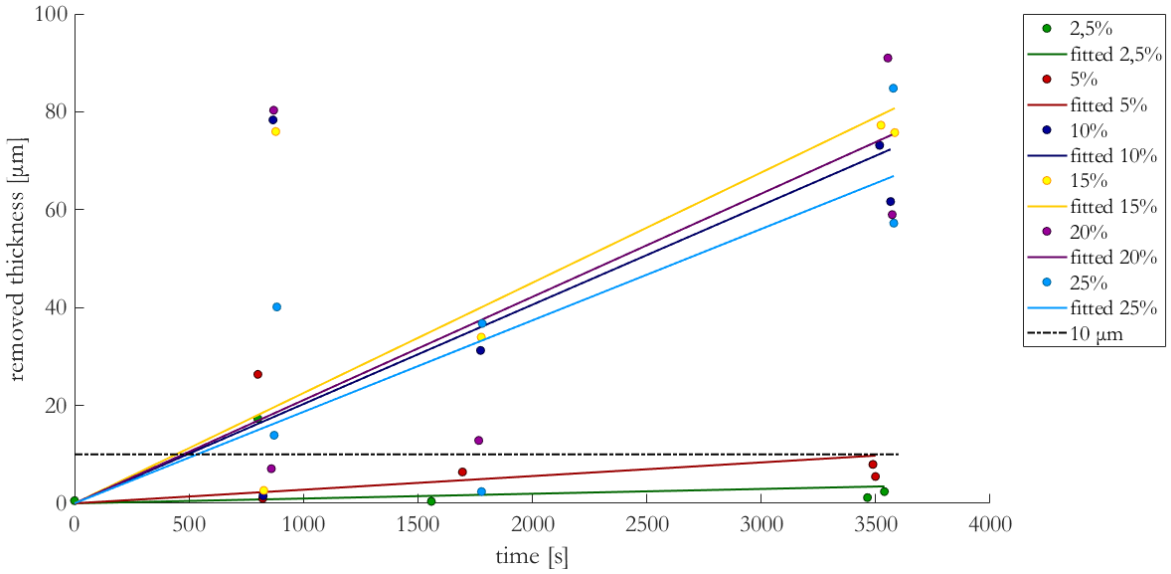

Fig. 5.10 *Removed thickness versus etching time plot for 80°C*

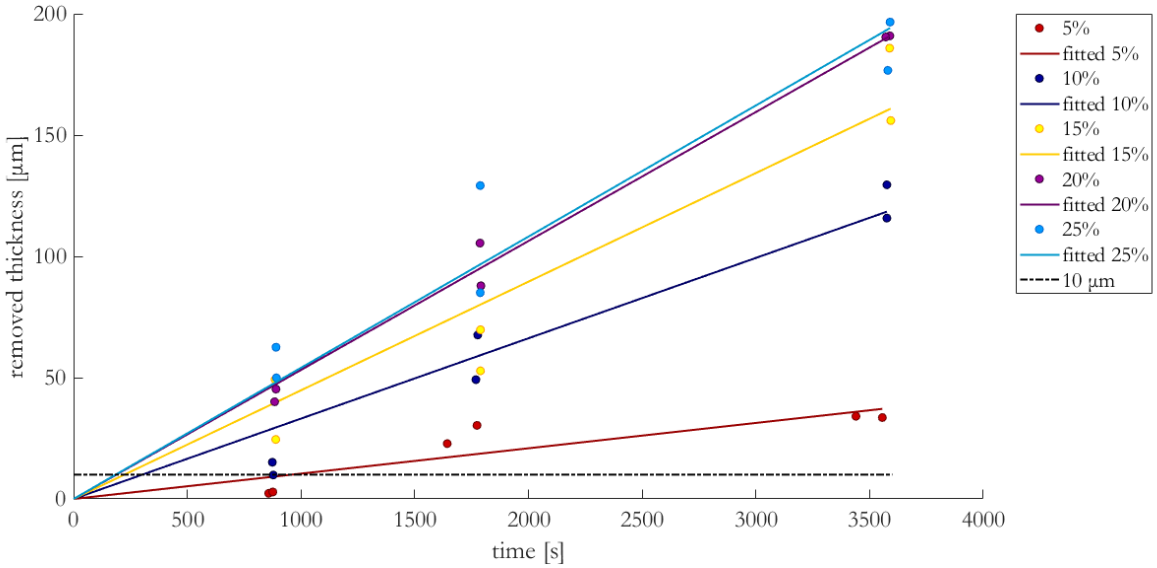

Fig. 5.11 *Removed thickness versus etching time plot for 90°C*

Tab. 5.7 Etching rates

		2,5 wt.%	5 wt.%	10 wt.%	15 wt.%	20 wt.%	25 wt.%
50°C	**r [µm/s]**			$5{,}3819 \cdot 10^{-4}$	$1{,}4729 \cdot 10^{-3}$	$2{,}3133 \cdot 10^{-3}$	$2{,}4016 \cdot 10^{-3}$
	R^2			0,1757	0,6459	0,9467	0,9057
60°C	**r [µm/s]**		$3{,}4911 \cdot 10^{-4}$	$1{,}0914 \cdot 10^{-3}$	$3{,}4853 \cdot 10^{-3}$	$4{,}7094 \cdot 10^{-3}$	$5{,}2235 \cdot 10^{-3}$
	R^2		-0,3627	0,3621	0,8419	0,8330	0,8601
70°C	**r [µm/s]**		$5{,}7592 \cdot 10^{-4}$	$1{,}7237 \cdot 10^{-2}$	$1{,}3137 \cdot 10^{-2}$	$1{,}8536 \cdot 10^{-2}$	$1{,}6963 \cdot 10^{-2}$
	R^2		-0,3042	0,5303	0,4578	0,8525	0,9421
80°C	**r [µm/s]**	$9{,}8022 \cdot 10^{-4}$	$2{,}7867 \cdot 10^{-3}$	$2{,}0290 \cdot 10^{-2}$	$2{,}2532 \cdot 10^{-2}$	$2{,}1090 \cdot 10^{-2}$	$1{,}8687 \cdot 10^{-2}$
	R^2	-0,3248	-0,5801	0,0266	0,2329	0,1389	0,5595
90°C	**r [µm/s]**		$1{,}0440 \cdot 10^{-2}$	$3{,}3117 \cdot 10^{-2}$	$4{,}4782 \cdot 10^{-2}$	$5{,}3168 \cdot 10^{-2}$	$5{,}4069 \cdot 10^{-2}$
	R^2		0,7529	0,9317	0,9137	0,9904	0,9085

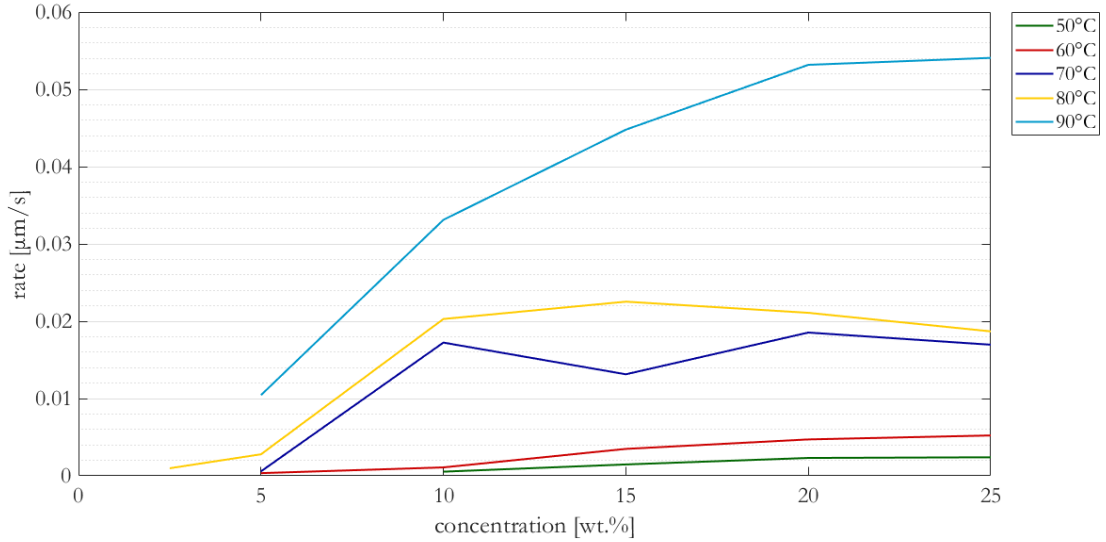

Fig. 5.12 *Etching rate versus solution concentration at 50÷90°C*

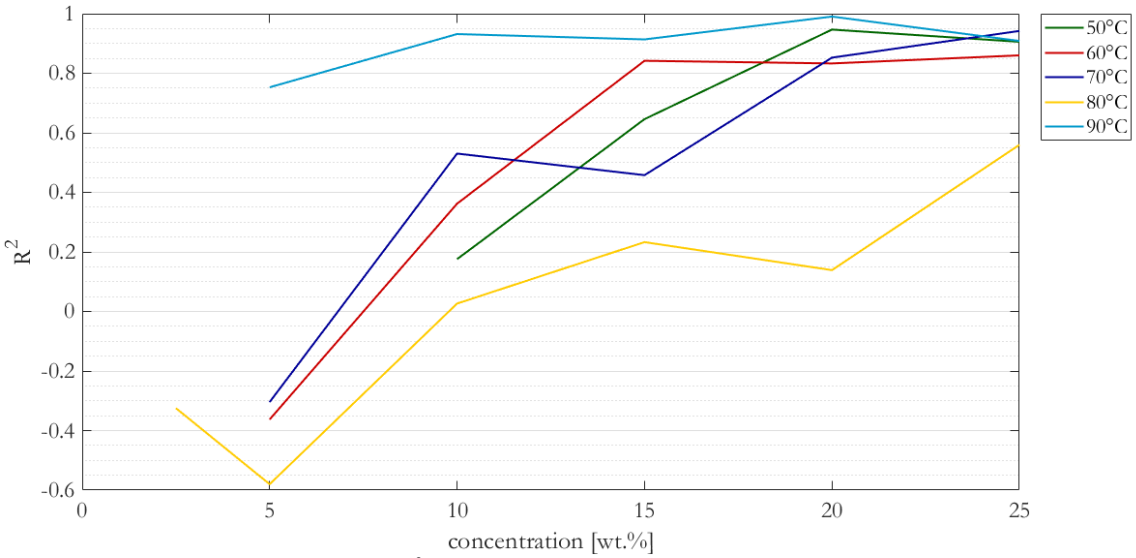

Fig. 5.13 *R^2 versus solution concentration at 50÷90°C*

The coloured marks in the graphs from Fig. 5.7 to Fig. 5.11 represent the removed thickness as function of the real etching time for the treated samples. The analysis has been done for the combinations of temperature and solution concentration that led to remarkable results, so the ones for which the incubation time was too long or the ones that led to a too small mass decreasing or even a mass increasing have been discarded. For example, at 30°C and 40°C the incubation time is longer than the treatment time in most cases, so they are not considered in the present model.

It is possible to observe that the coloured marks increase with time, apparently following a linear trend. So, a linear model has been applied to fit the data:

$$\Delta d(t) = r \cdot t \tag{5.11}$$

Where Δd is the removed thickness in micrometers, t the time in seconds and r the etching rate in µm/s. In Tab. 5.7 the etching rates and the R^2 values for the applied models have been reported

and in Fig. 5.12 and Fig. 5.13 it is displayed how this values change as function of the concentration for different temperatures.

5.3.1.1 Temperature dependence of the etching rate

From Fig. 5.12 it is possible to notice that the etching rate increases with increasing temperature, represented in the graph by the different curves. So, as the etching rate evolves as function of temperature has been studied. For this purpose, the etching rate considered in this part of the study is the moles of silicon dissolved from every square centimetre of the sample surface per second. If the surface area is multiplied to this rate, the total amount of moles per second dissolved in sodium hydroxide for each sample can be easily calculated, but, since we have different samples, this would be a size-dependent parameter. This rate is easily obtained from the thickness decreasing rate as follows:

$$r'\left[\frac{mol}{cm^2 s}\right] = r\left[\frac{\mu m}{s}\right] \cdot \frac{\varrho_{Si} \cdot 10^{-4}}{AW_{Si}} \tag{5.12}$$

Since an exponential trend can be identified from the coloured marks in Fig. 5.14, where the rate as function of the inverse of the absolute temperature is plotted, the following exponential model, attributable to the Arrhenius equation, has been used:

$$r' = A \cdot e^{\frac{b}{T}} \tag{5.13}$$

where A is the pre-exponential factor and $b = -E_a/R$, where E_a is the activation energy. In Fig. 5.14 the solid lines of the exponential model fit well the trend of the data. The model parameters can be found in Tab. 5.8. From the high R^2 values it is possible to state that the model fits well the experimental data.

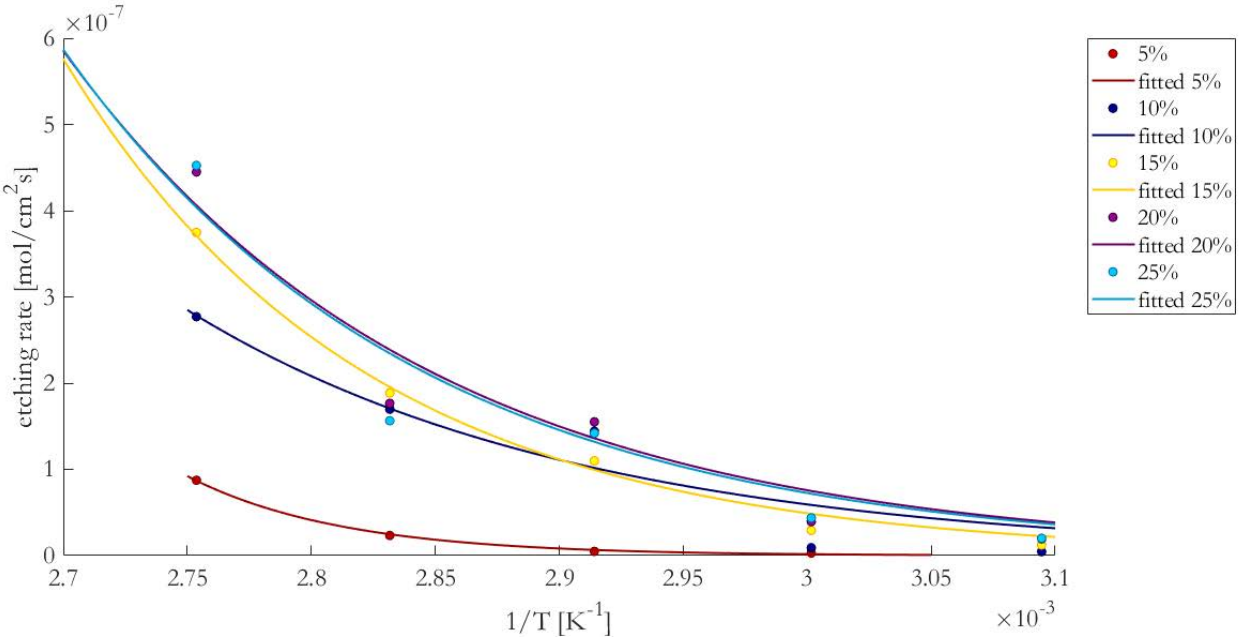

Fig. 5.14 *Etching rate as function of the inverse of temperature for different concentration of the solution*

Tab. 5.8 Exponential model and Arrhenius parameters

	A [mol/cm^{2}s]	b [K]	E_a [J/mol]	R^2
5 wt.%	$1{,}524 \cdot 10^{12}$	$-1{,}609 \cdot 10^4$	1935,40	0,9985
10 wt.%	8,898	-6275	754,75	0,9050
15 wt.%	2417	-8207	987,02	0,9925
20 wt.%	57,36	-6815	819,64	0,9358
25 wt.%	87,05	-6969	838,12	0,9187

5.3.2 Discussion

From the graphs from Fig. 5.9 to Fig. 5.11 it is possible to see that at 50°C the time for the removal of the required thickness to completely etch the back-surface field is too long: in one hour the target is not reached, also for the most concentrated solutions. So, it is possible to conclude that this temperature is not high enough to complete the process in a reasonable time.

At 60°C the target amount of removed material is reached for the three most concentrated solutions, namely 15, 20 and 25 wt.% sodium hydroxide solutions. However, the necessary time to reach this level is quite high: considering the model line, the necessary time to reach it is almost 30 minutes of pure etching for the 20 and 25 wt.% solutions, even more, like 45 minutes, for the 15 wt.% solution. At this time the incubation time must be added too, which is between 80 and 120 seconds for this temperature and these concentrations. Moreover, for the 20 and the 25 wt.% solutions, at 30 minutes the model removed thicknesses differ significantly from the experimental values, represented by the circular marks. For these reasons, also this temperature can be neglected for the further study.

From 70°C the etching time sufficient to get the target removal decreases up to almost 500 seconds, and for 90°C is even lower. This means that to get the etching in a reasonable amount of time, the treatment should be done at temperature from 70°C on.

The silicon which is on the free surface reacts with the sodium hydroxide and the product is dissolved in the solution. The average mass of the treated samples is 0,223 g, while the amount of solution used is 70 mL for temperatures between 30°C and 70°C. Supposing that all the sample is etched by the solution, and that a limited amount of solution is evaporated, considering a solution density of 1,02 g/mL for the 2,5 wt.% solution and of 1,26 g/mL for the 25 wt.% solution, the final concentration of silicon in the solution becomes 8÷99 times lower than the sodium hydroxide concentration. This value becomes even lower for the experiments made at 80°C and 90°C, where six samples have been treated in a ten times bigger volume of solution. Moreover, except for the one hour etch at 90°C, the dissolved amount of silicon is much less than the full sample. For this reason, it is possible to state that the increasing of the silicon concentration in the solution does not interfere with the chemical reaction, so the rate is not affected.

Given this, the linear model represents well the real behaviour of the etching, because the sodium hydroxide keeps dissolving the silicon on the surface in the same way during the whole

experiment. However, from Tab. 5.7 and Fig. 5.13 it is possible to see that in some cases the model does not fit perfectly the data, when the R^2 values are not close to 1. The reason of this can be identified with the difference between the etching rates for different plane orientations: multicrystalline samples that have grains favourably oriented etch faster than the others. The solution concentration affects this difference: for the lower concentrations the R^2 values are typically lower than for the 15, 20 and 25 wt.% solutions.

Another aim of the study is to define a process that should be reproducible, namely that the removed thickness should not differ too much between samples treated with the same combinations of the parameters, and they also should be as close as possible to the model. In Fig. 5.15 the difference between the real removed thickness and the one obtained from the linear model is represented for the 20 wt.% solution. It is possible to observe that as the temperature increases, the difference becomes larger, and so the reproducibility becomes lower. The only exception is at 90°C: in this case, even if the solution dissolves a large amount of material, the removed amount is almost always the same. For the other concentrations the reproducibility at 90°C is not this good, but still better than for the 70°C and 80°C treatments.

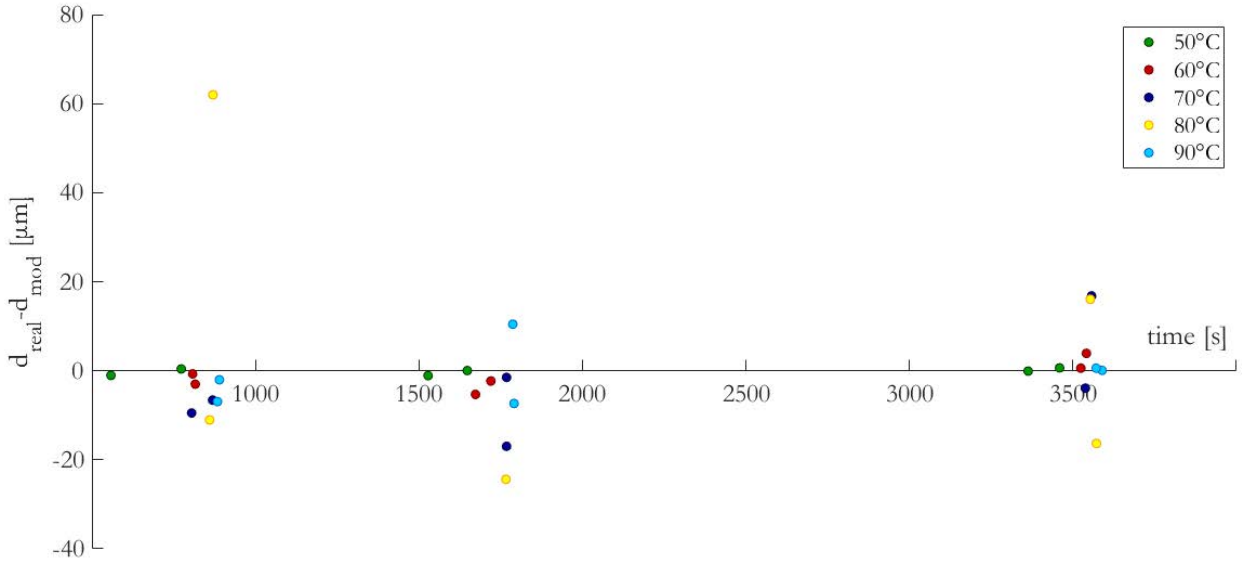

Fig. 5.15 *Difference between the real removed thickness and the one obtained from the model for the 20 wt.% solution at different temperatures*

About the reaction rates, it is possible to observe from Fig. 5.12 that for the most interesting temperatures (70°C÷90°C) the highest reduction rate is generally not found for the most concentrated solution, but around the 20 wt.% solution. This is in line with the preliminary results, where it was found that the solution concentration that gave the highest number of green boxes in Tab. 5.1 and Tab. 5.2 was the 20 wt.% one. The reason should be identified, as Huang proposed (Huang & Tao, 2015), in the reaction between silicon and sodium hydroxide, in equation 5.1: if the sodium hydroxide concentration increases too much, the available water is reduced, and so the reaction is slowed. However, also here the only exception is the 90°C treatment, where the highest rate is found for the 25 wt.% solution, even if the difference from the 20 wt.% one is small ($5{,}4069 \cdot 10^{-2}$ µm/s versus $5{,}3168 \cdot 10^{-2}$ µm/s).

The etching rates increases with the temperature too, as from Fig. 5.14, with an Arrhenius-like behaviour. While the pre-exponential factor differs significantly with the concentration, the activation energy has almost the same order for all the different solutions.

5.4 BACK-SURFACE FIELD REMOVAL

To recycle the silicon solar cells, the heavily doped layers should be completely removed, in order to get the lightly doped base. The back-surface field is the layer on the back surface of the silicon, the one which does not face directly the sun, which is heavily p-type because doped with aluminium. This layer is generally 5÷10 μm thick, so the required removed thickness is 10 μm, so to be sure that all the layer is effectively removed.

Silicon can be etched in sodium hydroxide solutions: the reaction is shown in equation 5.1. However, before this reaction starts, the native silicon oxide layer, which naturally forms on the surface of silicon, must be dissolved, as from equation 5.4.

Temperatures lower than 70°C are not suitable for the treatment, since the etching rate is too low, and so the required amount of material is dissolved in a too long time. Moreover, at these temperatures the oxide layer takes a long time to be removed, time which is wasted and that should be reduced as much as possible. As temperature increases, the etching rate increases too, with an exponential behaviour. Also the incubation time decreases as temperature increases. So, higher temperatures guarantee a faster process. On the contrary, the reproducibility of the experiment generally decreases as temperature increases, so a trade-off between these two parameters should be found to get a fast technology which at the same time allows to get always optimum results. However, the 90°C treatment ensures high etching rates with a good reproducibility.

As regards the solution concentration, accordingly with the preliminary results the one which provides the highest etching rate is generally the 20 wt.% one. The incubation time decreases as the concentration increases, so the best concentration would be the highest one. However, due to the negative exponential trend, the incubation time does not change too much between the 20 wt.% and 25 wt.% solutions.

5.4.0.1 High-temperature problems

It is right that high temperatures are favourable to get a fast process. To get a process which is not too long the process should be done at temperatures higher than 70°C, and the etching rate increases and the incubation time decreases as the temperature increases.

However, as temperature increases, the evaporation rate increases too. Since the generated vapour is richer in water than in sodium hydroxide, the remaining solution increase its concentration. Since the maximum of the etching rate is with a 20 wt.% solution, this would lead to a decreasing of the etching rate. In the technological point of view, it is expected that the solution is not changed every time the etching is done, but it should be used to treat different samples,

so, if the concentration changes during the solution lifetime, the reproducibility is jeopardized, since different samples will experience different conditions.

Closing the system, so that an equilibrium between the gas phase and the liquid phase is reached, is not a feasible option, since hydrogen gas is generated by the reaction, and if its concentration is too high it would cause explosions.

For these reason, the best treatment parameters are 70°C and 20 wt.% sodium hydroxide solution. Since the etching rate is $1{,}8536 \cdot 10^{-2}$ μm/s, the required removed thickness of 10 μm is reached in 9 minutes. Since the maximum of the measured incubation time is 95 seconds, an 11-minutes-long treatment is enough to reach the desired results.

5.4.1 Resistivity measurements

The resistivity measurements are still ongoing at Innolabor Kft. in Budapest. However, some interesting samples have already been measured, and the results are reported in Tab. 5.9. It is possible to observe that in most of the samples the target resistivity value for solar-grade silicon, namely 0,5÷2 Ω·cm, is obtained.

Tab 5.9 Preliminary resistivity results on a limited number of samples (replicates a)

T [°C]	c [wt.%]	t [s]	Δd [μm]	Voltage [mV]	Current [mA]	Resistance [Ω]	Resistivity [Ω·cm]
50	20	15	0,23	7,79 36,4	1,44 6,45	5,3889 5,6434	0,4734
50	20	30	2,43	221,4 25,2	14,18 1,6	15,6135 15,75	1,3220
50	20	60	7,69	24,4 134,2	1,61 9,19	15,1553 14,6028	1,2543
60	20	15	3,10	171,8 33,8	9,35 1,61	18,3743 20,9938	1,7903
60	20	30	2,57	16,1 63,78	1,61 6,04	10 10,5596	0,9411
60	20	60	20,58	28,9 7,12	1,535 0,53	18,8274 13,4340	1,3233
70	20	15	5,43	72,6 22,6	4,02 1,24	18,0597 18,2258	1,5678
70	20	30	15,80	24,4 111,7	1,24 5,35	19,6774 20,8785	1,7003
70	20	60	45,93	124,6 25,7	5,85 1,18	21,2992 21,7797	1,9720

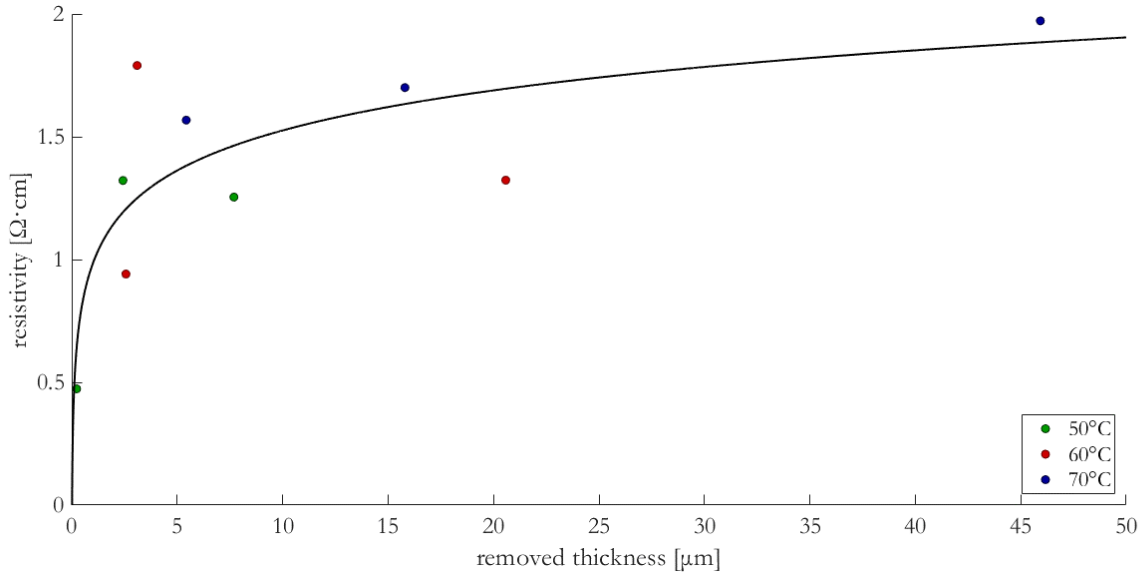

Fig. 5.16 *Measured resistivity versus removed thickness at different temperatures for the 20 wt.% solution*

From Fig. 5.16 it is possible to observe that as the removed thickness increases, the resistivity increases, tending asymptotically to the value of 2 Ω·cm. This leads to the conclusion that with the proposed treatment parameters of 70°C, 20 wt.% concentration and at least 11 minutes treatment, the required resistivity and grade of silicon is achieved. In fact, the 10 μm of removed thickness correspond to a resistivity of almost 1,5 Ω·cm, widely into the target range. However, resistivity measurements are still ongoing and for a more detailed analysis of the resistivity change as function of the process parameters and of the removed thickness all the measurements are needed. Furthermore, reference samples are going to be measured, and thus the resistivity measurements results can be corrected, but the difference is expected to be around 5÷10%.

5.4.2 Economics of the process

Sodium hydroxide market price is currently around 700 €/dmt NaOH. As regards the stoichiometry of the etching reaction, for each mole of silicon removed from the sample, one mole of NaOH is needed. For each cell, 180 μm thick on average, 10 μm of silicon are removed, which accounts for the 5,55% of the cell. So, to produce one kilogram of silicon with this process, 58,82 g are etched by the solution, which equals to 2,09 mol of silicon. This molar amount is the same needed for the sodium hydroxide to etch this quantity of silicon, which corresponds to 83,77 g of NaOH. Thus, the cost for the required amount of sodium hydroxide is 0,059 €/kg of Si produced. Clearly, this amount of solution is a theorical calculation made on the stoichiometry of the reaction, but it does not consider for example that the concentration of products would increase very fast, probably decreasing the reaction kinetics. For this reason, the volume of the solution should be increased, thus increasing also the cost for sodium hydroxide.

Fortunately, no energy is needed to heat up the solution. The dissolution of sodium hydroxide in water is known to be strongly exothermic: supposing to use 18°C water to prepare the solution, the heat of solution is equal to $\Delta H^{sol} = 42{,}59\ kcal/mol$ (D.W. Green, R.H. Perry, Perry's

Chemical Engineers' Handbook, 2008). Supposing now that the process happens at constant pressure (atmospheric pressure) and knowing that the heat capacity for the 20 wt.% sodium hydroxide solution at 20°C is $c_p = 4{,}06\ J/(g \cdot °C)$, the temperature increasing is:

$$\Delta T = \frac{\Delta H^{sol}}{\rho c_p} = \frac{253{,}38\ kJ/L}{1{,}18965\ kg/L \cdot 4{,}06\ kJ/(kg \cdot °C)} = 52{,}48°C \qquad (5.14)$$

Thus, the final temperature is 70°C. The only energy needed is the one to keep the temperature constant during the whole process, but it depends on the configuration of the industrial plant. Also, the cost related to the workers per each kilogram of produced silicon depends on the plant configuration and how much silicon can be treated. In conclusion, this purification process appears to be very cost effective.

6. FRONT-SIDE ETCHING

6.1 PROFILOMETER ANALYSIS

A total number of 30 samples have been treated with different combination of three temperatures (60, 70 and 80°C) and six different times (1, 2, 4, 8 and 16 minutes), two replicates for each combination, in a 20 wt.% sodium hydroxide solution. In every sample, almost half of the silicon nitride layer is removed in order to create a step: in fact, sodium hydroxide does not dissolve this layer, so the etching cannot happen in the silicon below; on the other part, instead, where the silicon nitride is removed, the etching regularly happens. At the end of the treatment, a step should be identified between the treated and untreated part.

For this reason, the treated samples have been measured with a profilometer, in order to measure the height different between the two sides of the step: the measuring line has been traced in such a way that the measurement starts on the unetched part and in finishes on the etched one.

Unfortunately, silicon wafers suffer of a micrometric surface roughness, due to the texturization process, as it is possible to observe from Fig. 6.1. The profilometer analysis relies on different levers: when the measurement is complete, the adjustment of two levers is needed to get the results. These levers should be placed on regions that are known to be at the same height: with a rough profile is impossible to determine ex ante two regions that really are at the same height. For this reason, the profiles change drastically when the levers' position is changed, causing different step heights for the same sample. So, these results have no sense and this technique is discarded.

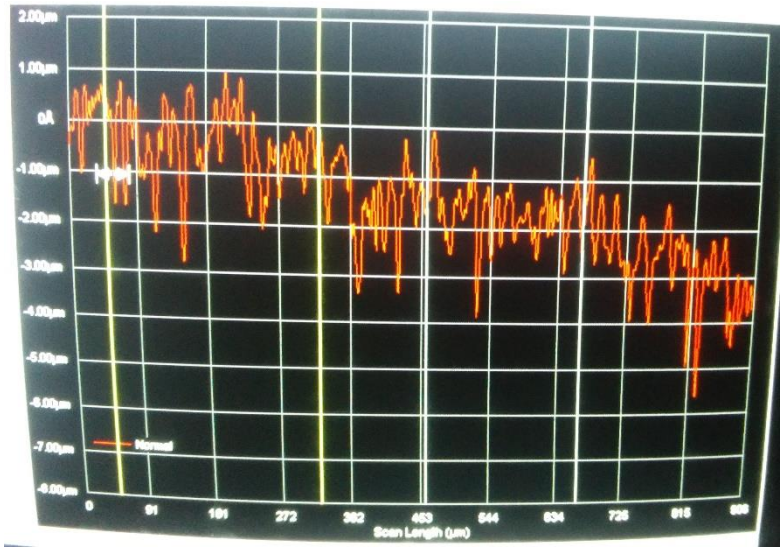

Fig. 6.1 *Typical profile of a treated sample*

6.2 FOUR-POINT-PROBE RESISTIVITY ANALYSIS

Five new samples have been used for the resistivity measurements. The nitride layer has been removed from all the surface and they have been treated in 70°C 20 wt.% sodium hydroxide solution for 1, 2, 4, 8 and 16 minutes. In another sample the silicon nitride layer has been removed too, but it has not been treated in the sodium hydroxide solution. Multicrystalline samples have been chosen, with grains large enough so that the equipment tips would have completely fallen inside one grain.

To calculate the resistivity, the thickness of the emitter should have been known. From the literature the information about it are conflicting, but the values are all in the range between 300 nm and 1 μm. Moreover, the profilometer analysis are not adequate, so it is impossible to know exactly the removed thickness after the etching, and so the remaining emitter thickness. For this reason, the resistivity if the sample cannot be calculated, but it is possible to use the sheet resistance data R_S, measured in Ω□. For the same reason, also the dopant concentration cannot be calculated, so the dose, measured in atoms/cm^2, is used.

In Tab. 6.1 the obtained data are reported. The correction factor used for the sheet resistance measurement, due to the large dimension of the sample respect to the distance between the tips, is 2, while the geometric factor for the Hall measurements is 1,8.

Tab. 6.1 Results from the resistivity measurements

Sample	Source current	Sheet Resistance [Ω□]	Dose [atoms/cm^2]
Untreated	300 μA	$2{,}476 \cdot 10^2 \pm 2.922 \cdot 10^1$	$1{,}077 \cdot 10^{15}$ (e^-)
1 min	100 μA	$1{,}009 \cdot 10^3 \pm 4{,}354 \cdot 10^1$	$4{,}554 \cdot 10^{14}$ (e^-)
2 min	100 μA	$1{,}852 \cdot 10^3 \pm 1{,}481 \cdot 10^2$	$5{,}237 \cdot 10^{13}$ (e^-)
4 min	1 mA	$1{,}553 \cdot 10^4 \pm 1{,}072 \cdot 10^2$	e^- & h^+
8 min	/	/	/
16 min	/	/	/

It is possible to observe that the lines for 8 and 16 minutes have no results. For this two samples it was impossible to calculate the sheet resistance or the dose. In fact, as it is possible to see from Fig. 6.2, their contacts present an ohmic behaviour (not linear), and this makes the correct calculation of the resistance and the dose impossible. This is also confirmed by the Hall measurements for the 4 minutes sample: when a positive field is applied, holes are measured, and vice versa. This is probably due to the inhomogeneous etching on the surface, depending on the plane orientation or due to the carving of pits. From 4 minutes on, the etching treatment removes almost completely the emitter, reaching the base, but some n-type tips are still present, and these compromise the measurement.

For this reason, also the resistivity measurements are not adequate for checking the emitter removal, since it does not measure accurately the resistivity and the dose as the treatment time increases. In fact, a proof of the emitter removal would have been the stabilization of the resistiv-

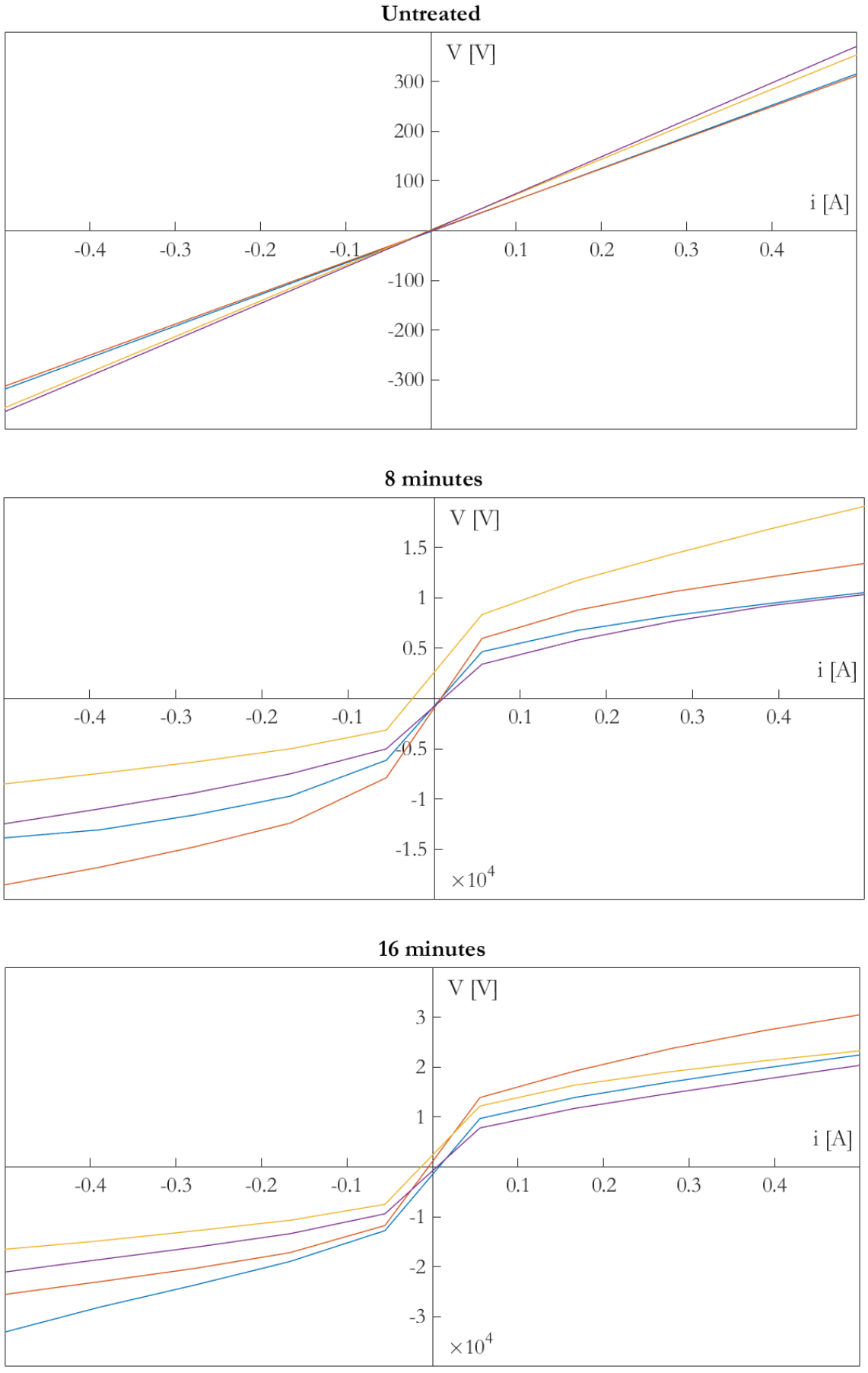

Fig. 6.2 *Ohmicity of the metal-semiconductor contacts for different treatment time*

ity at a value of 25÷100 Ω□, that is the sheet resistance of the base. From Fig. 6.3 it is possible to observe that the resistivity increases as the treatment time increases, due to the reduction of the thickness d ($R_S=\varrho/d$) and of the dopant concentration as the etching of the emitter proceeds (Dastgheib-Shirazi et al., 2013; Irvin, 1962). However, no data are available for a treatment time longer than 4 minutes, so it is impossible to determine when the emitter is completely removed.

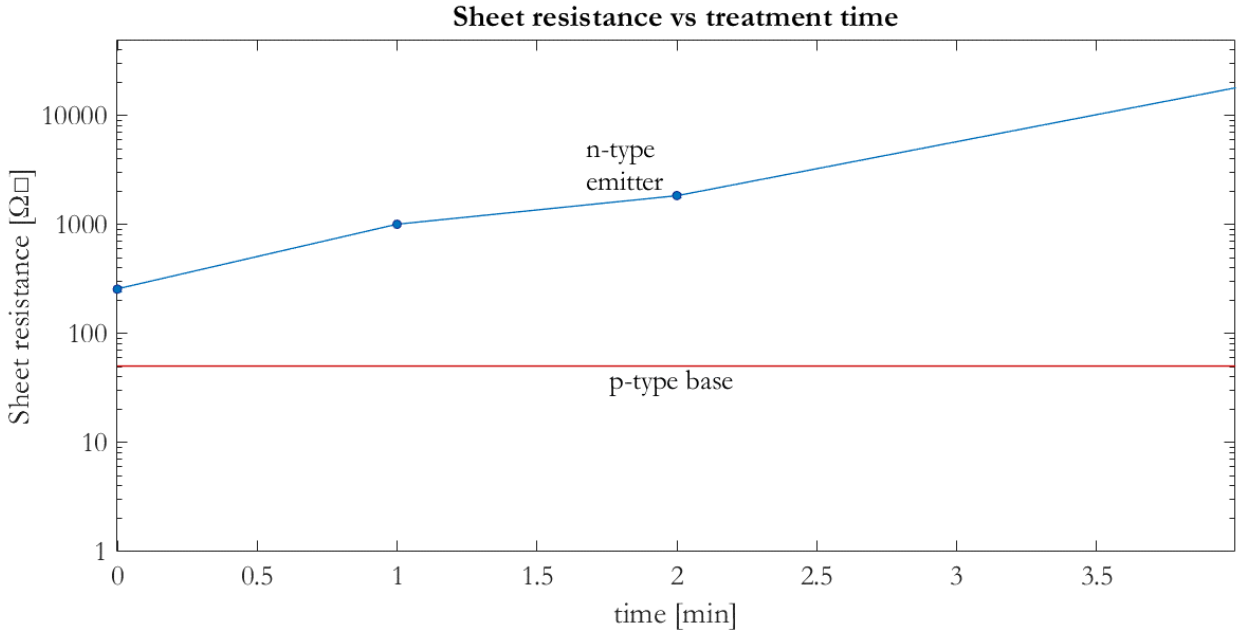

Fig. 6.3 *Sheet resistance versus treatment time plot for a 70°C in 20 wt.% NaOH treatment*

6.2.1 Compensated silicon

However, some interesting information can be derived from the calculated dose. The required phosphorus concentration for the solar-grade silicon is 0,79 ppm_w. When the solar cell is melted (necessary to generate new wafers), the phosphorus contained in the emitter diffuses in the whole thickness: in this way compensated silicon is obtained. The required dose for solar-grade silicon is thus easy to calculate:

$$0{,}79ppm_w = \frac{0{,}79 \cdot 10^{-6} g}{1g} = \frac{0{,}79 \cdot 10^{-6} g \cdot \frac{6{,}02 \cdot 10^{23}\ atoms/mol}{30{,}9737\ g/mol}}{\frac{1g}{2{,}32\ g/cm^3}} \tag{6.1}$$
$$= 3{,}5622 \cdot 10^{16} atoms/cm^3 \cdot 0{,}0180cm$$
$$= 6{,}412 \cdot 10^{14}\ atoms/cm^2$$

In Fig. 6.4 it is possible to see the dose calculated for the samples treated for 1 and 2 minutes and for the untreated sample. It is possible to observe that just after two minutes the phosphorus level is low enough to have solar-grade silicon.

However, the aim of the study is to completely remove the emitter layer, and from these results it is possible to conclude that the resistivity tests made are not appropriate do determine it. Also, the calculations on compensated silicon should be done in a more accurate way, since different factors should be considered: the phosphorus content of the base should be known, to which

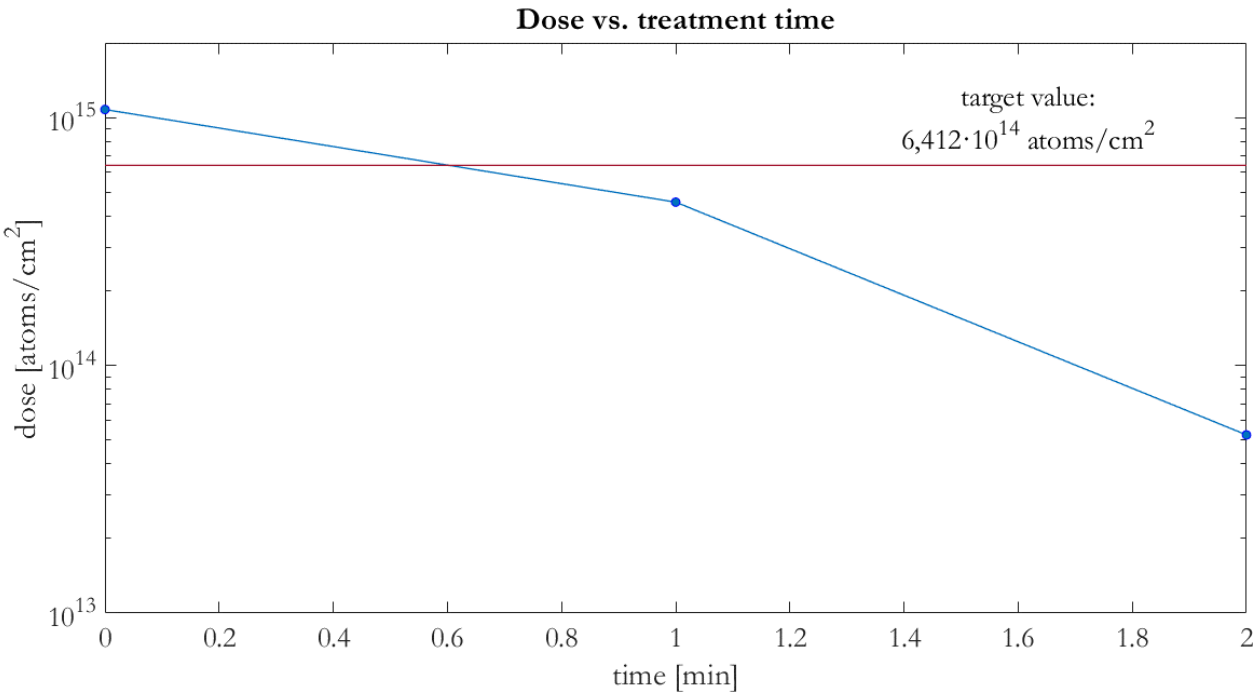

Fig. 6.4 *Dose versus treatment time plot for a 70°C in 20 wt.% NaOH treatment*

the one from the emitter is added, and it should be remembered that n-type base and p-type emitter cells also exist. However, these results, even if partial, show that this topic can be taken into consideration.

6.3 P/N ANALYSIS

All the samples have been measured with a PN-100 pen by Semilab. This equipment is able to determine the type of the majority carriers in the semiconductor. When the pen approaches the semiconductor and it is turned on, it sends a chopped light to the sample surface, and a probe measures the potential surface barrier. A LED display turns red if holes are measured, so if it is p-type, or green if electrons are measured, so if it is n-type.

All the samples have been prepared in such a way that the silicon nitride anti-reflection coating is removed on only almost half of the surface. In this way the etching treatment happens only in the uncovered part, and it is proved by the appearance of hydrogen bubbles. For this reason, if the emitter is effectively removed, the LED on the pen should display a different colour between the treated and the untreated part.

For all the samples measured, no change in the type of silicon is found between the regions with or without the anti-reflection layer. So, it is impossible to determine with precision if the emitter is effectively removed or not with this technique.

However, these results confirm the hypothesis stated in the previous section. The etching treatment is not homogeneous, but it is orientation-dependent, or, due to the absence of stirring, it could cause the carving of pits, or else the emitter layer has not a homogeneous thickness. For these reasons, it is probable that the emitter is not completely removed from the front side of

the cell, but some parts remains after the treatment. Thus, the p/n tester, as with the four-point-probe equipment, measures regions where the emitter is completely removed and ones where it is not, and since the emitter is heavily doped, while the base is lightly doped, the pen feels strongly the effect of the remaining parts of the emitter, even if they are small.

6.4 EMITTER REMOVAL

The treatments on the front-side of the cell have been done to find the right combination of the process parameters to completely remove the emitter. Different analytical techniques have been tried to measure if this layer is effectively removed, but none of them confirmed it, not even the resistivity measurements and the p/n pen tests.

The resistivity measurements went right for the samples treated less then four minutes in the 20 wt.% sodium hydroxide solution at 70°C. From that time on, the contact ohmicity started to deviate from the rectified behaviour, typical of the p-n junction, and both holes and electrons have been found in the Hall measurements. This means that after this time the emitter is completely removed in some points, thus reaching the base, but not on all the surface. This can be caused by some different effects, such as that the etching is not homogeneous, because of the orientation-dependency, the carving of pits during etching, caused by the absence of stirring, or the inhomogeneity of the thickness of the emitter, which is generated by diffusion of the dopant. For these reasons, the probes feel the differences of the silicon type between different zones where the emitter is removed or not, and so the measurements are affected by that. The p/n pen measurements are probably affected too by the not complete removal of the emitter: since it is heavily doped, the pen feels the remaining parts of the emitter more than the lightly-doped base, thus giving the same result of the untreated part.

Other experiments and measurements are currently being done to check when the emitter is completely removed. By now, it is only possible to state that the emitter is probably removed from the most part of the front surface in between 4 and 8 minutes at 70°C in the 20 wt.% NaOH solution. This time refers to the treatment time, so also the incubation time is considered. So, the 11 minutes treatment proposed in the previous chapter for the back-surface field removal is probably enough also for the emitter removal, but this should be confirmed by other experiments.

7. CONCLUSIONS

Due to the photovoltaic boom 15÷20 years ago, in the next years there will be lots of panels that will reach the end of life. In the panels, lots of valuable materials are present, such as silver, copper, aluminium and, mostly, solar-grade silicon. All these materials must be separated and recovered. Solar-grade silicon is the most important material in the solar panels: due to its semiconducting properties, it uses the energy coming from the sun to generate electrons-hole pairs, that flow into the material, generating a potential difference and, thus, direct electric current.

To take advantage of these photovoltaic properties of silicon, a p-n junction must be generated in the silicon by doping it with elements from the III and V group. Thus, the solar cell typically has a lightly p-type boron-doped base, a n^+-type phosphorus doped emitter, which is maximum 1 μm thick and is needed to create the p-n junction, and a p^+-type back-surface field, aluminium doped, 5÷10 μm thick, to reduce the recombination at the back surface. The emitter and the BSF are heavily doped, so they do not reach the required purity for solar grade silicon. For this reason, they must be removed from the cell to get one which meets the requirements, to create new wafers for new solar panels.

One way to do it is to chemically etch these layers with some acidic or basic solutions: removing the surface layer of silicon, also the contaminants are dissolved in the solution. Different chemicals are known to etch silicon, but most of them are hazardous and toxic acids. Sodium hydroxide gives basic solutions, that are corrosive, but it does not generate toxic gases, as most of acids do. The reaction with silicon is described by:

$$Si + 2NaOH + H_2O = Na_2SiO_3 + H_2 \tag{7.1}$$

Attention must be paid to the generation of gaseous hydrogen, that can violently react with the oxygen in the atmosphere, causing explosions. This must be taken care especially in the industrial plants, when large amounts of material are treated, so a large volume of gas is generated. The aim of this study is to determine the best process parameters for a fast removal of the doped layer in the end-of-life silicon solar cells.

When the silicon is immersed in the sodium hydroxide solution, the reaction does not start immediately, but after an incubation time. The native silicon oxide layer must be dissolved from the surface before the silicon etching starts. The reaction within silicon oxide and the sodium hydroxide solution is described by:

$$SiO_2 + 2NaOH = Na_2SiO_3 + H_2O \quad (7.2)$$

This reaction is faster when the temperature and the concentration of the solution are increased. In fact, the more the solution is concentrated, the more NaOH is available for the reaction.

Two different incubation times have been measured during the experiments: the first bubble time, namely the time when the first hydrogen bubbles, sign that the silicon reaction has started, can be seen, and the 50% covered surface, when almost half of the surface is covered by bubbles. For the process point of view, the second one is better, since it is more indicative of the real and effective etching of the silicon. This incubation time, in seconds, can be calculated with the following equation:

$$\tau_{50\%}(T, c) = 5{,}189 \cdot 10^4 \cdot e^{-0{,}1047 \cdot c} \cdot e^{-0{,}0657 \cdot T} \quad (7.3)$$

Then, the etching time has been studied, in relation to the back side of the cell, where 10 μm should be removed on order to completely remove the BSF. The removed amount of material linearly increases with the etching time, which is calculated as t-$\tau_{50\%}$. It is observed that the etching rate increases with temperature with an Arrhenius-like behaviour, but it is untrue that it increases as the concentration increases. In most of the cases the maximum of the etching rate is found around 20÷25 wt.% concentration.

Below 60°C the time to etch the required amount of material is too long for an industrial process, but if temperatures are too high, the solution evaporates fast, and the liquid enriches with the sodium hydroxide, this decreasing the etching rate. For this reason, the proposed combination of temperature and concentration for the process is 70°C and 20 wt.% solution. In this case, the etching rate equals to $1{,}8536 \cdot 10^{-2}$ μm/s, so the required 10 μm removal is achieved is nine minutes. The incubation time for this combination of parameters is 65 seconds, but since the maximum measured values during the experiment were around 90 seconds, two more minutes are proposed for the incubation time, thus giving a treatment time of 11 minutes. These results are different from the results by Huang (Huang & Tao, 2015), who affirmed that the best solution concentration is the 3 wt.% at 50°C: however, he proposed a three times longer treatment, lasting 30 minutes, to completely etch the back-surface field.

For the emitter removal, all the measurements that have been done are not accurate enough to state if it has been successfully removed, so other experiments and test are needed. However, it is possible to claim that, after four minutes in the 20 wt.% sodium hydroxide solution at 70°C, the emitter is removed in some areas, even if not in the whole front surface. This is proved by the fact that the electric measurements are not accurate for the samples treated more than four minutes, influenced by the differences of type between close regions of the surface. This means that after this time the emitter, even if not in the whole sample, is partially completely removed in some parts of the surface, so after this time the emitter removal is even better. So, the 11

minutes treatment proposed for the back side of the cell is probably enough also to get a good emitter removal, but more experiments are needed to precisely define the effective time.

The proposed mechanism for the purification of the cell consists on immersing the as-received silicon cell in a 20 wt.% sodium hydroxide solution at 70°C for a certain time, then pulling it out for a certain time to remove the silicon nitride layer in hydrofluoric, phosphoric, citric or tartaric acid, and then immersing it again in the same solution as before to complete the etching on both sides. The total treatment time proposed is 11 minutes in the NaOH solution: this time is enough to completely remove the back-surface field, and probably enough for the emitter removal too. However, the exact time to remove it is not precisely known yet, and other experiments are needed to define it.

When the emitter and the back-surface field are removed, the silicon is thus ready for the production of new wafers. The total silicon recovery is higher than the 90%, leading to a good recycling process with limited silicon losses. The process is very cost-effective, since the sodium hydroxide is not so expensive and that not so high temperatures are needed. Moreover, since the dissolution of NaOH in water is highly exothermic, and it reaches spontaneously the temperature of 70°C, only the energy to keep the solution warm is needed. When the treatment time will be precisely defined in all its parts, this proposed process will be ready for the upscaling, in order to reach TRL7 by year 2020.

8. ACKNOWLEDGMENTS

I would like to thank the Department of Materials Development of Bay Zoltán Nonprofit Ltd. for Applied Research, in Miskolc, Hungary. In the five months I have been there they made me feel like home, and it has been a pleasure to work with them. I would especially like to thank Szabó József, my mentor in the company. Our work together and our mutual suggestions made possible to upscale our embryonal ideas to a concrete process to be developed in the industrial scale. Our long talks taught me lots of useful things, also for my future career. I would like to thank Dr. Lévai Gábor, the Head of the Department, who helped me before my arrival and in my first days in Hungary, helping me to find an accommodation. I would also like to thank Juhász Koppány and Baranyai Viktor for the very important suggestions they gave me and for the help to achieve our common results. Most important, I would like to thank Tar Edit: her help in the laboratory was really appreciated. Without her, it would have taken ages to complete the experiments, and, mostly, the days run by in her company. I am really thankful also for all the important support she gave me outside the workplace, she made easier my staying abroad. I would also like to thank Szabó Dávid and Rezes József, very good and nice co-workers, and all the other people in the company.

A heartfelt thanks also to the University of Padova, for the big opportunity given to me to take part to such an important project. I would like to thank all the Metallurgy Department of the Industrial Engineering Department, all the professors and the researchers that proposed me to work on this topic and that helped me during the time I spent in the University laboratories. In particular, I would like to thank Pezzato Luca and Cerchier Pietro, who are involved in this project too and found me the contacts with the Hungarian company. I would also like to thank Prof. Dabalà Manuele and Napolitani Enrico for the useful discussions we had on the work made in Padova and Carraro Chiara, who helped me with the resistivity measurements.

A special thanks to my family which has been very supportive during all these years and during the time I was in Hungary. They have always taught me how to take care of myself, and this was very useful when I was living alone in a foreign country. They made lots of sacrifices to let me and my sister study, and I think that now we are adults we repaid them well. I would also like to thank my girlfriend: staying apart for five months has not been easy, but she has been very supportive during all that time and she waited for me. I am the luckiest person in the world to have her by my side.

9. REFERENCES

Akhter, P., Baig, A., & Mufti, A. (1989). Dissolution of Si (100) layers in NaOH aqueous solutions. Journal of Physics D: Applied Physics, 22, 1924–1927.

Al Hosani, M., & Emziane, M. (2013). Modeling and simulation of a thermophotovoltaic system with NaF heat storage. Energy Procedia, 42, 726–734. https://doi.org/10.1016/j.egypro.2013.11.075

Alemany, C., Trassy, C., Pateyron, B., Li, K.-I., & Delannoy, Y. (2002). Refining of metallurgical-grade silicon by inductive plasma. Solar Energy Materials and Solar Cells, 72, 41–48. https://doi.org/10.1016/S0927-0248(01)00148-9

Allongue, P., Costa-Kieling, V., & Gerisher, H. (1993). Etching of Silicon in NaOH Solutions II. Electrochemical Studies of n-Si(111) and (100) and Mechanism of the Dissolution. Journal of The Electrochemical Society, 140(4), 1018–1026.

Allongue, P., Costa-Kieling, V., & Gerisher, H. (1993). Etching of Silicon in NaOH Solutions I. In Situ Scanning Tunneling Microscopic Investigation of n-Si(111). Journal of The Electrochemical Society, 140(4), 1009–1018.

Ban, B., Zhang, T., Li, J., Bai, X., Pan, X., Chen, J., & Hadi Tabaian, S. (2018). Solidification refining of MG-Si by Al-Si alloy rotating electromagnetic field with varying frequencies. Separation and Purification Technology, 202, 266–274. https://doi.org/10.1016/j.seppur.2018.03.069

Barycka, I., Teterycz, H., & Znamirowski, Z. (1979). Sodium Hydroxide Solution Shows Selective Etching of Boron Doped Silicon. Journal of The Electrochemical Society, 345–346.

Bathey, B. R., & Cretella, M. C. (1982). Review Solar-grade silicon. Journal of Materials Science, 17, 3077–3096. https://doi.org/10.1007/BF01203469

Blakers, A. W., Wang, A., Milne, A. M., Zhao, J., & Green, M. A. (1989). 22.8% Efficient Silicon Solar Cell. Applied Physics Letters, 55(13), 1363–1365. https://doi.org/10.1063/1.101596

Braga, A. F. B., Moreira, S. P., Zampieri, P. R., Bacchin, J. M. G., & Mei, P. R. (2008). New processes for the production of solar-grade polycrystalline silicon: A review. Solar Energy Materials and Solar Cells, 92, 418–424. https://doi.org/10.1016/j.solmat.2007.10.003

Bridgman, P. W. (1925). Certain Physical Properties of Single Crystals of Tungsten, Antimony, Bismuth, Tellurium, Cadmium, Zinc, and Tin. Proceedings of the American Academy of Arts and Sciences, 60(6), 305–383.

Buldini, P. L., Mevoli, A., & Lal Sharma, J. (1998). LA-ICP-MS, IC and DPASV-DPCSV determination of metallic impurities in solar-grade silicon. Talanta, 47, 203–212. https://doi.org/10.1016/S0039-9140(98)00065-4

Buonassisi, T., Istratov, A. A., Pickett, M. D., Rakotoniaina, J. P., Breitenstein, O., Marcus, M. A., … Weber, E. R. (2006). Transition metals in photovoltaic-grade ingot-cast multicrystalline silicon: Assessing the role of impurities in silicon nitride crucible lining material. Journal of Crystal Growth, 287, 402–407. https://doi.org/10.1016/j.jcrysgro.2005.11.053

Bye, G., & Ceccaroli, B. (2014). Solar grade silicon: Technology status and industrial trends. Solar Energy Materials and Solar Cells, 130, 634–646. https://doi.org/10.1016/j.solmat.2014.06.019

Cai, J., Luo, X.-T., Lu, C.-H., Haarberg, G. M., Laurent, A., Kongstein, O. E., & Wang, S.-L. (2012). Purification of metallurgical grade silicon by electrorefining in molten salts. Transactions of Nonferrous Metals Society of China, 22, 3103–3107. https://doi.org/10.1016/S1003-6326(11)61577-X

Ceccaroli, B., & Lohne, O. (2003). Solar Grade Silicon Feedstock. Handbook of Photovoltaic Science and Engineering.

Ciftja, A. (2012). Refining of solar cell silicon through metallurgical routes. JOM, 64(8), 933–934. https://doi.org/10.1007/s11837-012-0385-2

Ciftja, A., Engh, T. A., & Tangstad, M. (2008). Refining and Recycling of Silicon : A Review.

Criado, A. J., Martínez, J. A., & Calabrés, R. (1997). Growth of eutectic silicon from primary silicon crystals in aluminium-silicon alloys. Scripta Materialia, 36(1), 47–54. https://doi.org/10.1016/S1359-6462(96)00332-6

Crystal Systems Inc. (2008). Development of Solar Grade (SoG) Silicon.

Dastgheib-Shirazi, A., Steyer, M., Micard, G., Wagner, H., Altermatt, P. P., & Hahn, G. (2013). Relationships between diffusion parameters and phosphorus precipitation during the POCl3 diffusion process. Energy Procedia, 38, 254–262. https://doi.org/10.1016/j.egypro.2013.07.275

Dawless, R. K., Troup, R. L., Meier, D. L., & Rohatgi, A. (1988). Production of extreme-purity aluminum and silicon by fractional crystallization processing. Journal of Crystal Growth, 89, 68–74. https://doi.org/10.1016/0022-0248(88)90073-5

Deckert, C. A. (1978). Etching of CVD Si3N4 in Acidic Fluoride Media. Journal of The Electrochemical Society, 125(2), 320–323.

del Coso, G., del Cañizo, C., & Sinke, W. C. (2010). The impact of silicon feedstock on the PV module cost. Solar Energy Materials and Solar Cells, 94, 345–349. https://doi.org/10.1016/j.solmat.2009.10.011

Delannoy, Y. (2012). Purification of silicon for photovoltaic applications. Journal of Crystal Growth, 360, 61–67. https://doi.org/10.1016/j.jcrysgro.2011.12.006

Ergül, E., Karakaya, İ., & Erdoğan, M. (2011). Electrochemical decomposition of SiO2 pellets to form silicon in molten salts. Journal of Alloys and Compounds, 509, 899–903. https://doi.org/10.1016/j.jallcom.2010.09.126

Esfahani, S. (2010). Solvent refining of metallurgical grade silicon using iron. https://doi.org/10.1016/0165-1633(87)90077-3

Fair, R. B. (1978). Analysis of Phosphorus-Diffused Layers in Silicon. Journal of The Electrochemical Society, 125(2), 323–327.

Fair, R. B., & Tsai, J. C. C. (1977). A Quantitative Model for the Diffusion of Phosphorus in Silicon and the Emitter Dip Effect. Journal of The Electrochemical Society, 124, 1107–1118. https://doi.org/10.1149/1.2133492

Fellmeth, T., Mack, S., Bartsch, J., Erath, D., Jäger, U., Preu, R., … Biro, D. (2011). 20.1% Efficient Silicon Solar Cell With Aluminum Back Surface Field. IEEE Electron Device Letters, 32(8), 1101–1103. https://doi.org/10.1109/LED.2011.2157656

Ferrazza, F. (2012). Crystalline Silicon: Manufacture and Properties. Practical Handbook of Photovoltaics. Elsevier Ltd. https://doi.org/10.1016/B978-0-12-385934-1.00004-0

Fertani-Gmati, M., & Jemal, M. (2011). Thermochemistry and kinetics of silica dissolution in NaOH aqueous solution. Thermochimica Acta, 513, 43–48. https://doi.org/10.1016/j.tca.2010.11.008

Flamant, G., Kurtcuoglu, V., Murray, J., & Steinfeld, A. (2006). Purification of metallurgical grade silicon by a solar process. Solar Energy Materials and Solar Cells, 90, 2099–2106. https://doi.org/10.1016/j.solmat.2006.02.009

Fossum, J. G., & Burgess, E. L. (1978). High-efficiency p+-n-n+ back-surface-field silicon solar cells. Applied Physics Letters, 33(3), 238–240. https://doi.org/10.1063/1.90311

Frisson, L., Lieten, K., Bruton, T., Declercq, K., Szlufcik, J., de Moor, H., … Aceves, O. (2000). Recent improvements in industrial PV module recycling. In 16th European Photovoltaic Solar Energy Conference.

Glöckner, R., & de Wild-Scholten, M. (2012). Energy Payback Time and Carbon Footprint of Elkem Solar Silicon®. In 27th European Photovoltaic Solar Energy Conference and Exhibition (pp. 4661–4666).

Glunz, S. W., Preu, R., & Biro, D. (2012). Crystalline Silicon Solar Cells – State-of-the-Art and Future Developments. In Comprehensive Renewable Energy (Vol. 1). https://doi.org/10.1016/B978-0-08-087872-0.00117-7

Gratz, A. J., Bird, P., & Quiro, G. B. (1990). Dissolution of quartz in aqueous basic solution, 106-236°C: Surface kinetics of "perfect" crystallographic faces. Geochimica et Cosmochimica Acta, 54, 2911–2922. https://doi.org/10.1016/0016-7037(90)90109-X

Green, D. W., & Perry, R. H. (2008). Perry's Chemical Engineers' Handbook (8th ed.). McGraw-Hill.

Green, M. A. (1987). High Efficiency Silicon Solar Cells. In Seventh E.C. Photovoltaic Solar Energy Conference (pp. 681–687).

Greenberg, S. A. (1956). The Depolymerization of Silica in Sodium Hydroxide Solutions.

Gu, X., Yu, X., & Yang, D. (2011). Low-cost solar grade silicon purification process with Al-Si system using a powder metallurgy technique. Separation and Purification Technology, 77, 33–39. https://doi.org/10.1016/j.seppur.2010.11.016

Guenther, K.-M., Baumann, A. L., Gimpel, T., Kontermann, S., & Schade, W. (2012). Tandem solar cell concept using Black Silicon for enhanced infrared absorption. Energy Procedia, 27, 555–560. https://doi.org/10.1016/j.egypro.2012.07.109

Guo, H., Su, B., Zhang, J., Shao, J., Zuo, H., & Ren, S. (2012). Energy conservation for granular coal injection into a blast furnace. Jom, 64(8), 1002–1010. https://doi.org/10.1007/s11837-012-0390-5

Haarberg, G. M., Famiyeh, Lord, Martinez, A. M., & Osen, K. S. (2013). Electrodeposition of silicon from fluoride melts. Electrochimica Acta, 100, 226–228. https://doi.org/10.1016/j.electacta.2012.11.052

Hampel, J., Boldt, F. M., Gerstenberg, H., Hampel, G., Kratz, J. V., Reber, S., & Wiehl, N. (2011). Fast determination of impurities in metallurgical grade silicon for photovoltaics by instrumental neutron activation analysis. Applied Radiation and Isotopes, 69, 1365–1368. https://doi.org/10.1016/j.apradiso.2011.05.024

Hargreaves, J. K., & Millard, D. (1962). The accuracy of four-probe resistivity measurements on silicon. British Journal of Applied Physics, 13, 231–234.

Hofstetter, J., Lelièvre, J. F., del Cañizo, C., & Luque, A. (2009). Acceptable contamination levels in solar grade silicon: From feedstock to solar cell. Materials Science and Engineering B, 159–160, 299–304. https://doi.org/10.1016/j.mseb.2008.05.021

Hopkins, R. L. (1958). Light Diffracting Striations in Silicon. Journal of Applied Physics, 29, 1378–1379. https://doi.org/10.1063/1.1723452

Huang, L., Danaei, A., Thomas, S., Xing, P., Li, J., Luo, X., & Barati, M. (2018). Solvent extraction of phosphorus from Si-Cu refining system with calcium addition. Separation and Purification Technology, 204, 205–212. https://doi.org/10.1016/j.seppur.2018.04.087

Huang, W.-H., & Tao, M. (2015). A Simple Green Process to Recycle Si from Crystalline-Si Solar Cells. In 2015 IEEE 42nd Photovoltaic Specialist Conference (PVSC). IEEE. https://doi.org/10.1109/PVSC.2015.7356259

Huang, W.-H., Shin, W. J., Wang, L., Sun, W.-C., & Tao, M. (2017). Strategy and technology to recycle wafer-silicon solar modules. Solar Energy, 144, 22–31. https://doi.org/10.1016/j.solener.2017.01.001

Huang, Z., Liu, C., Yuan, X., Liu, S., & Liu, F. (2013). Development of a Polysilicon Chemical Vapor Deposition Reactor Using the Computational Fluid Dynamics Method. ECS Journal of Solid State Science and Technology, 2(11), 457–464. https://doi.org/10.1149/2.027311jss

Irvin, J. C. (1962). Resistivity of Bulk Silicon and of Diffused Layers in Silicon. The Bell System Technical Journal, 49(2), 387–410.

Islam, M. S. (2015). Electrically Enhanced Slag-Metal Reactions.

Istratov, A. A., Buonassisi, T., Pickett, M. D., Heuer, M., & Weber, E. R. (2006). Control of metal impurities in "dirty" multicrystalline silicon for solar cells. Materials Science and Engineering B, 134, 282–286. https://doi.org/10.1016/j.mseb.2006.06.023

Jendoubi, F., Mgaidi, A., & El Maaoui, M. (1997). Kinetics of the Dissolution of Silica in Aqueous Sodium Hydroxide Solutions at High Pressure and Temperature. The Canadian Journal of Chemical Engineering, 75, 721–727.

Jester, T. (2014). Solar-grade silicon: Viable option to "EG." Renewable Energy Focus, 34–35. https://doi.org/10.1016/S1755-0084(14)70045-6

Johnston, M. D., & Barati, M. (2010). Distribution of impurity elements in slag-silicon equilibria for oxidative refining of metallurgical silicon for solar cell applications. Solar Energy Materials and Solar Cells, 94, 2085–2090. https://doi.org/10.1016/j.solmat.2010.06.025

Johnston, M. D., Khajavi, L. T., Li, M., Sokhanvaran, S., & Barati, M. (2012). High-temperature refining of metallurgical-grade silicon: A review. JOM, 64(8), 935–945. https://doi.org/10.1007/s11837-012-0384-3

Jung, E. J., Moon, B. M., & Min, D. J. (2011). Quantitative evaluation for effective removal of phosphorus for SoG-Si. Solar Energy Materials and Solar Cells, 95, 1779–1784. https://doi.org/10.1016/j.solmat.2011.02.001

Jung, E. J., Moon, B. M., Seok, S. H., & Min, D. J. (2014). The mechanism of boron removal in the CaO-SiO2-Al2O3 slag system for SoG-Si. Energy, 66, 35–40. https://doi.org/10.1016/j.energy.2013.08.010

Jung, I.-H., & Zhang, Y. (2012). Thermodynamic calculations for the dephosphorization of silicon using molten slag. JOM, 64(8), 973–981. https://doi.org/10.1007/s11837-012-0387-0

Khattak, C. P., Joyce, D. B., & Schmid, F. (2001). Production of Solar Grade (SoG) Silicon by Refining Liquid Metallurgical Grade (MG) Silicon.

Khattak, C. P., Joyce, D. B., & Schmid, F. (2002). A simple process to remove boron from metallurgical grade silicon. Solar Energy Materials and Solar Cells, 74, 77–89. https://doi.org/10.1016/S0927-0248(02)00051-X

Kim, K. Y. (2014). Separation of primary solid phases from Al-Si alloy melts. China Foundry, 11(4), 382–395.

Kluska, S., & Granek, F. (2011). High-Efficiency Silicon Solar Cells With Boron Local Back Surface Fields Formed by Laser Chemical Processing. IEEE Electron Device Letters, 32(9), 1257–1259.

Knotter, D. M., & Denteneer, T. J. J. (2001). Etching Mechanism of Silicon Nitride in HF-Based Solutions. Journal of The Electrochemical Society, 148(3), F43–F46. https://doi.org/10.1149/1.1348262

Kobayashi, K., Shingu, P. H., & Ozaki, R. (1975). Crystal growth of the primary silicon in an Al-16 wt % Si alloy. Journal of Materials Science, 10(2), 290–299. https://doi.org/10.1007/BF00540353

Kropp, M., & Lang, W. (2015). None hazardous chemical method for etching thin film silicon nitride using aqueous solutions of chelating agents. Procedia Engineering, 120, 1107–1110. https://doi.org/10.1016/j.proeng.2015.08.796

Krystad, E., Tang, K., & Tranell, G. (2012). The kinetics of boron transfer in slag refining of silicon. JOM, 64(8), 968–972. https://doi.org/10.1007/s11837-012-0382-5

Lai, C., Li, X. M., Xiang, Z., Tao, Z., Zhang, D. X., & Yang, W. J. (2014). Study on corrosion of porous silicon in KOH and NaOH solution. Corrosion Engineering, Science and Technology, 49(5), 386–389. https://doi.org/10.1179/1743278214Y.0000000151

Lai, C., Li, X., Zhang, D., Xiang, Z., & Yang, W. (2014). Fabrication and corrosion behavior of fresh porous silicon in sodium hydroxide solution. Materials Chemistry and Physics, 144, 355–360. https://doi.org/10.1016/j.matchemphys.2014.01.002

Lai, C., Xiang, Z., Liu, C., Zhu, C., Wang, H., & Zhu, H. (2015). Study on Corrosion of Macroporous Silicon in Sodium Hydroxide Solution by Electrochemical Methods and Scanning Electron Microscopy. International Journal of Corrosion.

Larbi, K. K. (2010). Synthesis of High Purity Silicon from Rice Husks. Retrieved from https://tspace.library.utoronto.ca/handle/1807/24595

Lee, J. Y., & Lee, S. H. (2016). Boron back surface field using spin-on dopants by rapid thermal processing. Journal of the Korean Physical Society, (July 2004).

Lee, J., Lee, C., & Yoon, W. (2012). Behavior of the impurity-rich phase in metallurgical grade silicon during fractional melting. Journal of Nanoscience and Nanotechnology, 12, 3473–3477. https://doi.org/10.1166/jnn.2012.5570

Lee, S.-C., Hur, J.-M., & Seo, C.-S. (2008). Silicon powder production by electrochemical reduction of SiO2 in molten LiCl-Li2O. Journal of Industrial and Engineering Chemistry, 14, 651–654. https://doi.org/10.1016/j.jiec.2008.04.010

Lee, W., Yoon, W., & Park, C. (2009). Purification of metallurgical-grade silicon in fractional melting process. Journal of Crystal Growth, 312, 146–148. https://doi.org/10.1016/j.jcrysgro.2009.09.050

Li, J., Bai, X., Ban, B., He, Q., & Chen, J. (2016). Mechanism of boron removal from Si–Al melt by Ar–H2 gas mixtures. Transactions of Nonferrous Metals Society of China, 26, 3046–3051. https://doi.org/10.1016/S1003-6326(16)64435-7

Li, J., Guo, Z., Tang, H., Wang, Z., & Sun, S. (2012). Si purification by solidification of Al-Si melt with super gravity. Transactions of Nonferrous Metals Society of China, 22, 958–963. https://doi.org/10.1016/S1003-6326(11)61270-3

Li, Y., Tan, Y., Li, J., Xu, Q., & Liu, Y. (2014). Effect of Sn content on microstructure and boron distribution in Si-Al alloy. Journal of Alloys and Compounds, 583, 85–90. https://doi.org/10.1016/j.jallcom.2013.08.145

Liang, Z. C., Chen, D. M., Liang, X. Q., Yang, Z. J., Shen, H., & Shi, J. (2010). Crystalline Si solar cells based on solar grade silicon materials. Renewable Energy, 35, 2297–2300. https://doi.org/10.1016/j.renene.2010.02.027

Limmanee, A., Sugiura, T., Yamamoto, H., Sato, T., Miyajima, S., Yamada, A., & Konagai, M. (2008). Boron-doped Microcrystalline Silicon Oxide Film for Use as Back Surface Field in Cast Polycrystalline Silicon Solar Cells. Japanese Journal of Applied Physics, 47(12), 8796–8798. https://doi.org/10.1143/JJAP.47.8796

Liu, T., Dong, Z., Zhao, Y., Wang, J., Chen, T., Xie, H., … Huo, D. (2012). Purification of metallurgical silicon through directional solidification in a large cold crucible. Journal of Crystal Growth, 355, 145–150. https://doi.org/10.1016/j.jcrysgro.2012.06.037

Lu, J.-C., Chen, P.-N., Chen, C.-M., & Wu, C.-H. (2013). Improvements to the solar cell efficiency and production yields of low-lifetime wafers with effective phosphorus gettering. Materials Science and Engineering B. https://doi.org/10.1016/j.mseb.2013.06.019

Luo, X., Cao, J., Gong, H., Yan, H., & He, L. (2018). Phase separation technology based on ultrasonic standing waves : A review. Ultrasonics - Sonochemistry, 48, 287–298. https://doi.org/10.1016/j.ultsonch.2018.06.006

Ma, X., Zhang, J., Wang, T., & Li, T. (2009). Hydrometallurgical purification of metallurgical grade silicon. Rare Metals, 28(3), 221–225. https://doi.org/10.1007/s12598-009-0043-1

Maoudj, M., Bouhafs, D., Bourouba, N., Boufnik, R., El Amrani, A., & Ferhat, A. H. (2015). Comparative study of etching silicon wafers with NaOH and KOH solutions. International Journal of Computational and Experimental Science and Engineering, 1(2), 7–11.

Martin, P. J., Netterfield, R. P., Sainty, W. G., & Pacey, C. G. (1984). The preparation and characterization of optical thin films produced by ionassisted deposition. Journal of Vacuum Science & Technology A, 341, 341–345. https://doi.org/10.1116/1.572735

Massot, L., Bieber, A. L., Gibilaro, M., Cassayre, L., Taxil, P., & Chamelot, P. (2013). Silicon recovery from silicon-iron alloys by electrorefining in molten fluorides. Electrochimica Acta, 96, 97–102. https://doi.org/10.1016/j.electacta.2013.02.065

Mauk, M. G. (2003). Silicon Solar Cells : Physical Metallurgy Principles. JOM, 38–42.

Mei, P. R., Moreira, S. P., Cardoso, E., Côrtes, A. D. S., & Marques, F. C. (2012). Purification of metallurgical silicon by horizontal zone melting. Solar Energy Materials and Solar Cells, 98, 233–239. https://doi.org/10.1016/j.solmat.2011.11.014

Meteleva-Fischer, Y. V., Yang, Y., Boom, R., Kraaijveld, B., & Kuntzel, H. (2012). Slag treatment followed by acid leaching as a route to solar-grade silicon. JOM, 64(8), 957–967. https://doi.org/10.1007/s11837-012-0383-4

Miki, T., Morita, K., & Sano, N. (1996). Thermodynamics of Phosphorus in Molten Silicon. Metallurgical and Materials Transactions B, 27B, 937–941. https://doi.org/10.1007/s11663-997-0071-x

Mitrašinović, A. (2010). Characterization of the Cu-Si System and Utilization of Metallurgical Techniques in Silicon Refining for Solar Cell Applications. Retrieved from https://tspace.library.utoronto.ca/handle/1807/26210

Morita, K., & Miki, T. (2003). Thermodynamics of solar-grade-silicon refining. Intermetallics, 11, 1111–1117. https://doi.org/10.1016/S0966-9795(03)00148-1

Morita, K., & Yoshikawa, T. (2011). Thermodynamic evaluation of new metallurgical refining processes for SOG-silicon production. Transactions of Nonferrous Metals Society of China, 21, 685–690. https://doi.org/10.1016/S1003-6326(11)60766-8

Mount, G., Wang, L., Putyera, K., & LePage, M. (n.d.). Characterization of Solar Grade Silicon Contaminants.

Mukashev, B. N., Abdullin, K. A., Tamendarov, M. F., Turmagambetov, T. S., Beketov, B. A., Page, M. R., & Kline, D. M. (2009). A metallurgical route to produce upgraded silicon and monosilane. Solar Energy Materials and Solar Cells, 93, 1785–1791. https://doi.org/10.1016/j.solmat.2009.06.011

Müller, A., Ghosh, M., Sonnenschein, R., & Woditsch, P. (2006). Silicon for photovoltaic applications. Materials Science and Engineering B, 134, 257–262. https://doi.org/10.1016/j.mseb.2006.06.054

Murray Bullid, W. (1974). Standard Measurements of the Resistivity of Silicon by the Four-Probe Method.

Murray, J. P., Flamant, G., & Roos, C. J. (2006). Silicon and solar-grade silicon production by solar dissociation of Si3N4. Solar Energy, 80, 1349–1354. https://doi.org/10.1016/j.solener.2005.11.009

Narasimha, S., Rohatgi, A., & Weeber, A. W. (1999). An Optimized Rapid Aluminum Back Surface Field Technique for Silicon Solar Cells. IEEE Transactions on Electron Devices, 46(7), 1363–1370.

Nordstrand, E. F., & Tangstad, M. (2012). Removal of boron from silicon by moist hydrogen gas. Metallurgical and Materials Transactions B, 43B, 814–822. https://doi.org/10.1007/s11663-012-9671-1

Obinata, I., & Komatsu, N. (1957). Method of refining silicon by alloying.

Odden, J. O., Halvorsen, G., Rong, H., & Gløckner, R. (2008). Comparison of the energy consumption in different production processes for solar grade silicon. Silicon for the Chemical and Solar Industry IX. Retrieved from https://elkem.com/Global/solar/innovation/research-papers/comparison-of-the-energy-consumption-in-different.pdf

Park, S., Park, H., Kang, Y., Lee, H., & Kim, D. (2016). Analysis of aluminum back surface field at different wafer specifications in crystalline silicon solar cells. Current Applied Physics, 16, 1062–1068. https://doi.org/10.1016/j.cap.2016.05.016

Petersen, K. E. (1982). Silicon as a Mechanical Material. In Proceedings of the IEEE (Vol. 70, pp. 420–457). IEEE. https://doi.org/10.1109/PROC.1982.12331

Petit, B., Pelletier, J., & Molins, R. (1985). A Novel Processing Technique for the Fabrication of Thick Silicon Grids by Anisotropic Etching. Journal of The Electrochemical Society, 982–984.

Pizzini, S. (2010). Towards solar grade silicon: Challenges and benefits for low cost photovoltaics. Solar Energy Materials and Solar Cells, 94, 1528–1533. https://doi.org/10.1016/j.solmat.2010.01.016

Ramos, A., Filtvedt, W. O., Lindholm, D., Ramachandran, P. A., Rodríguez, A., & Del Cañizo, C. (2015). Deposition reactors for solar grade silicon: A comparative thermal analysis of a Siemens reactor and a fluidized bed reactor. Journal of Crystal Growth, 431, 1–9. https://doi.org/10.1016/j.jcrysgro.2015.08.023

Ranjan, S., Balaji, S., Panella, R. A., & Ydstie, B. E. (2011). Silicon solar cell production. Computers and Chemical Engineering, 35, 1439–1453. https://doi.org/10.1016/j.compchemeng.2011.04.017

Rappich, J., & Lewerenz, H. J. (1993). The Surface of Si (111) during Etching in NaOH Studied by FTIR Spectroscopy in the ATR Technique RE CS RE ir light, 140(12), 187–189.

Reznichenko, M. (2016). Evolution of Requirements for Solar Grade Silicon. Procedia Engineering, 139, 41–46. https://doi.org/10.1016/j.proeng.2015.09.223

Richter, A., Benick, J., Feldmann, F., Fell, A., Hermle, M., & Glunz, S. W. (2017). n-Type Si solar cells with passivating electron contact: Identifying sources for efficiency limitations by wafer thickness and resistivity variation. Solar Energy Materials and Solar Cells, 173, 96–105. https://doi.org/10.1016/j.solmat.2017.05.042

Rimsza, J. M., Jones, R. E., & Criscenti, L. J. (2018). Interaction of NaOH solutions with silica surfaces. Journal of Colloid And Interface Science, 516, 128–137. https://doi.org/10.1016/j.jcis.2018.01.049

Ryu, H. Y., An, Y. S., Jang, B. Y., Lee, J. S., Nersisyan, H. H., Han, M. H., … Lee, J. H. (2012). Formation of high purity Si nanofiber from metallurgical grade Si by molten salt electrorefining. Materials Chemistry and Physics, 137, 160–168. https://doi.org/10.1016/j.matchemphys.2012.08.075

Safarian, J., & Tangstad, M. (2012). Vacuum refining of molten silicon. Metallurgical and Materials Transactions B, 43B, 1427–1445. https://doi.org/10.1007/s11663-012-9728-1

Safarian, J., & Tangstad, M. (2012). Kinetics and Mechanism of Phosphorus Removal from Silicon in Vacuum Induction Refining. High Temperature Materials and Processes, 31. https://doi.org/10.1515/htmp.2011.143

Safarian, J., Tranell, G., & Tangstad, M. (2012). Processes for upgrading metallurgical grade silicon to solar grade silicon. Energy Procedia, 20, 88–97. https://doi.org/10.1016/j.egypro.2012.03.011

Sarti, D., & Einhaus, R. (2002). Silicon feedstock for the multi-crystalline photovoltaic industry. Solar Energy Materials and Solar Cells, 72, 27–40. https://doi.org/10.1016/S0927-0248(01)00147-7

Schindler, F., Fell, A., Müller, R., Benick, J., Richter, A., Feldmann, F., … Glunz, S. W. (2018). Towards the efficiency limits of multicrystalline silicon solar cells. Solar Energy Materials and Solar Cells, 185, 198–204. https://doi.org/10.1016/j.solmat.2018.05.006

Schlosser, R., & Münzer, A. (2000). Solar Cell with a Back-Surface Field.

Schmid, F., & Joyce, D. B. (2009). Recent advances in upgrading Metallurgical Grade (MG) silicon for Solar Grade (SoG) silicon feedstock.

Seidel, H., Csepregi, L., Hauberger, A., & Baumgärtel, H. (1990). Anisotropic Etching of Crystalline Silicon in Alkaline Solutions II. Influence of Dopants. Journal of The Electrochemical Society, 137, 3626–3632.

Seidel, H., Csepregi, L., Hauberger, A., & Baumgärtel, H. (1990). Anisotropic Etching of Crystalline Silicon in Alkaline Solutions I. Orientation dependence and Behaviour of Passivation Layers. Journal of The Electrochemical Society, 137, 3612–3626.

Shi, S., & Yang, X. (2014). Development and situation of boron removal from solar grade silicon. In International Conference on Logistics, Engineering, Management and Computer Science, LEMCS 2014 (pp. 107–111).

Shin, J., Park, J., & Park, N. (2017). A method to recycle silicon wafer from end-of-life photovoltaic module and solar panels by using recycled silicon wafers. Solar Energy Materials and Solar Cells, 162, 1–6. https://doi.org/10.1016/j.solmat.2016.12.038

Silicor Materials. (2012). How did we revolutionize the solar industry? Photon Magazine.

Sio, H. C., Xiong, Z., Trupke, T., & Macdonald, D. (2012). Imaging crystal orientations in multicrystalline silicon wafers via photoluminescence. Applied Physics Letters, 101. https://doi.org/10.1063/1.4747801

Smits, F. M. (1958). Measurement of Sheet Resistivities with the Four-Point Probe. The Bell System Technical Journal, 711–718.

Søiland, A.-K., Dolmen, M. G., Heide, J., Thisted, U., Halvorsen, G., Ausland, G., … Tronstad, R. (2014). Solar Energy Materials & Solar Cells First results from a simpli fi ed Elkem

Solar route — Input to tolerance limits. Solar Energy Materials & Solar Cells, 130, 661–667. https://doi.org/10.1016/j.solmat.2014.04.012

Sun, Y.-H., Ye, Q.-H., Guo, C.-J., Chen, H.-Y., Lang, X., David, F., … Yang, C.-M. (2013). Purification of metallurgical-grade silicon via acid leaching, calcination and quenching before boron complexation. Hydrometallurgy, 139, 64–72. https://doi.org/10.1016/j.hydromet.2013.07.002

Swanson, R. M. (2006). A vision for crystalline silicon photovoltaics. Progress in Photovoltaics: Research and Applications, 14, 443–453. https://doi.org/10.1002/pip

Tang, K. (2012). A Novel Slag Treatment for B and P Removals in the UMG-Si.

Tang, K., Andersson, S., Nordstrand, E., & Tangstad, M. (2012). Removal of boron in silicon by H2-H2O gas mixtures. JOM, 64(8), 952–956. https://doi.org/10.1007/s11837-012-0368-3

Tao, J., & Yu, S. (2015). Review on feasible recycling pathways and technologies of solar photovoltaic modules. Solar Energy Materials and Solar Cells, 141, 108–124. https://doi.org/10.1016/j.solmat.2015.05.005

Theuerer, H. C. (1956). Removal of boron from silicon by hydrogen water vapor treatment. Journal of Metals, 1316–1319.

Thurber, W. R., Mattis, R. L., Liu, Y. M., & Filliben, J. J. (1980). Resistivity-Dopant Density Relationship for Boron-Doped Silicon. Journal of The Electrochemical Society, 2291–2294.

Thurber, W. R., Mattis, R. L., Liu, Y. M., & Filliben, J. J. (1980). Resistivity-Dopant Density Relationship for Phosphorus-Doped Silicon. Journal of The Electrochemical Society, 1807–1812.

Uhlir, A. (1955). The Potentials of Infinite Systems of Sources and Numerical Solutions of Problems in Semiconductor Engineering. The Bell System Technical Journal, 105–128.

Uruena, A., Horzel, J., Singh, S., Kuzma-filipek, I., Cornagliotti, E., John, B. J., … Poortmans, J. (2012). Rear contact and BSF formation for local Al-BSF solar cells. Energy Procedia, 27, 561–566. https://doi.org/10.1016/j.egypro.2012.07.110

Valdes, L. B. (1954). Reisitivity Measurements on Germanium for Transistors. In Proceedings of the IRE (pp. 420–427).

various authors. (2003). Research Trends. Membrane Technology, 12. https://doi.org/10.1016/S0958-2118(03)08019-4

Visnovec, K., Variawa, C., Utigard, T., & Mitrašinović, A. (2012). Elimination of impurities from the surface of silicon using hydrochloric and nitric acid. Materials Science in Semiconductor Processing. https://doi.org/10.1016/j.mssp.2012.06.009

von Roos, O. (1978). A simple theory of back surface field (BSF) solar cells. Journal of Applied Physics, 49, 3503–3511. https://doi.org/10.1063/1.325262

Wang, A., Zhao, J., & Green, M. A. (1990). 24% efficient silicon solar cells. Applied Physics Letters, 57, 602–604. https://doi.org/10.1063/1.103610

Wang, T. H., Ciszek, T. F., Schwerdtfeger, C. R., Moutinho, H., & Matson, R. (1996). Growth of silicon thin layers on cast MG-Si from metal solutions for solar cells. Solar Energy Materials and Solar Cells, 41/42, 19–30. https://doi.org/10.1016/0927-0248(95)00131-X

Won, C. W., Nersisyan, H. H., & Won, H. I. (2011). Solar-grade silicon powder prepared by combining combustion synthesis with hydrometallurgy. Solar Energy Materials and Solar Cells, 95, 745–750. https://doi.org/10.1016/j.solmat.2010.10.016

Wu, J., Ma, W., Yang, B., Dai, Y., & Morita, K. (2009). Boron removal from metallurgical grade silicon by oxidizing refining. Transactions of Nonferrous Metals Society of China, 19, 463–467. https://doi.org/10.1016/S1003-6326(08)60296-4

Xakalashe, B. S. (2011). Removal of Phosphorus from Silicon Melts by Vacuum Refining.

Xia, Z., Wu, J., Ma, W., Lei, Y., Wei, K., & Dai, Y. (2017). Separation of boron from metallurgical grade silicon by a synthetic CaO-CaCl2 slag treatment and Ar-H2O-O2 gas blowing refining technique. Separation and Purification Technology, 187, 25–33. https://doi.org/10.1016/j.seppur.2017.06.037

Xiao, W., Jin, X., Deng, Y., Wang, D., & Chen, G. Z. (2010). Rationalisation and optimisation of solid state electro-reduction of SiO2 to Si in molten CaCl2 in accordance with dynamic three-phase interlines based voltammetry. Journal of Electroanalytical Chemistry, 639, 130–140. https://doi.org/10.1016/j.jelechem.2009.12.001

Xu, Y., Li, J., Tan, Q., Peters, A. L., & Yang, C. (2018). Global status of recycling waste solar panels: A review. Waste Management, 75, 450–458. https://doi.org/10.1016/j.wasman.2018.01.036

Yadav, S., Chattopadhyay, K., & Singh, C. V. (2017). Solar grade silicon production: A review of kinetic, thermodynamic and fluid dynamics based continuum scale modeling. Renewable and Sustainable Energy Reviews, 78, 1288–1314. https://doi.org/10.1016/j.rser.2017.05.019

Yasuda, K., Morita, K., & Okabe, T. H. (2014). Processes for Production of Solar-Grade Silicon Using Hydrogen Reduction and/or Thermal Decomposition. Energy Technology, 2, 141–154. https://doi.org/10.1002/ente.201300131

Yasuda, K., Nohira, T., Hagiwara, R., & Ogata, Y. H. (2007). Direct electrolytic reduction of solid SiO2 in molten CaCl2 for the production of solar grade silicon. Electrochimica Acta, 53, 106–110. https://doi.org/10.1016/j.electacta.2007.01.024

Yasuda, K., & Okabe, T. H. (2010). Solar-grade silicon production by metallothermic reduction. JOM, 62(12), 94–101. https://doi.org/10.1007/s11837-010-0190-8

Yoshikawa, T., & Morita, K. (2012). An evolving method for solar-grade silicon production: Solvent refining. JOM, 64(8), 946–951. https://doi.org/10.1007/s11837-012-0371-8

Yoshikawa, T., & Morita, K. (2005). Thermodynamics of solid silicon equilibrated with Si-Al-Cu liquid alloys. Journal of Physics and Chemistry of Solids, 66, 261–265. https://doi.org/10.1016/j.jpcs.2004.08.036

Yoshikawa, T., & Morita, K. (2009). Refining of silicon during its solidification from a Si-Al melt. Journal of Crystal Growth, 311, 776–779. https://doi.org/10.1016/j.jcrysgro.2008.09.095

Yuge, N., Abe, M., Hanazawa, K., Baba, H., Nakamura, N., Kato, Y., … Aratani, F. (2001). Purification of metallurgical-grade silicon up to solar grade. Progress in Photovoltaics: Research and Applications, 9, 203–209. https://doi.org/10.1002/pip.372

Zhang, C., Wei, K., Zheng, D., Ma, W., & Dai, Y. (2017). Phosphorus removal from upgraded metallurgical-grade silicon by vacuum directional solidification. Vacuum, 146, 159–163. https://doi.org/10.1016/j.vacuum.2017.08.037

Zhao, L., Wang, Z., Guo, Z., & Li, C. (2011). Low-temperature purification process of metallurgical silicon. Transactions of Nonferrous Metals Society of China, 21, 1185–1192. https://doi.org/10.1016/S1003-6326(11)60841-8

Zheng, S., Engh, T. A., Tangstad, M., & Luo, X. (2011). Separation of Phosphorus from silicon by induction vacuum refining. Separation and Purification Technology, 82, 128–137. https://doi.org/10.1016/j.seppur.2011.09.001

Zheng, S. S., Engh, T. A., Tangstad, M., & Luo, X.-T. (2011). Separation of Phosphorus from silicon by induction vacuum refining. Separation and Purification Technology, 82(1), 128–137. https://doi.org/10.1016/j.seppur.2011.09.001

Zheng, S.-S., Chen, W.-H., Cai, J., Li, J. T., Chen, C., & Luo, X.-T. (2010). Mass transfer of phosphorus in silicon melts under vacuum induction refining. Metallurgical and Materials Transactions B: Process Metallurgy and Materials Processing Science, 41(6), 1268–1273. https://doi.org/10.1007/s11663-010-9422-0

Zheng, S., Safarian, J., Seok, S., Kim, S., Tangstad, M., & Luo, X.-T. (2011). Elimination of phosphorus vaporizing from molten silicon at finite reduced pressure. Transactions of Nonferrous Metals Society of China, 21, 697–702. https://doi.org/10.1016/S1003-6326(11)60768-1

A. EXPERIMENT RESULTS TABLES

Tab. A.1 displays the results of the sodium hydroxide etching experiments on silicon, and it can be found in the following pages.

From page A-2 to A-22 the values for the mass m, measured before and after the treatment, thickness d, measured before and after the treatment, average roughness Ra, measured after the experiment for the most interesting samples, surface area A and resistivity ϱ, measured after the experiment, are reported. Instead, the time when the first bubbles appear τ_{in} and when almost half of the surface is covered by bubbles $\tau_{50\%}$ are shown in pages A-23 and A-24.

In the surface area column, the grey boxes mean that after the treatment the sample broke. This new value of the surface area has been calculated with the final mass and the final average thickness (obtained by the thickness calculated in five points instead of three, to decrease the error due to the different thickness measured in points of the same samples after long time and high temperature etching).

The symbol *U.* at page A-22 stands for "unmeasurable": the sample has been almost completely dissolved in the sodium hydroxide solution after the treatment, so it was impossible to measure the thickness and the resistivity.

Tab A.1 Measured quantities for NaOH etching treatment

	30°C - 15 min								
	m_{in} [g]	d_{in} [µm]	avg d_{in} [µm]	m_{fin} [g]	d_{fin} [µm]	avg d_{fin} [µm]	$R_{a,fin}$ [µm]	avg $R_{a,fin}$ [µm]	A [mm^2]
2,5 wt. %	0,2656	192 195 192	193,0	0,2654	193 193 192	192,6667			593,1749
	0,2669	206 200 199	192,6667	0,2444	193 192 192	192,3333			546,7725
5 wt. %	0,2346	210 195 206	203,6667	0,2346	195 197 197	196,3333			416,0189
	0,2939	207 209 212	194,3333	0,2731	194 193 195	194,0			605,7402
10 wt. %	0,1964	193 193 195	193,6667	0,1961	195 193 191	193,0			437,1179
	0,2259	208 209 210	194,3333	0,1480	195 194 194	194,3333			239,8606
15 wt. %	0,2386	193 192 191	192,0	0,2382	189 192 190	190,3333			465,7441
	0,1737	212 212 206	196,0	0,2074	193 197 197	195,6667			462,3946
20 wt. %	0,1536	191 192 192	191,6667	0,1532	190 191 191	190,6667			345,4273
	0,1591	195 194 192	192,6667	0,2136	192 191 192	191,6667			313,9746
25 wt. %	0,2131	191 193 192	192,0	0,2124	188 192 191	190,3333			271,5017
	0,1594	193 192 191	210,0	0,3189	211 208 209	209,3333			655,3777

	30°C - 30 min								
	m_{in} [g]	**d_{in} [µm]**	**avg d_{in} [µm]**	**m_{fin} [g]**	**d_{fin} [µm]**	**avg d_{fin} [µm]**	**$R_{a,fin}$ [µm]**	**avg $R_{a,fin}$ [µm]**	**A [mm^2]**
2,5 wt. %	0,2444	192 193 193	201,6667	0,2666	206 200 199	201,6667			533,7221
	0,1829	188 189 188	188,3333	0,1801	190 189 189	189,3333			418,5993
5 wt. %	0,2731	194 194 195	209,3333	0,2939	207 209 210	208,6667			605,1642
	0,2189	184 192 189	188,3333	0,2194	189 192 185	188,6667			402,5401
10 wt. %	0,1481	195 194 194	209,0	0,2260	208 209 210	209,0			465,8885
	0,3300	207 207 207	207,0	0,3297	206 205 206	205,6667			375,3835
15 wt. %	0,2223	194 197 197	210,0	0,1733	210 211 207	209,3333			356,5271
	0,3155	216 211 220	215,6667	0,3154	215 211 219	215,0			630,5628
20 wt. %	0,2144	193 193 192	193,6667	0,1593	193 190 190	191,0			354,1011
	0,2893	198 200 200	199,3333	0,2888	201 200 198	199,6667			625,5766
25 wt. %	0,3193	211 208 211	192,0	0,1595	192 191 190	191,0			357,8484
	0,3690	209 206 210	208,3333	0,3678	210 208 204	207,3333			763,4483

	30°C - 60 min								
	m_{in} [g]	**d_{in} [µm]**	**avg d_{in} [µm]**	**m_{fin} [g]**	**d_{fin} [µm]**	**avg d_{fin} [µm]**	**$R_{a,fin}$ [µm]**	**avg $R_{a,fin}$ [µm]**	**A [mm^2]**
2,5 wt. %	0,2594	208 206 217	210,3333	0,2585	220 207 205	210,6667			531,5864
	0,2517	199 196 199	198,0	0,2519	204 203 204	203,6667			547,9363
5 wt. %	0,2425	188 189 188	188,3333	0,2424	188 187 187	187,3333			555,0046
	0,3151	199 197 197	197,6667	0,3151	204 202 202	202,6667			465,1192
10 wt. %	0,2015	200 200 200	200,0	0,2012	206 207 207	206,6667			376,7407
	0,2366	194 194 194	194,0	0,2366	199 202 199	200,0			505,3137
15 wt. %	0,1904	209 201 202	204,0	0,1905	208 201 204	204,3333			284,7906
	0,2021	188 188 187	187,6667	0,2009	187 190 190	189,0			464,1851
20 wt. %	0,3001	186 186 186	186,0	0,2985	183 184 183	183,3333			652,8630
	0,1987	187 184 185	185,3333	0,1979	185 185 184	184,6667			235,1949
25 wt. %	0,2459	190 187 187	188,0	0,2444	187 189 186	187,3333			361,5495
	0,2041	203 197 198	199,3333	0,2032	204 205 204	204,3333			441,3418

	40°C – 15 min								
	m_{in} [g]	**d_{in} [μm]**	**avg d_{in} [μm]**	**m_{fin} [g]**	**d_{fin} [μm]**	**avg d_{fin} [μm]**	**$R_{a,fin}$ [μm]**	**avg $R_{a,fin}$ [μm]**	**A [mm^2]**
2,5 wt. %	0,2693	202 198 199	199,6667	0,2691	208 202 206	205,3333			581,3569
	0,2785	208 204 207	206,3333	0,2782	209 208 210	209,0			506,2486
5 wt. %	0,1925	205 204 204	204,3333	0,1922	210 211 210	210,3333			406,0725
	0,1417	181 180 181	180,6667	0,1416	179 182 182	181,0			336,3591
10 wt. %	0,2077	198 201 198	199,0	0,2083	204 207 204	205,0			449,8787
	0,2001	205 204 207	205,3333	0,1998	201 205 200	202,0			299,3063
15 wt. %	0,2677	189 188 188	188,3333	0,2666	183 183 183	183,0			449,8787
	0,2100	190 188 185	187,6667	0,2095	188 187 187	187,3333			482,3299
20 wt. %	0,3772	209 207 207	188,0	0,3247	187 188 189	188,0	1,06 0,86 0,95	0,9567	590,8304
	0,2227	190 190 187	189,0	0,2220	188 190 190	189,3333	0,82 0,98 0,96	0,92	507,8909
25 wt. %	0,3260	189 187 188	207,6667	0,3772	208 207 208	207,6667			411,1180
	0,1443	207 205 205	205,6667	0,1440	201 204 206	203,6667			302,4227

	40°C - 30 min								
	m_{in} [g]	d_{in} [µm]	avg d_{in} [µm]	m_{fin} [g]	d_{fin} [µm]	avg d_{fin} [µm]	$R_{a,fin}$ [µm]	avg $R_{a,fin}$ [µm]	A [mm^2]
2,5 wt. %		208			207				
	0,2058	210	207,6667	0,2059	210	208,6667			427,1600
		205			209				
		186			189				
	0,1617	189	188,6667	0,1617	191	190,6667			369,4255
		191			192				
5 wt. %		187			186				
	0,2513	183	183,3333	0,2515	184	183,3333			440,0440
		180			180				
		186			188				
	0,1930	188	186,6667	0,1932	191	189,3333			274,8191
		186			189				
10 wt. %		202			206				
	0,2778	204	202,6667	0,2574	209	207,6667			547,0168
		202			208				
		188			190				
	0,1869	188	187,3333	0,1867	190	190,3333			430,0374
		186			191				
15 wt. %		208			202				
	0,2572	207	207,3333	0,2759	206	204,3333			380,8455
		207			205				
		206			210				
	0,1564	204	204,6667	0,1566	210	210,0			329,3834
		204			210				
20 wt. %		192			191		0,76		
	0,1606	190	191,0	0,1597	189	190,3333	0,76	0,7633	362,4300
		191			191		0,77		
		196			201		1,14		
	0,2377	197	198,0	0,2364	200	201,0	1,05	1,1333	517,4591
		201			202		1,21		
25 wt. %		205			207				
	0,2429	208	207,6667	0,2423	207	207,6667			504,1651
		210			209				
		190			193				
	0,1798	190	191,0	0,1792	191	193,0			405,7592
		193			195				

	40°C - 60 min								
	m_{in} [g]	**d_{in} [μm]**	**avg d_{in} [μm]**	**m_{fin} [g]**	**d_{fin} [μm]**	**avg d_{fin} [μm]**	**$R_{a,fin}$ [μm]**	**avg $R_{a,fin}$ [μm]**	**A [mm^2]**
2,5 wt. %	0,2011	193 193 196	194,0	0,2011	193 196 199	196,0			396,4371
	0,1993	208 206 206	206,6667	0,1991	208 206 210	208,0			415,6702
5 wt. %	0,2155	210 209 213	210,6667	0,2159	208 211 209	209,3333			440,9237
	0,1695	183 183 185	180,3333	0,2631	184 183 178	181,6667			388,3129
10 wt. %	0,2023	200 203 194	199,0	0,1984	200 202 193	198,3333			438,1823
	0,2642	176 181 184	183,6667	0,1690	178 184 183	183,0			397,7877
15 wt. %	0,2094	203 205 204	204,0	0,2070	203 204 202	203,0			442,4442
	0,1725	214 215 210	213,0	0,1711	214 213 207	211,3333			349,0772
20 wt. %	0,2318	209 208 211	209,3333	0,2271	209 206 204	206,3333	1,49 0,88 1,04	1,1367	477,2952
	0,2308	189 187 193	189,6667	0,2279	187 190 189	188,6667	0,99 0,69 0,85	0,8433	283,7335
25 wt. %	0,2803	200 200 199	199,6667	0,2746	198 197 196	197,0			605,1033
	0,2886	183 186 186	185,0	0,2840	177 181 178	178,6667			672,4138

	50°C -15 min								
	m_{in} [g]	d_{in} [µm]	avg d_{in} [µm]	m_{fin} [g]	d_{fin} [µm]	avg d_{fin} [µm]	$R_{a,fin}$ [µm]	avg $R_{a,fin}$ [µm]	A [mm^2]
2,5 wt. %		191			190				
	0,2374	191	191,0	0,2374	192	191,0			535,7465
		191			191				
		185			184				
	0,1861	186	185,0	0,1816	185	184,0			433,5974
		184			183				
5 wt. %		202			190				
	0,2216	190	194,0	0,2211	191	192,0			455,3854
		190			195				
		212			213				
	0,1966	211	211,6667	0,1966	212	212,0			374,6185
		212			211				
10 wt. %		210			211		0,92		
	0,2431	210	210,3333	0,2427	210	210,3333	0,99	0,8167	410,9004
		211			210		0,54		
		207			207		0,68		
	0,1959	211	209,6667	0,1955	210	209,0	0,72	0,7333	402,7329
		211			210		0,8		
15 wt. %		208			207		0,56		
	0,2226	209	208,0	0,2222	211	208,6667	0,56	0,6667	461,2898
		207			208		0,88		
		214			212		0,92		
	0,1950	211	212,3333	0,1949	213	212,3333	0,92	0,8267	268,0725
		212			212		0,64		
20 wt. %		191			191		0,91		
	0,2491	191	190,0	0,2488	189	189,3333	0,92	0,87	295,1849
		188			188		0,78		
		189			187		1,4		
	0,2504	191	188,6667	0,2475	191	188,6667	2,01	1,54	355,0388
		186			188		1,21		
25 wt. %		184			182				
	0,1826	185	184,3333	0,1826	180	181,0			262,4828
		184			181				
		187			190				
	0,2104	191	187,3333	0,2101	192	191,0			386,5884
		184			191				

	50°C - 30 min								
	m_{in} [g]	**d_{in} [μm]**	**avg d_{in} [μm]**	**m_{fin} [g]**	**d_{fin} [μm]**	**avg d_{fin} [μm]**	**$R_{a,fin}$ [μm]**	**avg $R_{a,fin}$ [μm]**	**A [mm^2]**
2,5 wt. %		209			209				
	0,2176	210	209,3333	0,2176	209	209,0			448,0562
		209			209				
		188			188				
	0,2092	188	187,3333	0,2096	187	187,6667			281,6888
		186			188				
5 wt. %		216			213				
	0,1901	211	212,3333	0,1898	212	212,0			385,9010
		210			211				
		182			181				
	0,2232	185	182,6667	0,2229	181	180,6667			318,1671
		181			180				
10 wt. %		208			208		0,89		
	0,1809	210	209,0	0,1806	208	208,3333	1,03	0,9333	373,0820
		209			209		0,88		
		184			186		0,8		
	0,1579	183	185,0	0,1563	182	183,3333	1,16	0,9233	367,8938
		188			182		0,81		
15 wt. %		179			176		0,83		
	0,2366	179	179,0	0,2331	179	178,0	0,63	0,6933	205,0929
		179			179		0,62		
		187			187		1,31		
	0,2233	186	186,6667	0,2226	186	186,0	0,93	1,196666667	515,6250
		187			185		1,35		
20 wt. %		185			185		1,71		
	0,2077	188	186,6667	0,2050	187	186,0	1,21	1,2133	429,8657
		187			186		0,72		
		183			176		1,49		
	0,2411	182	182,0	0,2360	178	178,0	0,7	0,96	571,0023
		181			180		0,69		
25 wt. %		189			188				
	0,2484	190	190,0	0,2441	186	187,0			407,9351
		191			187				
		191			189				
	0,1774	189	189,3333	0,1734	189	188,3333			403,8672
		188			187				

	50°C - 60 min								
	m_{in} [g]	d_{in} [µm]	avg d_{in} [µm]	m_{fin} [g]	d_{fin} [µm]	avg d_{fin} [µm]	$R_{a,fin}$ [µm]	avg $R_{a,fin}$ [µm]	A [mm^2]
2,5 wt. %		205			204				
	0,2911	206	205,3333	0,2906	205	204,3333			611,0753
		205			204				
		184			184				
	0,1533	185	184,3333	0,1531	183	184,0			245,3402
		184			185				
5 wt. %		191			188				
	0,2225	188	187,3333	0,2221	182	182,6667			511,9493
		183			178				
		186			177				
	0,2077	180	181,3333	0,2075	181	181,6667			493,7088
		178			187				
10 wt. %		191			191		0,83		
	0,2515	190	191,0	0,2486	186	188,0	1,04	1,1933	384,0717
		192			187		1,71		
		191			190		1,06		
	0,2175	190	190,3333	0,2167	190	190,3333	0,81	0,8933	485,1392
		190			191		0,81		
15 wt. %		209			198		0,87		
	0,2710	207	206,0	0,2669	204	203,0	1,27	1,15	567,0405
		202			207		1,31		
		207			206		2,1		
	0,2196	206	207,0	0,2115	204	205,3333	1,41	1,54	457,2714
		208			206		1,11		
20 wt. %		189			187		1,22		
	0,1955	187	188,0	0,1875	186	186,0	1,35	1,2167	361,2811
		188			185		1,08		
		185			181		0,48		
	0,2063	185	185,6667	0,1967	178	179,0	0,71	0,54	349,9128
		187			178		0,43		
25 wt. %		190			183				
	0,1545	184	186,3333	0,1467	180	181,0			285,3496
		185			180				
		186			184				
	0,1576	187	186,3333	0,1508	186	184,3333			321,2694
		186			183				

	60°C - 15 min								
	m_{in} [g]	**d_{in} [μm]**	**avg d_{in} [μm]**	**m_{fin} [g]**	**d_{fin} [μm]**	**avg d_{fin} [μm]**	**$R_{a,fin}$ [μm]**	**avg $R_{a,fin}$ [μm]**	**A [mm^2]**
2,5 wt. %	0,2427	208 211 211	210,0	0,2470	209 210 211	210,0			495,6488
	0,2754	181 183 197	187,0	0,2748	199 184 183	188,6667			329,2117
5 wt. %	0,2611	191 194 195	193,3333	0,2602	193 193 192	192,6667	1,12 0,94 0,96	1,0067	503,5471
	0,1434	178 183 179	180,0	0,1433	181 184 181	182,0	0,73 0,71 0,76	0,7333	343,3908
10 wt. %	0,2012	206 216 206	209,3333	0,2009	207 218 206	210,3333	1,01 0,75 0,74	0,8333	414,2873
	0,1892	199 198 197	198,0	0,1889	199 197 199	198,3333	1,22 1,51 1,13	1,2867	411,8774
15 wt. %	0,1737	184 182 182	182,6667	0,1728	178 180 179	179,0	0,68 0,57 0,95	0,7333	384,5785
	0,2096	200 198 201	199,6667	0,2079	199 199 199	199,0	0,59 1,12 1,38	1,03	225,0861
20 wt. %	0,1981	207 206 201	204,6667	0,1951	200 203 199	200,6667	1,15 0,56 0,97	0,8933	417,2049
	0,3350	197 198 197	197,3333	0,3336	197 198 197	197,3333	1,14 1,09 1,34	1,19	731,7393
25 wt. %	0,2965	196 192 182	190,0	0,2902	178 184 195	185,6667	0,49 1,13 0,58	0,7333	460,1832
	0,3019	187 189 190	188,6667	0,2979	185 188 192	188,3333	0,57 0,63 0,67	0,6233	377,7837

	60°C - 30 min								
	m_{in} [g]	d_{in} [µm]	avg d_{in} [µm]	m_{fin} [g]	d_{fin} [µm]	avg d_{fin} [µm]	$R_{a,fin}$ [µm]	avg $R_{a,fin}$ [µm]	A [mm^2]
2,5 wt. %		215			215				
	0,2646	210	214,0	0,2643	209	213,6667			532,9520
		217			217				
		198			199				
	0,2382	200	198,6667	0,2387	199	198,3333			516,8075
		198			197				
5 wt. %		194			192		0,78		
	0,2004	188	188,3333	0,2001	188	187,6667	0,78	0,88	424,1121
		183			183		1,08		
		181			181		0,97		
	0,1507	186	184,6667	0,1503	186	185,6667	0,89	0,8767	351,7521
		187			190		0,77		
10 wt. %		198			202		0,91		
	0,3339	199	200,0	0,3301	199	199,6667	1,12	0,9967	544,2910
		203			198		0,96		
		193			191		1,03		
	0,1866	190	191,3333	0,1864	190	191,3333	1,13	1,0567	420,3713
		191			193		1,01		
15 wt. %		201			197		1,26		
	0,2781	203	201,6667	0,2747	203	199,0	1,5	1,1433	594,4001
		201			197		0,67		
		203			200		0,65		
	0,1810	201	201,3333	0,1780	198	200,3333	0,88	0,83	387,5029
		200			203		0,96		
20 wt. %		203			201		1,23		
	0,3165	204	203,0	0,3125	204	202,0	1,07	1,06	352,7799
		202			201		0,88		
		206			205		0,88		
	0,2406	209	208,0	0,2339	209	207,3333	0,91	0,9733	498,5908
		209			208		1,13		
25 wt. %		190			187		0,77		
	0,2547	190	190,0	0,2464	187	187,6667	1,28	0,97	577,8131
		190			189		0,86		
		211			207		1,04		
	0,2086	207	210,0	0,2049	205	203,6667	1,09	1,0133	207,3602
		212			199		0,91		

	60°C - 60 min								
	m_{in} [g]	**d_{in} [μm]**	**avg d_{in} [μm]**	**m_{fin} [g]**	**d_{fin} [μm]**	**avg d_{fin} [μm]**	**$R_{a,fin}$ [μm]**	**avg $R_{a,fin}$ [μm]**	**A [mm^2]**
2,5 wt. %		201			207				
	0,1769	207	205,3333	0,1766	206	204,6667			371,3474
		208			201				
		183			182				
	0,2450	181	181,0	0,2448	183	183,3333			583,4445
		179			185				
5 wt. %		211			192		0,77		
	0,1752	192	198,0	0,1744	191	193,3333	0,97	0,83	180,5439
		191			197		0,75		
		186			187		1,12		
	0,1730	191	187,0	0,1726	186	186,3333	1	1,05	398,7645
		184			186		1,03		
10 wt. %		179			179		0,95		
	0,1884	181	181,0	0,1878	181	181,3333	1,05	0,9967	448,6569
		183			184		0,99		
		187			192		0,74		
	0,2237	190	192,0	0,2154	188	187,6667	0,91	0,7733	490,9766
		199			183		0,67		
15 wt. %		187			181		0,62		
	0,1919	189	188,0	0,1783	185	183,6667	0,63	0,6633	439,9762
		188			185		0,74		
		189			184		1,51		
	0,2360	187	188,0	0,2177	186	185,6667	1,27	1,25	541,0858
		188			187		0,97		
20 wt. %		188			180		2,22		
	0,1915	188	187,6667	0,1705	184	181,0	1,34	1,4233	345,6858
		187			179		0,71		
		194			191		1,26		
	0,2829	194	193,6667	0,2578	187	188,6667	0,62	0,7767	629,6368
		193			188		0,45		
25 wt. %		203			188		0,7		
	0,1959	204	203,6667	0,1749	188	187,6667	0,55	1,0167	382,6010
		204			187		1,8		
		205			199		0,81		
	0,2616	206	205,6667	0,2370	194	196,0	0,76	0,9167	480,3082
		206			195		1,18		

	70°C - 15 min								
	m_{in} [g]	d_{in} [µm]	avg d_{in} [µm]	m_{fin} [g]	d_{fin} [µm]	avg d_{fin} [µm]	$R_{a,fin}$ [µm]	avg $R_{a,fin}$ [µm]	A [mm^2]
2,5 wt. %		184			185		0,81		
	0,1723	178	179,6667	0,1722	178	180,0	0,98	0,94	408,4111
		177			177		1,03		
		202			200		0,74		
	0,2401	202	201,3333	0,2388	202	201,3333	0,9	0,8267	232,6558
		200			202		0,84		
5 wt. %		184			184		1,16		
	0,2906	185	185,0	0,2901	187	185,6667	1,31	1,3367	644,2243
		186			186		1,54		
		202			202		1,23		
	0,2873	214	206,0	0,2862	206	203,3333	0,84	1,1033	601,1466
		202			202		1,24		
10 wt. %		204			206		1,11		
	0,2028	206	205,6667	0,2024	206	204,6667	0,84	0,9267	425,0265
		207			202		0,83		
		214			211		0,92		
	0,2729	212	212,0	0,2699	212	211,6667	0,74	0,7867	318,1737
		210			212		0,7		
15 wt. %		209			210		1,27		
	0,3124	209	209,3333	0,3081	209	209,6667	1,44	1,4367	279,3054
		210			210		1,6		
		208			208		1,03		
	0,2232	206	206,6667	0,2192	205	206,6667	0,99	1,01	237,9713
		206			207		1,01		
20 wt. %		188			187		1,84		
	0,1615	192	190,6667	0,1569	192	190,6667	1,37	1,56	365,0983
		192			193		1,47		
		197			192		0,69		
	0,2810	194	193,6667	0,2672	188	188,3333	1,36	0,9167	211,5097
		190			185		0,7		
25 wt. %		204			206		1,29		
	0,1811	207	205,6667	0,1771	204	203,0	1,43	1,35	379,5479
		206			199		1,33		
		196			201		1,35		
	0,2104	194	197,3333	0,1988	182	191,3333	1,38	1,4767	459,5760
		202			191		1,7		

	70°C - 30 min								
	m_{in} [g]	**d_{in} [µm]**	**avg d_{in} [µm]**	**m_{fin} [g]**	**d_{fin} [µm]**	**avg d_{fin} [µm]**	**$R_{a,fin}$ [µm]**	**avg $R_{a,fin}$ [µm]**	**A [mm^2]**
2,5 wt. %		197			201		1,35		
	0,2642	201	200,0	0,2638	201	200,0	0,85	1,1833	569,3966
		202			198		1,35		
		191			194		1,48		
	0,1705	192	191,3333	0,1702	195	194,6667	1,46	1,52	384,1013
		191			195		1,62		
5 wt. %		206			205		0,95		
	0,1941	206	206,3333	0,1934	207	206,6667	1,31	1,1567	321,5987
		207			208		1,21		
		183			194		1,12		
	0,2572	190	188,0	0,2562	191	190,3333	1,5	1,1933	589,1573
		191			186		0,96		
10 wt. %		194			193		0,8		
	0,2210	190	190,3333	0,2170	187	189,0	0,74	0,7767	501,4831
		187			187		0,79		
		221			219		1,21		
	0,1901	220	218,6667	0,1888	219	217,0	1,09	1,0633	374,7240
		215			213		0,89		
15 wt. %		203			203		1,42		
	0,2565	206	206,6667	0,2471	206	205,0	1,1	1,5267	534,9694
		211			206		2,06		
		203			200		2,12		
	0,3336	207	209,0	0,3029	204	206,3333	1,24	1,6467	333,4779
		217			215		1,58		
20 wt. %		190			183		1,45		
	0,2754	199	193,3333	0,2529	185	185,0	1,57	1,3533	614,0012
		191			187		1,04		
		206			201		1,17		
	0,2780	206	206,0	0,2358	200	200,6667	1,34	1,1933	581,6873
		206			201		1,07		
25 wt. %		206			196		0,81		
	0,2130	207	206,3333	0,1822	197	198,0	1,35	1,0467	444,9613
		206			201		0,98		
		208			200		1,13		
	0,2689	208	208,3333	0,2280	204	200,6667	0,85	0,9567	556,3448
		209			198		0,89		

	70°C - 60 min								
	m_{in} [g]	**d_{in} [µm]**	**avg d_{in} [µm]**	**m_{fin} [g]**	**d_{fin} [µm]**	**avg d_{fin} [µm]**	**$R_{a,fin}$ [µm]**	**avg $R_{a,fin}$ [µm]**	**A [mm^2]**
2,5 wt. %		213			225		0,92		
	0,3021	210	215,3333	0,3004	210	214,6667	0,95	0,9533	604,7160
		223			209		0,99		
		205			205		1,15		
	0,2164	200	202,3333	0,3056	201	201,6667	0,74	0,95	653,5818
		202			199		0,96		
5 wt. %		203			202		1		
	0,1820	206	205,6667	0,2150	206	205,0	1,02	1,0533	453,5293
		208			207		1,14		
		202			203		0,72		
	0,2154	201	202,0	0,1825	200	201,3333	0,74	0,7267	391,5586
		203			201		0,72		
10 wt. %		198			199		0,59		
	0,1692	198	197,0	0,1798	198	197,6667	0,85	0,7033	398,2146
		195			196		0,67		
		201			197		0,83		
	0,3809	203	202,0	0,2144	202	201,0	0,97	0,9133	468,3766
		202			204		0,94		
15 wt. %		216			215		1,59		
	0,3068	220	217,0	0,1833	218	212,6667	1,63	1,3767	427,8563
		215			205		0,91		
		207			205		1,5		
	0,1835	205	205,0	0,1672	205	204,3333	0,73	1,64	187,9683
		203			203		2,69		
20 wt. %		206			200		1,1		
	0,2195	207	206,6667	0,1316	202	202,0	0,89	1,2367	352,8921
		207			204		1,72		
		204			201		1,25		
	0,2001	207	205,3333	0,1400	202	202,0	0,83	1,1233	371,5573
		205			203		1,29		
25 wt. %		213			199		0,94		
	0,1770	210	211,0	0,3038	180	185,6667	0,31	0,4967	705,8372
		210			178		0,24		
		205			199		0,86		
	0,2678	203	204,0	0,1850	167	187,3333	0,73	0,78	192,7950
		204			196		0,75		

	80°C - 15 min								
	m_{in} [g]	**d_{in} [μm]**	**avg d_{in} [μm]**	**m_{fin} [g]**	**d_{fin} [μm]**	**avg d_{fin} [μm]**	**$R_{a,fin}$ [μm]**	**avg $R_{a,fin}$ [μm]**	**A [mm^2]**
2,5 wt. %	0,1747	191 188 191	190,0	0,1742	189 189 191	189,6667	0,81 0,87 1	0,8933	388,9823
	0,2297	185 193 195	191,0	0,2089	195 190 182	189,0	0,84 0,87 1,31	1,0067	472,3326
5 wt. %	0,1655	205 203 203	203,6667	0,1647	201 201 202	201,3333	0,67 0,67 0,7	0,68	350,2596
	0,2208	186 190 187	187,6667	0,1898	186 188 187	187,0	1,1 1,11 1,05	1,0867	437,0827
10 wt. %	0,1817	199 204 197	200,0	0,1803	198 203 195	198,6667	1,45 1,45 1,23	1,3767	391,5948
	0,2606	187 187 190	188,0	0,1520	184 184 182	183,3333	1,16 1,36 1,08	1,2	367,5257
15 wt. %	0,1524	204 201 201	202,0	0,1504	200 204 202	202,0	0,44 1,43 1,04	0,97	325,1963
	0,2969	187 187 188	187,3333	0,1765	185 185 184	184,6667	0,79 1,65 0,74	1,06	329,1579
20 wt. %	0,2457	192 208 200	200,0	0,2370	196 207 194	199,0	1,27 1,36 1,3	1,31	529,5259
	0,2847	187 187 186	186,6667	0,1622	185 172 184	180,3333	1,27 0,62 0,9	0,93	326,4349
25 wt. %	0,2151	209 208 211	209,3333	0,2008	206 195 206	202,3333	0,42 0,45 0,47	0,4467	401,2633
	0,2522	189 190 196	191,6667	0,1994	195 188 189	190,6667	0,91 1,24 1,19	1,1133	474,0630

	80°C - 30 min								
	m_{in} [g]	d_{in} [µm]	avg d_{in} [µm]	m_{fin} [g]	d_{fin} [µm]	avg d_{fin} [µm]	$R_{a,fin}$ [µm]	avg $R_{a,fin}$ [µm]	A [mm^2]
2,5 wt. %		186			184		0,92		
	0,2093	187	186,0	0,2293	185	184,3333	0,87	0,9233	532,3044
		185			184		0,98		
		203			209		1,7		
	0,2026	204	205,0	0,2022	204	205,0	0,84	1,3333	425,9882
		208			202		1,46		
5 wt. %		198			198		0,73		
	0,1903	199	198,6667	0,2189	198	198,0	0,94	0,8433	479,0558
		199			198		0,86		
		200			198		0,71		
	0,2943	202	200,6667	0,2849	198	197,6667	0,73	0,8067	338,8253
		200			197		0,98		
10 wt. %		203			201		0,75		
	0,1603	202	202,6667	0,2245	193	196,6667	1,23	1,06	312,9550
		203			196		1,2		
		199			183		1,36		
	0,2031	194	194,6667	0,1705	188	188,0	1,54	1,2533	165,9251
		191			193		0,86		
15 wt. %		195			182		0,47		
	0,1931	190	191,6667	0,2454	156	173,3333	0,55	0,4933	374,4462
		190			182		0,46		
		202			191		0,75		
	0,2461	200	200,3333	0,2044	187	190,6667	1,31	0,9667	529,5054
		199			194		0,84		
20 wt. %		184			171		1,13		
	0,1767	192	190,3333	0,2276	180	176,0	0,97	0,85	644,7400
		195			177		0,45		
		197			196		1,07		
	0,2979	196	196,3333	0,2784	195	195,0	0,67	0,9567	486,8599
		196			194		1,13		
25 wt. %		201			200		0,51		
	0,2108	201	202,0	0,2083	200	200,6667	1,3	0,9567	316,2222
		204			202		1,06		
		195			186		0,52		
	0,2270	195	196,3333	0,1845	172	183,6667	1,38	0,8433	498,3608
		199			193		0,63		

	80°C - 60 min								
	m_{in} [g]	**d_{in} [µm]**	**avg d_{in} [µm]**	**m_{fin} [g]**	**d_{fin} [µm]**	**avg d_{fin} [µm]**	**$R_{a,fin}$ [µm]**	**avg $R_{a,fin}$ [µm]**	**A [mm^2]**
2,5 wt. %	0,3283	185 186 191	187,3333	0,3241	185 187 191	187,6667	1,72 1,83 1,35	1,6333	406,1323
	0,2342	193 196 202	197,0	0,2328	200 191 195	195,3333	1,37 0,89 0,82	1,0267	512,4278
5 wt. %	0,2177	186 192 190	189,3333	0,2114	183 192 188	187,6667	1 1,01 1,45	1,13	495,6138
	0,1719	188 187 187	187,3333	0,1646	186 186 187	186,3333	0,72 0,92 0,86	0,8333	205,5738
10 wt. %	0,2789	196 194 189	193,0	0,1732	142 143 147	144,0	0,88 1,53 1,45	1,2867	160,0643
	0,2043	194 195 197	195,3333	0,1398	191 176 191	186,0	1,48 1,41 1,32	1,4033	93,9771
15 wt. %	0,2920	195 192 190	192,3333	0,1747	191 115 134	146,6667	0,25 0,23 0,2	0,2267	179,3864
	0,1651	188 189 188	188,3333	0,0987	139 109 145	131,0	0,31 0,22 0,29	0,2733	129,7834
20 wt. %	0,1881	200 186 189	191,6667	0,0988	135 185 189	169,6667	1,19 1,41 1,28	1,2933	182,0661
	0,1851	192 201 194	195,6667	0,1293	187 194 176	185,6667	0,65 0,27 1,27	0,73	304,3306
25 wt. %	0,2743	202 192 193	195,6667	0,1554	187 176 196	186,3333	1,19 0,94 3,23	1,7867	107,4201
	0,2048	190 190 191	190,3333	0,1432	189 142 185	172,0	0,18 0,36 0,53	0,3567	463,7961

	90°C - 15 min								
	m_{in} [g]	d_{in} [µm]	avg d_{in} [µm]	m_{fin} [g]	d_{fin} [µm]	avg d_{fin} [µm]	$R_{a,fin}$ [µm]	avg $R_{a,fin}$ [µm]	A [mm^2]
2,5 wt. %		196			198		0,7		
	0,2316	198	197,3333	0,2312	198	198,0	0,93	0,7767	505,8830
		198			198		0,7		
		187			192		0,94		
	0,1922	193	190,6667	0,1917	194	191,3333	0,88	0,89	434,5008
		192			188		0,85		
5 wt. %		196			202		0,94		
	0,4148	199	198,3333	0,4100	199	198,6667	1,02	0,88	461,0100
		200			195		0,68		
		178			179		1,05		
	0,2434	179	179,3333	0,2395	177	177,3333	0,93	0,9267	585,0212
		181			176		0,8		
10 wt. %		202			193		1,22		
	0,3213	203	200,0	0,2970	199	198,0	1,02	1,2233	208,0477
		195			202		1,43		
		204			202		1,02		
	0,3181	203	203,6667	0,3027	201	201,0	1,69	1,7133	673,2180
		204			200		2,43		
15 wt. %		200			147		0,95		
	0,3005	196	196,6667	0,2253	182	170,6667	1,61	1,3167	384,4295
		194			183		1,39		
		186			178		1,52		
	0,1789	188	186,6667	0,1554	183	179,6667	1,43	1,37	413,1004
		186			178		1,16		
20 wt. %		190			191		1,66		
	0,2767	188	189,0	#RIF!	165	182,3333	0,57	1,19	201,1163
		189			191		1,34		
		198			155		0,91		
	0,3049	198	197,3333	0,2430	160	159,0	0,31	0,51	450,7004
		196			162		0,31		
25 wt. %		190			154		0,23		
	0,2875	189	189,3333	0,2117	147	149,0	0,37	0,2933	629,9326
		189			146		0,28		
		188			163		0,88		
	0,1993	193	192,0	0,1344	180	168,3333	1,45	1,2367	285,9362
		195			162		1,38		

	90°C - 30 min								
	m_{in} [g]	**d_{in} [μm]**	**avg d_{in} [μm]**	**m_{fin} [g]**	**d_{fin} [μm]**	**avg d_{fin} [μm]**	**$R_{a,fin}$ [μm]**	**avg $R_{a,fin}$ [μm]**	**A [mm^2]**
2,5 wt. %	0,2877	185 186 186	185,6667	0,2864	185 185 185	185,0	0,65 0,81 0,91	0,79	667,9100
	0,2179	195 198 198	197,0	0,2175	196 198 194	196,0	0,78 0,74 0,25	0,59	476,7635
5 wt. %	0,1911	198 198 201	199,0	0,1692	186 185 198	189,6667	0,9 0,76 1,28	0,98	413,9231
	0,2506	183 183 186	184,0	0,2093	175 168 164	169,0	0,98 0,53 1,28	0,93	587,0502
10 wt. %	0,3141	197 199 198	198,0	0,2069	193 192 193	192,6667	0,97 0,87 1,52	1,12	112,4341
	0,2758	202 202 205	203,0	0,2090	195 183 200	192,6667	0,81 0,63 1,65	1,03	467,5206
15 wt. %	0,2754	200 207 204	203,6667	0,2040	150 142 178	156,6667	0,27 0,4 1,5	0,7233	469,1179
	0,2822	195 199 206	200,0	0,1838	196 170 183	183,0	1,4 1,2 1,46	1,3533	146,2918
20 wt. %	0,2039	197 199 203	199,6667	0,0962	81 192 139	137,3333	1,28 1,31 1,49	1,36	115,0092
	0,1840	184 181 180	181,6667	0,0950	101 106 107	104,6667	0,24 0,22 0,32	0,26	94,8609
25 wt. %	0,2800	184 184 184	184,0	0,0834	155 134 118	135,6667	0,94 0,87 0,83	0,88	655,9220
	0,3048	199 197 197	197,6667	0,1737	121 121 123	121,6667	0,24 0,23 0,24	0,2367	229,5963

	90°C - 60 min								
	m_{in} [g]	d_{in} [µm]	avg d_{in} [µm]	m_{fin} [g]	d_{fin} [µm]	avg d_{fin} [µm]	$R_{a,fin}$ [µm]	avg $R_{a,fin}$ [µm]	A [mm^2]
2,5 wt. %		200			199		0,44		
	0,2468	199	199,6667	0,2451	199	199,0	0,88	0,7467	532,7845
		200			199		0,92		
		195			194		1		
	0,1812	192	193,6667	0,1787	191	193,3333	0,7	0,8233	403,2880
		194			195		0,77		
5 wt. %		197			184		1		
	0,2898	194	195,6667	0,2401	182	184,3333	0,97	0,9367	638,4010
		196			187		0,73		
		198			194		1,16		
	0,2705	198	198,6667	0,2241	179	186,0	1,27	1,4567	661,3053
		200			185		1,94		
10 wt. %		200			111		2,09		
	0,2319	200	200,3333	0,0979	111	123,3333	0,84	1,22	183,6261
		201			148		0,73		
		198			113		1,19		
	0,3048	198	198,6667	0,1061	127	143,3333	1,36	1,8767	U.
		200			190		3,08		
15 wt. %		201			104		1,33		
	0,2743	199	199,0	0,0593	91	98,3333	2,04	1,54	U.
		197			100		1,25		
		201			U.		U.		
	0,2457	200	198,0	0,0151	U.		U.		U.
		193			U.		U.		
20 wt. %		197			U.		U.		
	0,3533	200	197,3333	0,0115	U.		U.		U.
		195			U.		U.		
		201			U.		U.		
	0,3422	202	201,3333	0,0185	U.		U.		U.
		201			U.		U.		
25 wt. %		184			U.		U.		
	0,1613	184	184,3333	0,0067	U.		U.		U.
		185			U.		U.		
		197			U.		U.		
	0,4264	197	196,6667	0,0002	U.		U.		U.
		196			U.		U.		

	30°C		40°C		50°C		60°C
	τ_{in}	$\tau_{50\%}$	τ_{in}	$\tau_{50\%}$	τ_{in}	$\tau_{50\%}$	τ_{in}
2,5 wt. %	>15’	>15’	>15’	>15’	>15’	>15’	>15’
	>30’	>30’	>30’	>30’	08’ 06’’	08’ 06’’	26’ 58’’
	>60'	>60'	>60'	>60'	49’ 09’’	49’ 29’’	03’ 46’’
	>15’	>15’	>15’	>15’	04’ 27’’	04’ 27’’	>15’
	>30’	>30’	>30’	>30’	>30’	>30’	05’ 54’’
	>60'	>60'	>60'	>60'	>60'	>60'	>60’
5 wt. %	>15’	>15’	>15’	>15’	>15’	>15’	06’ 37’’
	>30’	>30’	>30’	>30’	22’ 51’’	23’ 38’’	04’ 20’’
	>60'	>60'	>60'	>60'	39’ 29’’	>60'	12’ 23’’
	>15’	>15’	>15’	>15’	>15’	>15’	>15’
	>30’	>30’	>30’	>30’	23’ 01’’	23’ 58’’	04’ 39’’
	>60'	>60'	>60'	>60'	>60'	>60'	07’ 59’’
10 wt. %	>15’	>15’	>15’	>15’	06’ 21’’	09’ 51’’	03’ 32’’
	>30’	>30’	>30’	>30’	09’ 07’’	09’ 36’’	02’ 04’’
	>60'	>60'	19' 40"	20' 10"	13’ 40’’	14’44’’	05’ 29’’
	>15’	>15’	>15’	>15’	03’ 24’’	03’ 43’’	02’ 27’’
	>30’	>30’	>30’	>30’	04’ 21’’	04’ 40’’	01’ 30’’
	28’ 21’’	30’ 14’’	29’ 40’’	36’ 14’’	04’ 31’’	06’ 17’’	02’ 13’’
15 wt. %	>15’	>15’	06’ 33’’	06’ 41’’	02’ 32’’	04’ 30’’	02’ 08’’
	>30’	>30’	06’ 38’’	06’ 54’’	03’ 08’’	03’ 53’’	56’’
	>60'	>60'	21' 21"	24' 50"	04’ 05’’	05’ 12’’	54’’
	>15’	>15’	09’ 52’’	10’ 31’’	02’ 19’’	03’ 14’’	59’’
	>30’	>30’	14’ 13’’	16’ 26’’	02’ 38’’	03’ 25’’	01’ 09’’
	12’ 23’’	20’ 49’’	08’ 44’’	10’ 02’’	03’ 07’’	03’ 33’’	01’ 37’’
20 wt. %	>15’	>15’	06’ 13’’	07’ 06’’	04’ 03’’	05’ 42’’	01’ 02’’
	>30’	>30’	07’ 44’’	08’ 23’’	03’ 44’’	04’ 32’’	54’’
	11’ 41’’	13’ 26’’	06’ 04’’	06’ 33’’	02’ 32’’	03’ 57’’	52’’
	>15’	>15’	03’ 58’’	05’ 21’’	01’ 47’’	02’ 07’’	01’ 01’’
	25’ 45’’	26’ 24’’	06’ 02’’	06’ 38’’	02’ 11’’	02’ 32’’	57’’
	10’ 06’’	12’ 10’’	08’ 14’’	11’ 24’’	01’ 37’’	02’ 21’’	01’ 00’’
25 wt. %	09’ 24’’	12’ 11’’	06’ 37’’	10’ 06’’	02’ 00’’	02’ 23’’	58’’
	>30’	>30’	07’ 33’’	15’ 12’’	02’ 46’’	03’ 26’’	54"
	08’ 14’’	09’ 49’’	05’ 37’’	06’ 26’’	02’ 13’’	02’ 42’’	49’’
	09’ 32’’	13’ 58’’	03’ 01’’	04’ 05’’	02’ 27’’	03’ 02’’	45’’
	09’ 36’’	12’ 15’’	04’ 03’’	05’ 52’’	01’ 16’’	01’ 30’’	01’ 01’’
	11’ 58’’	14’ 40’’	18’ 36’’	18’ 56’’	01’ 47’’	02’ 18’’	01’ 22’’

60°C	70°C		80°C		90°C	
$\tau_{50\%}$	τ_{in}	$\tau_{50\%}$	τ_{in}	$\tau_{50\%}$	τ_{in}	$\tau_{50\%}$
>15’	07’ 36”	>15’	04’ 12”	>15'	40”	>15'
27’ 24”	>30’	>30’	01’ 08”	02’ 31”	43”	>30'
>60'	04’ 46”	04’ 53”	01’ 02”	01’ 22”	57”	>60'
>15’	05’ 06”	>15’	01’ 07”	01’ 39”	54”	>15'
07’ 44”	10’ 15”	>30’	25”	04’ 01”	52”	>30'
>60’	03’ 43”	>60'	50”	02’ 16”	25”	>60'
09’ 11”	09’ 20”	13’ 20”	01’ 05”	01’ 18”	24”	42”
09’ 48”	05’ 42”	07’ 18”	58”	01’ 37”	22”	02’ 37”
17’ 21”	03’ 47”	04’ 41”	01’ 09”	01’ 41”	27”	44”
>15’	04’ 13”	06’ 30”	01’ 05”	01’ 39”	12”	24”
05’ 07”	03’ 39”	04’ 36”	01’ 01”	01’ 45”	23”	26”
>60’	03’ 59”	>60'	54”	01’ 52”	29”	02’ 40”
09’ 07”	03’ 07”	04’ 57”	01’ 00”	01’ 16”	20”	26”
02’ 48”	01’ 17”	01’ 50”	22”	28”	16”	23”
06’ 38”	01’ 42”	03’ 15”	38”	01’ 23”	18”	24”
03’ 09”	01' 05"	01' 35"	24”	33”	18”	22”
02’ 03”	01’ 05”	01’ 29”	19”	26”	19”	31”
04’ 07”	01’ 55”	07’ 07”	21”	35”	18”	24”
03’ 57”	58”	01’ 33”	59”	01’ 13”	10”	14”
01’ 17”	01’ 08”	01’ 43”	14”	20”	10”	11”
01’ 39”	38”	01’ 00”	31”	01’ 17”	7"	7"
01’ 16”	36"	50"	16”	21”	10”	11”
01’ 28”	31”	36”	17”	23”	10”	11”
02’ 09”	31”	01’ 01”	12”	17”	11"	12"
01’ 32”	01’ 25”	01’ 35”	25”	40”	9”	10”
02’ 07”	25"	32"	22”	30”	12”	13”
59”	37”	43”	27”	47”	10"	11"
01’ 24”	26”	31”	21”	30”	15”	16”
01’ 20”	28”	32”	25”	34”	8”	9”
01’ 16”	37”	01’ 02”	20”	28”	27"	29"
01’ 03”	34”	41”	18”	28”	7”	8”
01' 15"	31”	38”	14”	22”	11”	12”
57”	33”	40”	20”	23”	19"	20"
53”	38”	56”	8”	16”	9”	10”
01’ 17”	30”	33”	12”	19”	11”	12”
02’ 02”	20”	23”	15”	21”	9"	10"